Volume 69, Issue 9 2010

Telecommunications
and
Radio Engineering

begell house, inc.
publishers

Aims and Scope

This journal consists of translations from two Ukrainian journals: *Radio Physics and Electronics*, *Radio Engineering* and one Russian journal: *Telecommunications*. What is more, the original papers by Russian an Ukrainian authors as well as the scientists from other states are published. The papers and articles are devoted to new mathematical approaches in electromagnetic theory, microwave electrodynamics, microwave and satellite telecommunications, signal processing, telephony, wave propagation, radar and radio navigation engineering, antennas, feeder systems and waveguides, electronic devices, nanotechnology in electronics, applied radio physics, and radio technology in biomedical studies. The scope of Telecommunication and Radio Engineering will appeal to theoreticians and engineers working on communication theory and networks, signal processing, protection of information and electromagnetic compatibility, radar and navigation systems, receiver and transmission equipment and instrumentation.

TELECOMMUNICATIONS AND RADIO ENGINEERING™ (ISSN 0040-2508) is owned by Begell House, Inc., 50 Cross Highway, Redding, Connecticut 06896, telephone (203) 938-1300. In 2010 one volume consisting of 20 issues is being published at a price of $4,518.00. Add $10.00 per issue for airmail service outside the United States and Canada. All subscriptions are payable in advance. Subscriptions are entered on an annual basis, i.e., January to December. Orders should be sent to Begell House, Inc, 50 Cross Highway, Redding, Connecticut 06896. Payments should be made by dollar checks drawn on a U.S. bank.

Printed TBD, 2010

TELECOMMUNICATIONS

AND RADIO ENGINEERING

Volume 69, 2010 **Number 9**

CONTENTS

Telecommunications and Radio Engineering, 69(9):751-762 (2010)

MICROWAVE ELECTRODYNAMICS

ELECTROMAGNETIC WAVE FOCUSING IN A DIELECTRIC CYLINDER

N.N. Gorobets & N.N. Statsyuk

V. Karazin National University of Kharkiv,
4, Svoboda Sq., Kharkiv, 61077, Ukraine

*Address all correspondence to N.N. Gorobets E-mail:
Nikolay.N.Gorobets@univer.kharkov.ua

The geometrical-optics approximation was used to perform calculations and analysis of amplitudes of the electric and magnetic fields in the point of their focusing inside the lossy dielectric cylinder irradiated with a plane electromagnetic wave of linear polarization. It has been established that in the focal region the amplitudes are changing according to the oscillating laws and the heavy longitudinal field gradients, the larger cylinder diameter and the higher its dielectric permeability. Experimental results allow one to explain the effects of subthreshold (nonthermal) influence of low-intensity millimeter and submillimeter electromagnetic waves on the man and other biological objects.

KEY WORDS: *electromagnetic field, focusing, losses, irradiation*

1. INTRODUCTION

In recent years an increased interest has been shown in application of microwaves for the improvement of the efficiency of various technological processes and for the stimulant influence on living organisms. To develop new a domain of microwave application in medicine and industry, purposefully and with complete understanding of used phenomena, it is necessary to know what the processes occur inside the material medium and biological objects under irradiation, how their parameters and properties are changing. The results obtained in practice do not give a comprehensive picture of processes, they do not agree because of many factors and it is impossible to take into account all of them [1,2]. Therefore, to describe comprehensively the mechanisms of electromagnetic wave influence onto biological objects it is necessary to develop physical-and-mathematical models of these effects.

The results of numerous experiments show [3] that during irradiation of living tissues there are such processes in them: ionization of molecules in the cells or cell membrane near-surface layers, that can change the cell permeability; change of the cell reproduction rate; polarization of molecules, that can change the process of fermentative reactions; influence on the neuromuscular system; excitation of elastic

acoustic vibrations in body tissues (acoustic effect). Enough studied and explained is the thermal effect – heating of tissues enabling to inhibit the tumor development. The mechanism of thermoelastic tissue dilatation has also therapeutic effect.

To date the most unclear and obscure is the effect of a subthreshold (nonthermal) influence of very low-intensity electromagnetic radiations on biological objects, in particular, on a man. On the one hand, the therapeutic effect of electromagnetic radiation in the medical treatment of many diseases is proved, on the other hand, the electromagnetic field intensity in these cases is less many times than the maximum permissible levels corresponding to the norms of factory hygiene in the radioindustry. That is the reason that the physical mechanism of the subthreshold action is not determined. We assume this mechanism to be the effect of electromagnetic wave focusing by cylindrical, spherical or ellipsoid formations having different, relatively to the environment, permitivity (or mepmeability for blood).

A goal of the paper is to investigate the amplitudes of electric and magnetic field strengths in the point of transmitted wave focusing in the dielectric cylinder.

2. PROBLEM STATEMENT

On the lateral surface of an infinitely extended lossy dielectric cylinder the plane linearly polarized wave is incident. Within the framework of geometrical optics the surface of a cylinder is illumined within the limits of angles of wave incidence $\varphi \in \left(-\frac{\pi}{2}; \frac{\pi}{2} \right)$ relatively to the external normal to the surface.

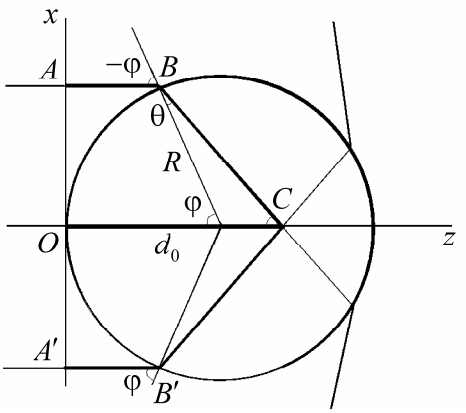

FIG. 1: Geometry of the problem

In the case of the ray incidence onto the interface of media the reflected and refracted rays are formed. The transmitted rays, formed as a result of the flat wave incidence onto the surface of a dielectric cylinder, will be focused in some region on

the focal axis inside the cylinder or, after the repeated refraction, on the continuation of this axis outside the cylinder.

It is necessary to define amplitudes of the fields $\left|\dot{\vec{E}}\right|$ and $\left|\dot{\vec{H}}\right|$ in the focusing points, formed by crossing of three rays OC, ABC and $A'B'C$, the angles of incidence of which are equal to $\varphi_1 = 0$, $\varphi_2 = \varphi$, $\varphi_3 = -\varphi$ respectively (Fig. 1).

In the problem solving the approximations accepted in the geometrical optics (GO) are taken. In particular, in the point of ray incidence we consider the surface to be locally flat (as $R >> \lambda$), therefore all the laws of GO are valid, and the boundary conditions of electrodynamics are valid in the form obtained for the media with different electrophysical parameters.

We assume that the amplitudes of repeatedly reflected rays in the dielectric cylinder are negligible. The ray trajectories are determined in accordance with the Snell laws.

The problem will be solved in two steps. At first, by the method of geometrical optics we find two rays ABC and $A'B'C$, which get the given point C on the focal axis of the cylinder. In the second step with the help of the method of optical physics we find the amplitudes and phases of all the three waves getting the point C by the rays OC, ABC and $A'B'C$. Thus, the field of every transmitted ray is a complex quantity, the amplitude of which is determined by the incident wave amplitude, the refraction coefficient module, the coefficient of wave attenuation in the medium and by the projection of the traveled distance in the cylinder onto its radius to the incidence point.

The phase is determined by the length of an optical path between the plane of equal incident wave phases (point A in Fig. 1) and the point of ray incidence onto the cylinder (point B), by the refraction coefficient argument and the BC distance, which the ray has passed inside the dielectric cylinder to the observation point. Now we consider two problems: when the plane of incident electromagnetic wave polarization is either parallel, or perpendicular to the element of cylinder. As the orthogonally polarized waves do not interfere, the solutions obtained can be used to study the effects of dielectric cylinder focusing of waves with a different polarization – oblique, linear, elliptic or circular.

Using the known equations [4,5] for the wave refraction coefficients the expressions for the transmitted wave are written as follows:

a) The incident wave is parallel polarized

$$\dot{\vec{E}}_{np} = \left(\vec{x}^0 \beta_z - \vec{z}^0 \left(\beta_x - i\alpha\right)\right) \cdot \frac{\dot{E}_0 \dot{D}_p}{k_2} \cdot e^{-\alpha x} \cdot e^{-i(\beta_x x + \beta_z z)}, \qquad (1)$$

$$\dot{\vec{H}}_{np} = \vec{y}^0 \cdot \frac{\dot{E}_0 \dot{D}_p}{\dot{W}_2} \cdot e^{-\alpha x} \cdot e^{-i(\beta_x x + \beta_z z)}. \qquad (2)$$

b) The incident wave is perpendicularly polarized

$$\dot{\vec{E}}_{np} = \vec{y}^0 \cdot \dot{E}_0 \dot{D}_s \cdot e^{-\alpha x} \cdot e^{-i(\beta_x x + \beta_z z)}, \qquad (3)$$

$$\dot{\vec{H}}_{np} = -\left(\vec{x}^0\beta_z - \vec{z}^0\left(\beta_x - i\alpha\right)\right)\cdot\frac{\dot{E}_0\dot{D}_s}{\dot{W}_2 k_2}\cdot e^{-\alpha x}\cdot e^{-i(\beta_x x+\beta_z z)}, \qquad (4)$$

where $\beta_x = \mathrm{Re}(k_2\cos\theta)$, $\beta_z = k_2\sin\theta = k_1\sin\varphi$, and $k_2 = \beta - i\alpha$.

The problem is considered in the Cartesian coordinate system, its origin being in the superposition with the point of incidence of the ray perpendicular to the cylinder surface ($\varphi = 0$), the axis *ox* coincides with the cylinder focal axis, the axis *oy* is parallel to the cylinder axis (Fig. 1). In this case the summarized amplitudes of the fields $\left|\dot{\vec{E}}\right|$ and $\left|\dot{\vec{H}}\right|$ of three rays in the observation points $\left(x = d_0 = R\left(1-\cos\varphi+\frac{\sin\varphi}{\tan(\varphi-\mathrm{Re}\,\theta)}\right), z = 0\right)$ are determined by their interference and are described by the following equations

a) Parallel polarization:

$$\left|\dot{E}_p\right| = E_0\sqrt{\left|\dot{D}_{p0}\right|^2\cdot e^{-2\alpha d_0} + A_E'^2 - 2\left|\dot{D}_{p0}\right|A_E'\cdot e^{-\alpha d_0}\cdot\cos\left(\psi_{E1}' + \psi_{E2}' + \mathrm{Re}\,k_2 d_0 - \arg\dot{D}_{p0}\right)}, \quad (5)$$

where $A_E' = -2\left|\frac{\dot{D}_p}{k_2}\right|\cdot e^{-\alpha(d_0 - R(1-\cos\varphi))}\cdot\sqrt{\left(k_1\sin^2\varphi + \cos\varphi\cdot\mathrm{Re}\left(k_2\cos\theta\right)\right)^2 + \alpha^2\cos^2\varphi}$,

$$\psi_{E1}' = \arctan\frac{b}{a+\cos\varphi} + \arctan\frac{b\cos\varphi}{a\cos\varphi+\sin^2\varphi} -$$

$$-\arctan\frac{\chi}{\eta} + \arctan\frac{-\alpha}{\beta} - \mathrm{Re}\left(k_2\cos\theta\right)\cdot\left(d_0 - R\left(1-\cos\varphi\right)\right) - \mathrm{Re}\left(k_2\cos\theta\right)\times$$

$$\times\left(d_0 - R\left(1-\cos\varphi\right)\right) + k_1 R\left(\sin^2\varphi - 1 + \cos\varphi\right),$$

$$\psi_{E2}' = \arctan\frac{-\alpha\cos\varphi}{k_1\sin^2\varphi + \cos\varphi\cdot\mathrm{Re}\left(k_2\cos\theta\right)},$$

$$\left|\dot{H}_p\right| = \frac{1}{|W_2|}E_0\sqrt{\left|\dot{D}_{p0}\right|^2\cdot e^{-2\alpha d_0} + \left|\dot{D}_p\right|^2\cdot e^{-2\alpha(x-R(1-\cos\varphi))} + 2\left|\dot{D}_{p0}\right|\left|\dot{D}_p\right|\cdot e^{-\alpha(2d_0 - R(1-\cos\varphi))}\cdot\cos\left(\psi_{H1}' - \psi_{H2}'\right)}, \quad (6)$$

where $\psi_{H1}' = \arctan\frac{\chi}{\eta+1} - \mathrm{Re}\,k_2 d_0$,

$$\psi_{H2}' = \arctan\frac{b}{a+\cos\varphi} + \arctan\frac{b\cos\varphi}{a\cos\varphi+\sin^2\varphi} -$$

$$-\arctan\frac{\chi}{\eta} - \mathrm{Re}\left(k_2\cos\theta\right)\cdot\left(d_0 - R\left(1-\cos\varphi\right)\right) + \qquad k_1 R\left(\sin^2\varphi - 1 + \cos\varphi\right) \qquad ,$$

$\dot{D}_{p0} = \dfrac{2}{\eta - i\chi + 1}$ is the refraction coefficient of the parallel polarized wave being incident perpendicularly to the medium-medium interface.

To simplify the calculations, similarly to [6], the subsidiary quantities are introduced.

$$n = \eta - i\chi,\ \chi = \sqrt{\frac{\varepsilon}{2}} \cdot \sqrt{\sqrt{1+\tan\delta^2} - 1},\ \eta = \sqrt{\frac{\varepsilon}{2}} \cdot \sqrt{\sqrt{1+\tan\delta^2} + 1},$$

$$(\eta - i\chi)\cos\theta = a - ib = \sqrt{(\eta - i\chi)^2 - \sin^2\varphi},$$

$$a = \sqrt{\frac{1}{2}\left[\sqrt{\left(\eta^2 - \chi^2 - \sin^2\varphi\right)^2 + 4\eta^2\chi^2} + \left(\eta^2 - \chi^2 - \sin^2\varphi\right)\right]},$$

$$b = \sqrt{\frac{1}{2}\left[\sqrt{\left(\eta^2 - \chi^2 - \sin^2\varphi\right)^2 + 4\eta^2\chi^2} - \left(\eta^2 - \chi^2 - \sin^2\varphi\right)\right]}.$$

b) Perpendicular polarization:

$$\left|\dot{E}_s\right| = E_0 \times \sqrt{\left|\dot{D}_{s0}\right|^2 \cdot e^{-2\alpha d_0} + \left|\dot{D}_s\right|^2 \cdot e^{-2\alpha(d_0 - R(1-\cos\varphi))} + 2\left|\dot{D}_{s0}\right|\left|\dot{D}_s\right| \cdot e^{-\alpha(2d_0 - R(1-\cos\varphi))} \cos\left(\psi_{E1} - \psi_{E2}\right)}, \quad (7)$$

where $\psi_{E1} = \arctan\dfrac{\chi}{\eta + 1} - \mathrm{Re}\, k_2 d_0$,

$$\psi_{E2} = \arctan\frac{b}{a + \cos\varphi} - \mathrm{Re}\left(k_2\cos\theta\right) \cdot \left(d_0 - R\left(1 - \cos\varphi\right)\right) + k_1 R\left(\sin^2\varphi - 1 + \cos\varphi\right),$$

$$\left|\dot{H}_s\right| = -\frac{1}{|W_2|} \times E_0 \sqrt{\left|\dot{D}_{s0}\right|^2 \cdot e^{-2\alpha d_0} + A_H^2 - 2\left|\dot{D}_{s0}\right| A_H \cdot e^{-\alpha d_0} \cos\left(\psi_{H1} + \psi_{H2} + \mathrm{Re}\, k_2 d_0 - \arg\dot{D}_{s0}\right)}, \quad (8)$$

where

$$A_H = -2\left|\frac{\dot{D}_s}{k_2}\right| \cdot e^{-\alpha(d_0 - R(1-\cos\varphi))} \sqrt{\left(k_1\sin^2\varphi + \cos\varphi \cdot \mathrm{Re}\left(k_2\cos\theta\right)\right)^2 + \alpha^2\cos^2\varphi},$$

$$\psi_{H1} = \arctan\frac{b}{a + \cos\varphi} + \arctan\frac{-\alpha}{\beta} - \mathrm{Re}\left(k_2\cos\theta\right) \times$$

$$\times\left(d_0 - R\left(1 - \cos\varphi\right)\right) + k_1 R\left(\sin^2\varphi - 1 + \cos\varphi\right),$$

$$\psi_{H2} = \arctan \frac{-\alpha \cos\varphi}{k_1 \sin^2\varphi + \cos\varphi \cdot \mathrm{Re}\left(k_2 \cos\theta\right)},\ \dot{D}_{s0} = \dot{D}_{p0} = \frac{2}{\eta - i\chi + 1}\ .$$

For the case of a loss-free medium the end formulae for the calculation of fields are simplified.

a) Parallel polarization:

$$\left|\dot{E}_p\right| = E_0 \sqrt{D_{p0}{}^2 + 4\cos^2\left(\varphi-\theta\right) D_p{}^2 + 4 D_{p0} D_p \cos\left(\varphi-\theta\right)\cos\left(k_2 d_0 + \xi_1\right)}\,, \qquad (9)$$

$$\left|\dot{H}_p\right| = \frac{E_0}{W_2} \sqrt{D_{p0}{}^2 + D_p{}^2 + 2 D_{p0} D_p \cos\left(k_2 d_0 + \xi_1\right)}\,, \qquad (10)$$

where $\xi_1 = k_2\left(R\cos\theta - R\cos\left(\varphi+\theta\right) - d_0\cos\theta\right) - k_1 R\left(1-\cos\varphi\right)$, $\dot{D}_{p0} = \dfrac{2}{\sqrt{\varepsilon}+1}$.

b) Perpendicular polarization:

$$\left|\dot{E}_s\right| = E_0 \sqrt{D_{s0}{}^2 + D_s{}^2 + 2 D_{s0} D_s \cos\left(k_2 d_0 + \xi_1\right)}\,, \qquad (11)$$

$$\left|\dot{H}_s\right| = \frac{E_0}{W_2} \sqrt{D_{s0}{}^2 + 4\cos^2\left(\varphi-\theta\right) D_s{}^2 + 4 D_{s0} D_s \cos\left(\varphi-\theta\right)\cos\left(k_2 d_0 + \xi_1\right)}\,, \qquad (12)$$

$$\dot{D}_{s0} = \dot{D}_{p0} = \frac{2}{\sqrt{\varepsilon}+1}\ .$$

To calculate total values of $\left|\dot{E}_\Sigma\right|$ and $\left|\dot{H}_\Sigma\right|$ for both variants of the incident wave polarization we have developed computer codes and constructed the diagrams of their dependence on the coordinates of observation points normalized to the circular cross-section radius of the dielectric cylinder for different ε.

3. ANALYSIS OF CALCULATION RESULTS

Let us consider the circular cross-section of a dielectric cylinder. We do not apply restrictions to its radius, except $R >> \lambda$. The dielectric permeability will be varied in the wide range, and the magnetic permeability is taken as $\mu = 1$. It is assumed that the medium outside the cylinder has the following characteristics: $\varepsilon = 1$, $\mu = 1$ and $\tan\delta = 0$. In the loss-free medium the dielectric operates as a converging lens: the incoming rays are parallel to the wave propagation direction, and the rays, passing through the medium, are refracting and focusing in/or outside the cylinder. The focal region takes place on the focal axis (along the direction of incident wave propagation), the ray path is symmetric relatively to this axis. In the lossy medium the propagating wave is attenuating and gets an additional phase incursion.

Now we consider the electromagnetic wave focusing points on the axis *ox* of a dielectric lossy cylinder cross-section. A plane wave is incident onto every point of the cylinder surface at an angle φ changing from $-\frac{\pi}{2}$ to $\frac{\pi}{2}$. Let us imagine the cylinder surface as a set of infinitesimal linear sections. In the approximation we can observe separately the ray incidence onto the plane interface of two media at an angle φ.

In every point of the axis *oz*, starting from the circle center, three rays can be intersected: a ray normal to the surface and two rays refracted at angles θ. The ray paths, the place of points of intersection of refracted rays with a normally incident ray and the field amplitude in these points will depend on the cylinder radius-to-incident wave length ratio, and also on the dielectric permeability and loss-angle tangent.

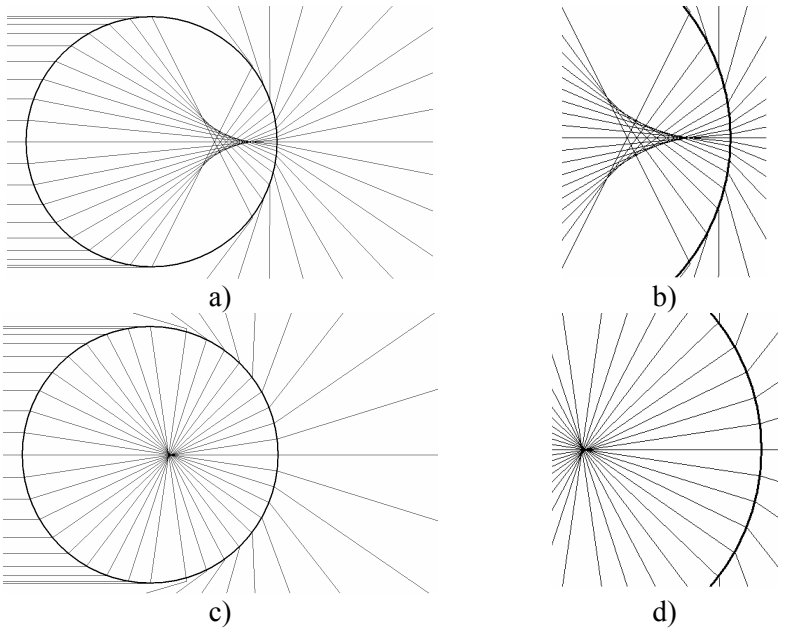

FIG. 2: The ray paths and the field caustic in the loss-free dielectric cylinder with $\varepsilon = 5$ (a, b) and $\varepsilon = 50$ (c, d)

The geometrical-optics illustrations of the process of ray refraction and focusing in the circular cross-section of the dielectric cylinder are shown in Fig. 2 for the comparative analysis. In the calculations, here and below, is assumed that the amplitude vector of the electric field strength being incident onto the dielectric plane wave cylinder is $E_0 = 1$ B/m, the wave length $\lambda = 1$ mm. Figure 2 demonstrates the fact that the transmitted rays form the caustic inside the dielectric body. And, as the dielectric permeability increases, the ray focusing converges into the point.

Further let us consider the dependences of the strength amplitudes of electric and magnetic fields on the normalized coordinate z/R with the cylinder radius R being changing and ε for the case of parallel (a, b) and perpendicular (c, d) polarization of the incident wave (see Figs. 3-6).

The presented calculation results allows one to analyze the effects of electric field focusing in the circular cross-section of the dielectric cylinder by changing its radius and medium parameters.

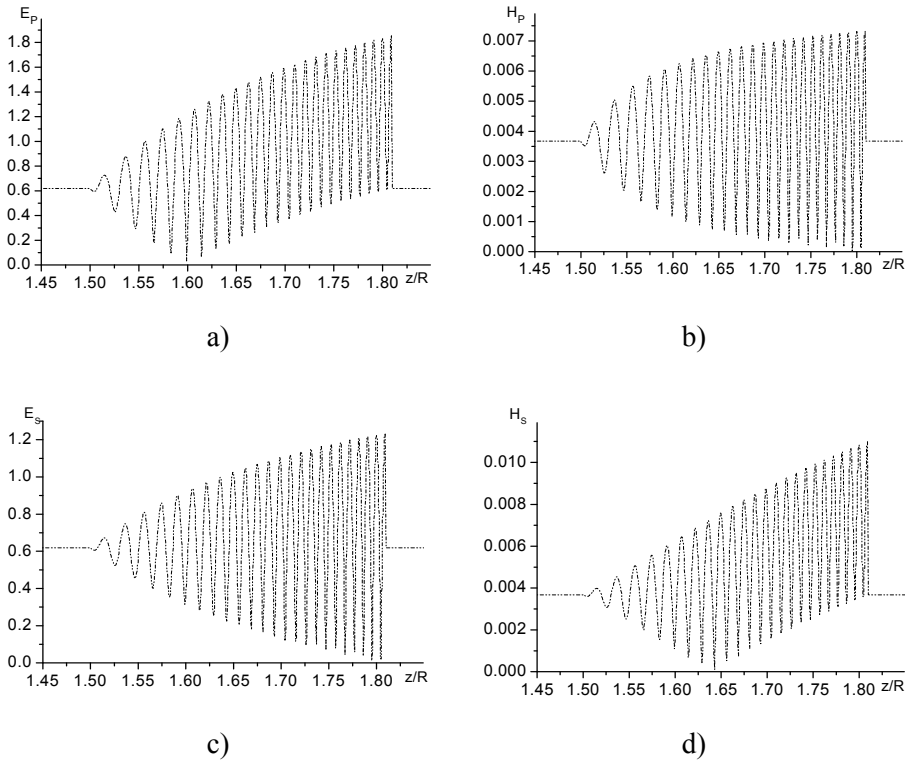

FIG. 3: Focusing of electric (a, b) and (c, d) magnetic fields by means of a dielectric cylinder ($R = 10\lambda$, $\varepsilon = 5$, $\tan\delta = 0$)

Inside the dielectric cylinder the incident electromagnetic wave power concentrates in some volume. But, in consequence of a phenomenon of wave interference inside this volume, the amplitudes of fields E and H are changing depending on the observation point position by the oscillating laws with very great gradients. Therefore, in the dielectric cylinder the waves do not focus into the point as in the case of classic focusing systems. However, the proved phenomenon of field concentration and very heavy gradients in the focal region of the dielectric cylinder can be a physical cause of the subthreshold action of electromagnetic waves on the

man and other biological objects. Apparently, it is particularly true for the millimeter and submillimeter waves when the heavy field gradients are observed at the distances comparable with molecule sizes.

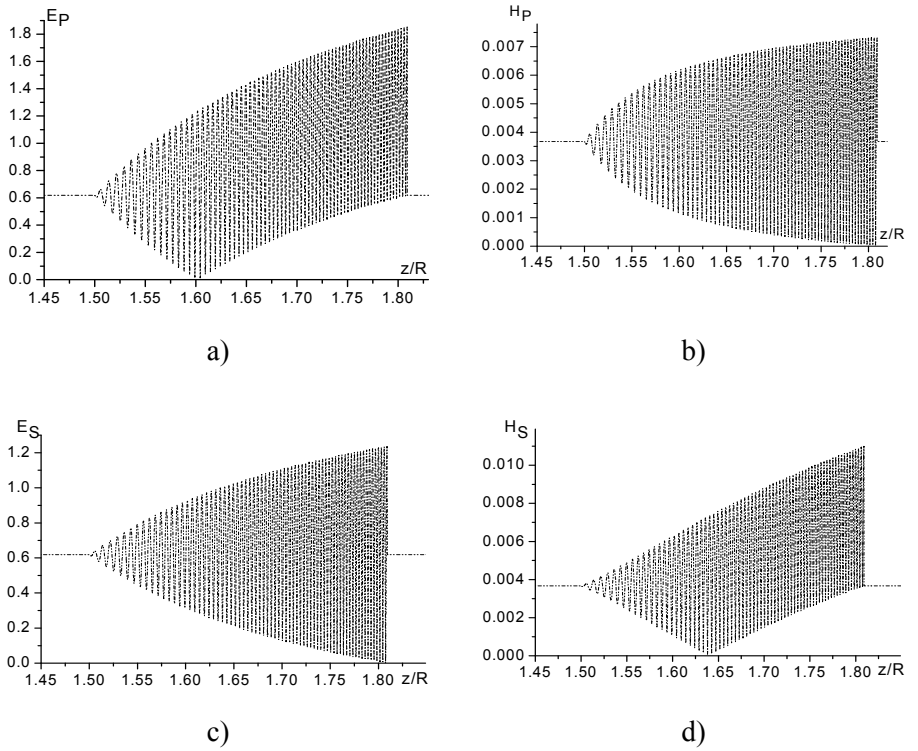

FIG. 4: Focusing of electric (a, b) and (c, d) magnetic fields by means of a dielectric cylinder ($R = 30\lambda$, $\varepsilon = 5$, $\tan\delta = 0$)

The maxima and minima of fields in the area of power concentration inside the dielectric cylinder (we name it "focusing region") are depending on the radius and permittivity of the cylinder. The amplitudes of E and H fields in this region are increasing in all the cases as they are moving away from the cylinder center for both the vertical and horizontal polarization. The pattern and rate of field amplitude rise in this case are different for E - and H fields.

As the cylinder radius increases with equal ε , the focusing region length extent is constant, as is seen from Figs. 3-6, however, the number of field oscillations per length unit increases without changing the field maximum value. This can be explained by the fact that as the radius increases the rate of change of the angle of plane wave incidence onto the cylinder plane is decreasing, as well as, the rate of change of the phase of the rays under consideration. Consequently, because of the difference in the rates of change of the normal ray and the ray refracted at an angle θ, there occurs an inphase and antiphase summation of waves in the focusing region.

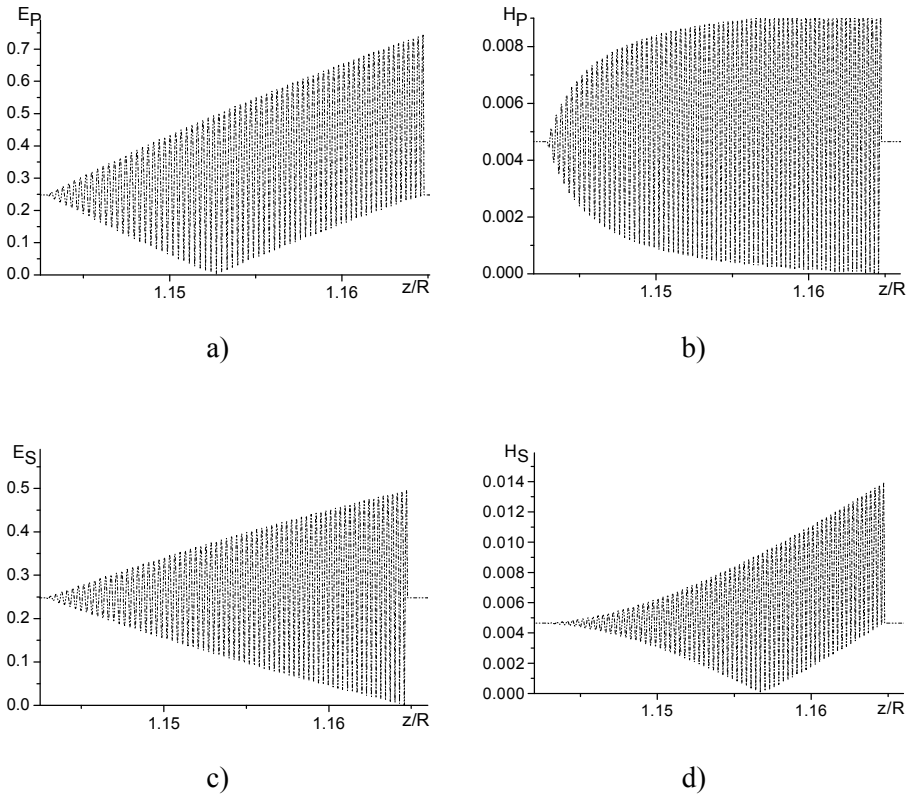

FIG. 5: Focusing of electric (a, b) and (c, d) magnetic fields by means of a dielectric cylinder ($R = 10\lambda$, $\varepsilon = 50$, $\tan\delta = 0$)

When the dielectric permeability ε increases, the rays focusing takes place and the number of oscillations is increasing too, as is seen from the comparison of Figs. 3-6. The amplitude of the field E decreases and that of the field H increases. As ε increases the envelope of oscillations is bending towards the region that it confines. The field focusing region moves towards the cylinder center and its extent decreases. The effect of the field gradient increase in the focal region with ε increasing is shown in Fig. 2(d).

Let us consider the loss influence on the electric induction vector in the focal area for the case of vertical and horizontal polarization of the wave being incident onto the dielectric cylinder. The calculation results for $R = 10\lambda, \varepsilon = 5$ are given in Fig. 7. One can see that as the dielectric loss-angle tangent increases, the displacement of focusing points is negligible. In the case of low loss ($\tan\delta \le 10^{-3}$) the law of field amplitude rise D remains unchanged as moving away from the cylinder center for both the horizontal and vertical polarization of the wave being incident of the dielectric cylinder. The loss increase leads to the increase of the curvature of oscillation envelope

and to the significant decrease of the electric-induction vector amplitude in the focusing region. Evidently, that it is explained by the increase of the wave optical path length in the absorbing medium.

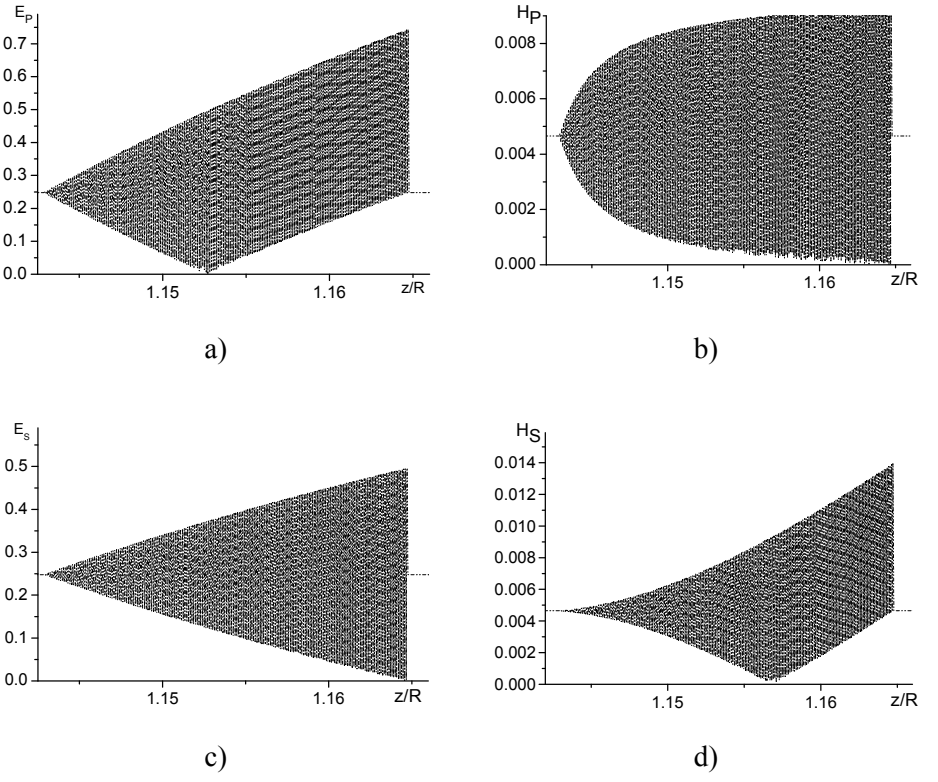

FIG. 6: Focusing of electric (a, b) and magnetic fields (c, d) by means of a dielectric cylinder ($R = 30\lambda$, $\varepsilon = 50$, $\tan\delta = 0$)

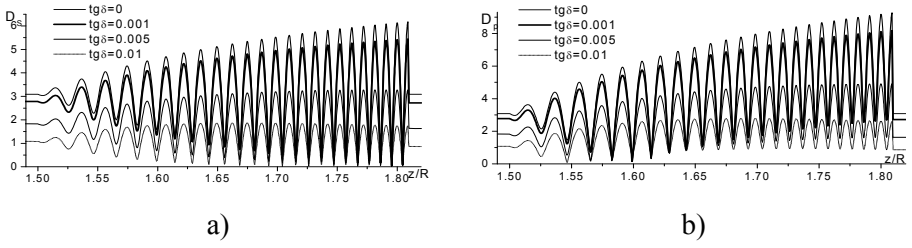

FIG. 7: Influence of the loss on the electric induction vectors in the focal area ($R = 10\lambda$, $\varepsilon = 5$)

4. CONCLUSIONS

Using the quasi-optical approximation, the authors solved the problem of finding the amplitudes of electric and magnetic field strengths inside the infinite dielectric cylinder, having an arbitrary radius, arbitrary value of the dielectric permeability, as well as, the dielectric loss-angle tangent for two model cases: when the electric field vector is parallel and perpendicular to the element of cylinder. In the calculations the field phase jumping in the process of wave passage through the cylinder surface is taken into account. By the algorithm developed a computer code was developed for calculation of amplitude and phase characteristics of the field inside the cylinder.

Analysis of calculation results has shown that the beams refraction at the dielectric cylinder boundary leads to their focusing. It has been established, that the region with the increased local density of electromagnetic wave power displaces towards the cylinder center and the higher dielectric permeability of the medium, the longer its displacement path. As a result of the wave interference in the focal area the rays are focused not in the point but in the rather fuzzy region inside the cylinder. This phenomenon leads to great gradients of field amplitudes. The results show that because of the loss in the medium not only the field amplitudes are decreasing in the local maxima, but the field gradients too.

The results of investigated phenomena allow one to explain the effects of subthreshold (nonthermal) influence of low-intensity millimeter and submillimeter electromagnetic waves on the man and other biological objects.

REFERENCES

1. Morozov, G.A. and Sedelnikov, Yu.E., (eds.) (2003), *Low-intensity microwave technologies (problems realizations)*, Radiotekhnika, Moscow: 112 p. (in Russian).
2. *Microwave energy. Vol.3: Application of microwave frequencies in medicine, science and engineering*, (1971), Mir, Moscow: 248 p. (in Russian).
3. Sakalo, S.M., Semenets, V.V., and Azarkhow, O.Yu., (2005), *Microwave frequencies in medicine (therapy and diagnostics) Manual*, KhNURE, Kollegium, Kharkov: 264 p. (in Russian).
4. Pimenov, Yu.V., Volman, V.I, and Muravtsov, A.D., (2002), *Engineering electrodynamics: Manual*. Radio i svyaz', Moscow: 536 p. (in Russian).
5. Goldstein, L.D. and Zernov, N.V., (1972), *Electromagnetic fields and waves*, Sov. Radio, Moscow: 464 p. (in Russian).
6. Prishivalko, A.P., (1963), *Light reflection from absorbing media*, Publ. by Byelorussian Academy of Sciences, USSR, Minsk: 430 p. (in Russian).
7. Kovneristy, Yu.K., Lazareva, I.Yu., and Ravayev, A.A., (1982), *Materials absorbing microwave radiations*, Nauka, Moscow: 167 p. (in Russian).

Telecommunications and Radio Engineering, 69(9):763-771 (2010)

ELECTROMAGNETIC WAVE RADIATION BY A SET OF LONGITUDINAL AND TRANSVERSE SLOTS IN A WIDE WALL OF A RECTANGULAR WAVEGUIDE *

S.L. Berdnik

V. Karazin National University of Kharkov,
4, Svoboda Sq., Kharkiv, 61077, Ukraine

*Address all correspondence to S.L. Berdnik E-mail: afis@ire.kharkov.ua

The Galerkin method has been used to find a solution to the problem on e.m. wave radiation by a two-frequency multielement multimode slotted-waveguide array. A radiating aperture comprises two sets of transverse and longitudinal slots in a rectangular waveguides wide wall. This structure has been studied in terms of its energy and directional characteristics. The computational procedure involved the parameters such as waveguide wall thickness, total interaction between the slots around the waveguides external and internal volume.

KEY WORDS: *antenna array, set of slots, multimode rectangular waveguide*

1. INTRODUCTION

The multifrequency multichannel system designed as a set of several antenna arrays placed in a single aperture makes it possible to increase the operational efficiency of airborne as well as ground based radio engineering facilities [1]. In some instances when the high performance capabilities of the above facilities are implemented in practice it makes sense to use multifunctional antennas in the shape of slot arrays which have different geometric dimensions of radiating multimode waveguide elements. In the literature no reference is essentially made to computational algorithms and the results from the study into electrodynamic properties of multielement multifrequency, multimode slotted waveguide antennas. Clearly it cannot but lead to their limited application in antenna-waveguide engineering.

The present paper describes the Galerkin method for calculating the radiation characteristics of multielement waveguide slot arrays comprising two subarrays in which slots are of different lengths and orientations, these elements being intended to operate at different frequencies and rectangular waveguide.

* Originally published in *Bulletin (Vestnik) of the Kharkiv University*, No 712, 2006, pp. 25–29.

2. STATEMENT OF THE PROBLEM AND ITS SOLUTION

In [2] a description is given of the study into the two-frequency slot antenna arrays on multimode rectangular waveguides. A radiating aperture makes up two systems of longitudinal slots in a wide wall of H_{10} and H_{30} mode-excited waveguide. In this particular instance a minimal magnitude of the reciprocal coupling between the HF and LF subarrays is obtained by means of the H_{10} mode-excited LF subarray slot radiators cut through at points where the H_{30} mode surface currents traversing these slots on the waveguides internal wall are equal to zero.

Given the physical considerations, it is quite obvious that the reciprocal coupling in these types of antennas can be further reduced if the HF subarray slots are arranged transverse to the waveguide axis, specifically to the orthogonal LF subarray slots. It is exactly due to the radiating fields orthogonally that a limiting attainable minimum of inter-subarray coupling can be assured.

The radiating aperture constitutes two systems of slots positioned in a wide wall of thickness h of the rectangular waveguide at $a \times b$ section (see Fig. 1).

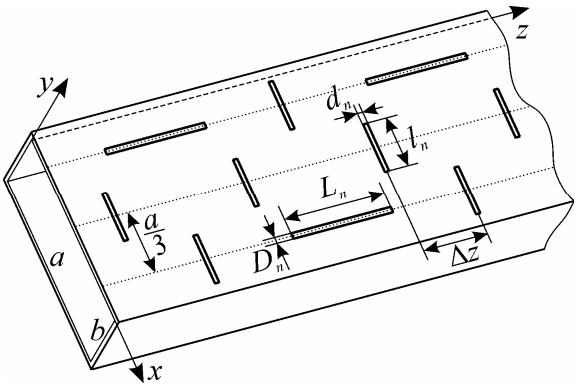

FIG. 1: Slot system positioned at the wide wall of waveguide

The longitudinal slots of lengths L_n and of widths D_n are excited by the fundamental H_{10} mode at a frequency of f_{10} (λ_{10} wavelength) whereas the transverse slots of lengths l_n and of widths d_n get excited by the H_{30} mode at a frequency of f_{30} (λ_{30} wavelength). The former system is operated over a long-wave range, the latter is run in a short-wave range. We represent the field in each slot as an expansion in linearly-independent vector-functions of longitudinal and transverse slots $\vec{E}_{nq}, \vec{e}_{n'q'}$ along with complex coefficients $V_{nq}, W_{n'q'}$ [3]. The total electric field in the multifunctional antenna aperture on the waveguide side (index "1") and the half-space above the infinite perfectly conducting shield (index "2") can then be expressed as follows

$$\vec{E}^{(1)} = \sum_{n=1}^{N}\sum_{q=1}^{Q} V_{nq}^{(1)} \vec{E}_{nq}^{(1)} + \sum_{n'=1}^{N'}\sum_{q'=1}^{Q'} W_{n'q'}^{(1)} \vec{e}_{n'q'}^{(1)}, \quad \vec{E}^{(2)} = \sum_{n=1}^{N}\sum_{q=1}^{Q} V_{nq}^{(2)} \vec{E}_{nq}^{(2)} + \sum_{n'=1}^{N'}\sum_{q'=1}^{Q'} W_{n'q'}^{(2)} \vec{e}_{n'q'}^{(2)}, \quad (1)$$

where N, N' are the numbers of longitudinal and transverse slots respectively; n, n' are their ordinal numbers; Q, Q' is the number of the field approximation functions on the surfaces of the above-mentioned slots; q, q' are the ordinal numbers of vector-functions.

Substituting (1) into the continuity equations of the tangential components of the magnetic intensity vector on the internal and external surface of each of the slots and using the Galerkin method for solving the derived integral equations, we obtain a system of linear algebraic equations (SLAE) with respect to the unknown quantities $V_{nq}^{(1),(2)}$ and $W_{n'q'}^{(1),(2)}$:

$$\begin{cases} \sum_{n=1}^{N}\sum_{q=1}^{Q} V_{nq}^{(1)} \left(Y_{mn,pq}^{1} + Y_{m,pq}^{V_{11}} \delta_{mn} \delta_{pq} \right) + \sum_{n'=1}^{N'}\sum_{q'=1}^{Q'} W_{n'q'}^{(1)} Y_{mn',pq'}^{1} + \sum_{q=1}^{Q} V_{mq}^{(2)} Y_{m,pq}^{V_{12}} \delta_{pq} = F_{mp}, \\ \sum_{q=1}^{Q} V_{mq}^{(1)} Y_{m,pq}^{V_{21}} \delta_{pq} + \sum_{n=1}^{N}\sum_{q=1}^{Q} V_{nq}^{(2)} \left(Y_{mn,pq}^{e} + Y_{m,pq}^{V_{22}} \delta_{mn} \delta_{pq} \right) + \sum_{n'=1}^{N'}\sum_{q'=1}^{Q'} W_{n'q'}^{(2)} Y_{mn',pq'}^{e} = 0, \\ m = 1,2,....N, \quad p = 1,2,...,Q, \\ \sum_{n=1}^{N}\sum_{q=1}^{Q} V_{mq}^{(1)} Y_{m'n,p'q}^{1} + \sum_{n'=1}^{N'}\sum_{q'=1}^{Q'} W_{nq}^{(1)} \left(Y_{m',p'q}^{1} + Y_{mn',p'q'}^{V_{11}} \delta_{m'n'} \delta_{p'q'} \right) + \sum_{q'=1}^{Q'} W_{m'q'}^{(2)} Y_{m',p'q'}^{V_{12}} \delta_{p'q'} = F_{m'p'}, \\ \sum_{q'=1}^{Q'} W_{m'q'}^{(1)} Y_{m',p'q'}^{V_{21}} \delta_{p'q'} + \sum_{n=1}^{N}\sum_{q=1}^{Q} V_{nq}^{(2)} Y_{m'n,p'q}^{e} + \sum_{n'=1}^{N'}\sum_{q'=1}^{Q'} W_{n'q'}^{(2)} \left(Y_{m'n',pq}^{e} + Y_{m',p'q'}^{V_{22}} \delta_{m'n'} \delta_{p'q'} \right) = 0, \\ m' = 1,2,...,N', \quad p = 1,2,...,Q'. \end{cases}$$

The coefficients of the derived SLAEs are the intrinsic and mutual internal and external conductances of slots as well as the slots bolume:

$$Y_{mn,pq}^{i(e)} = \mp \int_{S_m^{(1),(2)}} \left[\vec{E}_{mp}^{(1),(2)}, \vec{H}^{i,(e)} \left(\vec{E}_{nq}^{(1),(2)} \right) \right] \vec{n}\, ds, \quad Y_{m'n',p'q'}^{i,(e)} = \mp \int_{S_{m'}^{(1),(2)}} \left[\vec{e}_{m'p'}^{(1),(2)}, \vec{H}^{i,(e)} \left(\vec{e}_{n'q'}^{(1),(2)} \right) \right] \vec{n}\, ds,$$

$$Y_{m'n,p'q}^{i,(e)} = \mp \int_{S_m^{(1),(2)}} \left[\vec{e}_{m'p'}^{(1),(2)}, \vec{H}^{i(e)} \left(\vec{E}_{nq}^{(1),(2)} \right) \right] \vec{n}\, ds,$$

$$Y_{m,pq}^{V_{11},(V_{22}),(V_{12})} = \mp \int_{S_m^{(1),(2),(1)}} \left[\vec{E}_{mp}^{(1),(2),(1)}, \vec{H}^{V} \left(\vec{E}_{mq}^{(1),(2),(2)} \right) \right] \vec{n}\, ds,$$

$$Y_{m',p'q'}^{V_{11},(V_{22}),(V_{12})} = \mp \int\limits_{S_{m'}^{(1),(2),(1)}} \left[\vec{e}_{m'p'}^{(1),(2),(1)}, \vec{H}^{V} \left(\vec{e}_{m'q'}^{(1),(2),(2)} \right) \right] \vec{n}\, ds.$$

Here $F_{mp} = \int\limits_{S_m} \left[\vec{E}_{mp}, \vec{H}^{0} \right] \vec{n}\, ds$, $F_{m'p'} = \int\limits_{S_{m'}} \left[\vec{e}_{m'p'}, \vec{H}^{0} \right] \vec{n}\, ds$ are the partial magnetomotive forces; $\vec{H}^{i,(e),(V)} \left(\vec{E}_{nq}^{(1),(2)} \right)$, $\vec{H}^{i,(e),(V)} \left(\vec{e}_{nq}^{(1),(2)} \right)$ are the magnetic fields in regions "i" (waveguide internal region); "e" (half-space above the slot) and "V" (the slots internal region) being excited by the electric fields $\vec{E}_{nq}^{(1),(2)}$, $\vec{e}_{n'q'}^{(1),(2)}$ on the surfaces of slots; $\vec{H}^{0}$ is the magnetic field of extraneous sources; S_m is the area of the slot surface with number "m"; $\vec{n}$ is the vector of the normal to the surface of the slot oriented directed inside the waveguide; δ_{mn}, δ_{pq} are the Kronecker symbols.

Now consider the case which is typical of practical applications, where the width of slots is by far shorter as compared to their length and the wavelength itself. Here due to the boundary electrodynamics conditions the electric field around them is oriented crosswise and is not dependent upon the transversal coordinate. We may then take the following relation in terms of the intrinsic vector-functions of longitudinal and transverse slots respectively:

$$\vec{E}_{nq}^{(1),(2)} = \frac{\vec{x}^{0}}{D_n} \sin \frac{q\pi}{L_n} \left(z - \left(z_n - \frac{L_n}{2} \right) \right), \quad \vec{e}_{n'q'}^{(1),(2)} = \frac{\vec{z}^{0}}{d_{n'}} \sin \frac{q'\pi}{l_{n'}} \left(x - \left(x_{n'} - \frac{l_{n'}}{2} \right) \right), \quad (2)$$

where $\vec{z}^{0}, \vec{x}^{0}$ are the unit vectors oriented along the x and z axis; $z_n, x_{n'}$ are the corresponding coordinates of the centers of slots numbered as n and n'.

After the electric field in the antenna aperture has been determined according to expression (1) we find the energy and directional characteristics of the multifrequency antenna [3]. The radiation factor of the entire system is equal to:

$$\left| S_{\Sigma} \right|^2 = \left| S_{\Sigma}^{\text{long}} \right|^2 + \left| S_{\Sigma}^{\text{trans}} \right|^2 = \frac{1}{2} \text{Re} \sum_{n=1}^{N} \sum_{p=1}^{Q} \sum_{q=1}^{Q} V_{np}^{(2)} V_{nq}^{*(2)} Y_{nn,pq}^{e} +$$

$$+ \frac{1}{2} \text{Re} \sum_{n'=1}^{N'} \sum_{p'=1}^{Q'} \sum_{q'=1}^{Q'} W_{n'p'}^{(2)} W_{n'q'}^{*(2)} Y_{n'n',p'q'}^{e}.$$

The augends corresponds to the factor of longitudinal slot radiation; the addend is for the same factor of transverse slots. The reflection factor is expressed as

$$\left| S_{11} \right| = -\frac{1}{4} \sum_{n=1}^{N} \sum_{p=1}^{Q} V_{np}^{(1)} F_{np} - \frac{1}{4} \sum_{n'=1}^{N'} \sum_{p'=1}^{Q'} W_{n'p'}^{(1)} F_{n'p'}$$

The pattern of the system in the $x=0$ plane is defined by two mutually perpendicular electric fields components E_x and E_z.

$$F_{E_x}(\theta)=\sum_{n=1}^{N}\sum_{p=1}^{Q}V_{np}^{(2)}\frac{q\pi}{L_n}\frac{1-(-1)^q e^{ikL_n\cos\theta}}{L_n\left(\frac{q\pi}{L_n}\right)^2-(k\cos\theta)^2}e^{jkz_n\cos\theta}\sin\theta,$$

$$F_{E_z}(\theta)=\sum_{n'=1}^{N'}\sum_{q'=1}^{Q'}W_{n'q'}^{(2)}\frac{\sin\left(\frac{kd_{n'}}{2}\cos\theta\right)}{\frac{kd_{n'}}{2}\cos\theta}\frac{l_{n'}}{q'n}\left(1-(-1)^{q'}\right)e^{jkz_{n'}\cos\theta},$$

where angle θ is measured from the z axis.

3. NUMERICAL RESULTS

In order to get a more profound insight into the physical properties of slot interaction each of subarrays, as in the case with the longitudinal slots [2]. We think it wise to present some results of investigation into the radiation characteristics of a single transverse slot cut through in a wall of the waveguide whose dimensions allow propagating higher-order modes.

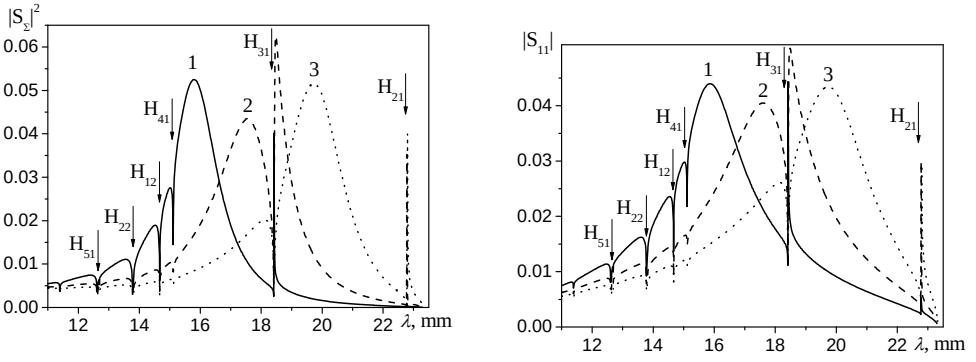

a) b)

FIG. 2: Wavelength-dependent radiation (a) and reflection (b) factors for the H_{30} mode-excited slots of different lengths ($\lambda_{30}^{cr}=23.33$ mm)

Figure 2 presents the calculated curves of radiation $|S_\Sigma|^2$ and field reflection $|S_{11}|$ factors of the H_{30} mode-excited transverse slot over the define wavelength ranges. Curves 1, 2, 3 correspond to the slots of different lengths: 7.5 mm, 8.5 mm, 9.5 mm at $x_1 = a/6$. The waveguide cross-sectional dimensions $a \times b = 35 \times 15$ mm^2, whereas the slot width and waveguide wall thickness are equal to 1 mm. As seen from the graphs in Fig. 2, the values of radiation and reflection factors are much lower against the corresponding values with the slots being excited by the waveguides fundamental mode H_{10}. The most remarkable feature that can be discovered in the graphs in Fig. 2 is that the dependencies $|S_\Sigma|^2 = f(\lambda)$ and $|S_{11}| = f(\lambda)$ have the minimal values of radiation and reflection factors at wavelengths that give rise to higher-order modes. This peculiar feature of $|S_\Sigma|^2 = f(\lambda)$ and $|S_{11}| = f(\lambda)$ has to be taken into account in selecting the electrical lengths of slotted radiators and the operating frequency band of a multielement short-wave antenna.

Figure 3(a) presents the wavelength-dependent radiation and reflection factors; Fig. 3(b) depicts the directivity (D) and gain (G) coefficients (DC, GC) as a function of the wavelength of the two-frequency waveguide slotted array comprising 17 transverse ($l = 8$ mm, $d = 1$ mm, $\Delta z = 16.25$ mm) and 8 longitudinal ($L = 20$ mm, $D = 1$ mm) H_{10} mode-excited slots. The transverse slots are positioned on the waveguide wall ($a \times b = 35 \times 15$ mm^2, $h = 1.5$ mm) just at a point where their excitation set up by the H_{30} mode comes up to a maximum level, whereas the longitudinal slot centers are arranged where the H_{30} mode surface currents transversing a slot are equal to zero (see Fig. 1). As will be apparent from the graphs, the maximum DC ($D = 55.7$) is attained at $\lambda_{30} = 18.33$ mm. In this case $|S_\Sigma|^2 = 0.44$ and $|S_{11}| = 0.06$. Figure 4(a) illustrates the amplitude-related field distribution in the antenna aperture at a given wavelength, and Fig. 4(b) presents the corresponding pattern. The dashed curves indicate the field distribution in the aperture of longitudinal slots. Although these slots are placed at point where the H_{30} mode surface currents are equal to zero, they become excited due to the reciprocal effect. The antenna pattern operating over a long-wave range and excited in the H -vector plane is shown by curve 2 in Fig. 4(b). The spacings between the slotted radiators in the subarrays is chosen so as to guard against the effect of the normal.

Note that for the array under examination, which is excited by the H_{30} mode at $\lambda_{30} = 18.33$ mm, the radiation and directivity factors are equal to $|S_\Sigma|^2 = 0.44$, $D = 55.7$, and with this array being excited by H_{10} mode at $\lambda_{10} = 38$ mm the above coefficients are equal to $|S_\Sigma|^2 = 0.85$, $D = 23$. These factors (DF) and (G) can be increasing by adding to the number of radiators along with a simultaneous change in the geometrical dimensions of slots just as it had been depicted in [2].

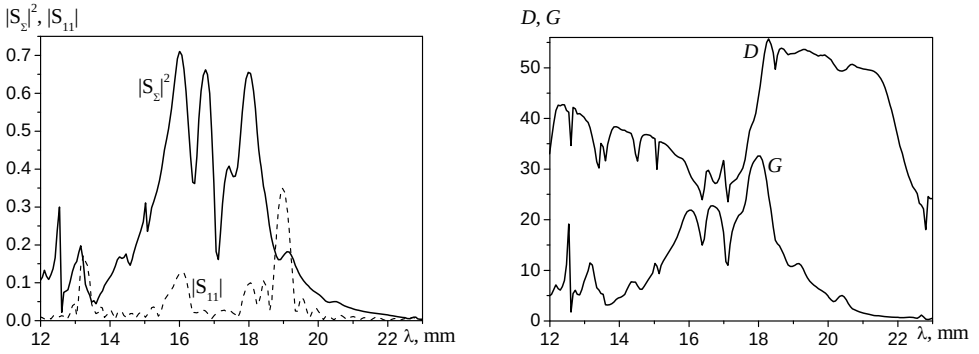

a) b)

FIG. 3: Wavelength-dependent radiation and reflection factors (a), directivity and gain coefficients (b) of the two-frequency H_{30} mode-excited array

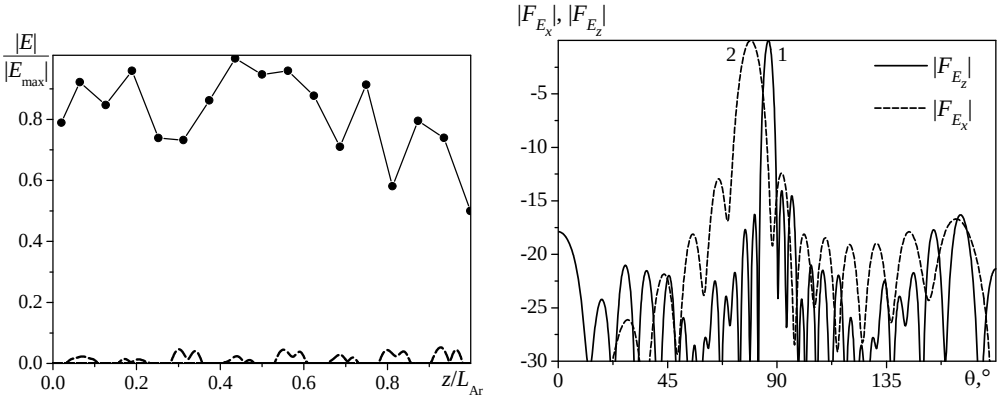

a) b)

FIG. 4: Amplitude-related electric field distribution (a) in the two-frequency H_{30} mode-excited array aperture at $\lambda_{30} = 18.33$ mm and in the AP (b) of the two-frequency array at $\lambda_{30} = 18.33$ mm $\left(F_{E_z}\right)$ and $\lambda_{10} = 38$ mm $\left(F_{E_x}\right)$

The amplitude of the electric fields induced in the longitudinal slots, as the array, is being operated over a short-wave range and, consequently, the contribution of the longitudinal slots to the total radiation power are dependent upon the electrical length of the above slots. This particular case is to be allowed for the process of designing and developing a two-frequency antenna. It is by varying the length of the longitudinal slots and their position that one might succeed in reducing the amplitude of the electrical field induced in the slots with L_n and thereby in diminishing the impact of

the long-wave array on the performance characteristics of the short-wave array. As an illustration of the structure discussed above, Fig. 5 graphically displays the longitudinal slots radiating power related to that of the transverse slots as a function of the longitudinal slots length. The excitation of the array is set up by the H_{30} mode at $\lambda_{30} = 18.33$ mm.

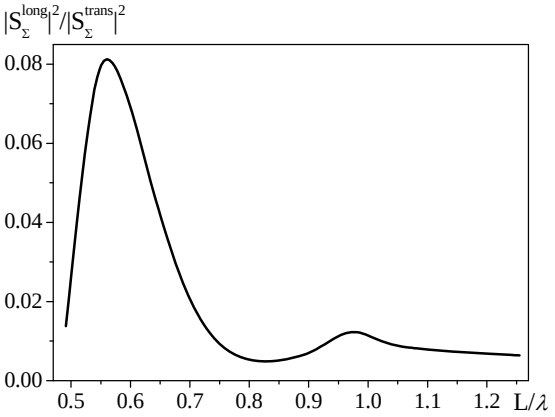

FIG. 5: Radiation power from the longitudinal slot system as a function of electrical length of longitudinal slots (λ_{30} = 18.33mm)

When the entire system is running over the long-wave range at f_{10}, no excitation of the transverse slots occurs $\left(\left|S_\Sigma^{trans}\right| < 0.001\right)$, because their electrical length is considerably shorter than the resonance length and thus produce no effect upon the radiation characteristics of the entire array.

It should be noted that the HF and LF subarray interaction in the system under study appears to be far less pronounced as compared to the processes in the array that analyzed in [2].

4. CONCLUSION

Hence we can state that the Galerkin method has proved to be helpful in finding the solution of the problem on the e.m. wave radiation by the system of longitudinal and transverse slots in a waveguides wide wall. This solution allows one to calculate and optimize the characteristics of two-frequency, multielement slotted multimode waveguide systems with regard to the total reciprocal effect of both types of slots having an arbitrary electrical length both along the internal and the external interaction

space. It is shown that due to the appropriate selection of dimensions and arrangement of slots one can scale down the impact of a long-wave array upon the characteristics of a short-wave array.

REFERENCES

1. Bakhrakha, L.D. and Voskresensky, O.I., (eds). (1989), *Problems of antenna engineering*, Radio and Svyaz, Moscow: 107-141 p. (in Russian).
2. Berdnik, S.L., Katrich, V.A., and Lyashchenko, V.A., (2002), Two frequency slot antennas on multimode waveguides, *Vestnik KhNU. Radiofizika and electronika*. 570:18-21 (in Russian).
3. Feld, Ya.N. and Benson, S.L., (1959), *Antenna-Feed Facilities*, Izd. VVIA, Moscow: 260-360 p. (in Russian).

Telecommunications and Radio Engineering, 69(9):773-784 (2010)

WAVE PROPAGATION AND SCATTERING

SIMULATION OF CENTIMETER WAVE PROPAGATION IN EVAPORATION DUCT OVER THE ROUGH SEA SURFACE *

Yu.V. Levadnyi, V.K. Ivanov, & V.N. Shalyapin

A. Usikov Institute of Radio Physics and Electronics,
National Academy of Sciences of Ukraine
12, Academician Proskura St., Kharkiv 61085, Ukraine

*Address all correspondence to Yu.V. Levadnyi E-mail: yulev@ire.kharkov.ua

In the previous investigations of centimeter wave propagation by the numerical stepwise partition method the scattering from the rough sea surface was taken into account in the tangent plane approximation. Such an approach prevents from taking into account the lighted surface shadowing and deviation of the sea surface height probability distribution from the normal law. The given work is concerned with the methods of registration of these effects and dependences of the attenuation factor on the height and distance in the presence of the evaporation duct. It is shown that shadowing exerts significantly greater impact on the centimeter radio waves propagation in the evaporation duct as compared to registration of the non-gaussianity. The obtained results make it possible to increase the precision prediction of the waves propagation in the lower troposphere.

KEY WORDS: *wave propagation, evaporation duct, parabolic equation, numerical methods*

1. INTRODUCTION

A wide use of various radio engineering systems in the ships and coastal radar stations define the increased attention to the problems of analysis and prediction of the wave propagation over the sea. Specifically, prediction of wave propagation in the evaporation duct, taking account of its random-inhomogeneous structure, is of great interest to increase the operation efficiency of the antennae placed at low heights. The evaporation duct depends upon a high humidity gradient near the sea surface. The main parameters of the duct are its height, i.e., such a height z_0, where derivative

* Originally published in *Radiophysics and Electronics*, Vol. 14, No 1, 2009, pp. 28–34.

$dM(z)/dz\big|_{z=z_0} = 0$ (typical value is 2-30 m), and *M*-deficit, i.e., difference of values of the mentioned refraction index M at the height z_0 and on the surface of the sea (generally up to 10 *M*-units). Such parameters of the duct make it possible to lock-on adequately radio waves in the centimeter-wave band shorter than 10 cm. Nowadays the systems of radio waves propagation prediction based on the numerical solution of the parabolic equation using stepwise method, have received a wide recognition [1]. The given method makes it possible to calculate efficiently the electromagnetic radiation distribution along the route given both height and distance dependence of the refraction index and also take into account nonhomogeneity of the underlying surface properties along the propagation route. But with the increase in the radio frequency the atmosphere refraction index turbulent fluctuations and the sea surface rough state, leading to energy outflow from the duct followed by decrease in its efficiency, exert the increasingly more significant action on the radio waves propagation over the sea [2]. In [3] we have fully considered the problem of taking account of the action of statistically non-uniform fluctuations of the atmosphere refraction coefficient on the radio waves propagation in the evaporation duct. In the present work we will describe the registration methods of the sea disturbance action on the propagation of the microwave frequency radio waves in the evaporation duct and estimate the extent of action on the centimeter waves in the evaporation duct of two additional factors taking into account:

- shadowing of the waves being propagating at narrow slip angles to the surface;
- non-gaussianity of the sea disturbance statistics.

2. REFLECTION FROM THE ROUGH SEA SURFACE

Account of scattering from the rough sea surface in the framework of the parabolic equation approximation for the middle field is realized through introduction of the efficient rough surface reflection coefficient, i.e., such a reflection coefficient wherein the field over the smooth surface will be the same as the field over the rough surface. For the microwave frequency radio waves the efficient reflection coefficient (efficient impedance) from the rough sea surface can be obtained in approximation of the small perturbation method [4,5]. The conditions of the small perturbations method applicability begin to be violated with the decrease in the radiation wave length and the solution is in the framework of tangent plane approximation. As we consider the microwave radio waves propagation within the evaporation duct, then the further analysis should be carried out within the framework of the tangent plane approximation. The efficient reflection coefficient represents the product of Fresnel reflection coefficient and the coefficient incorporating the underlying surface roughness ρ. In the hypothesis, that the probability distribution function of the sea surface altitude is of the Gaussian nature, Isakovich [6] and Ament [7] derived the expression for the coefficient incorporating the underlying surface roughness

$$\rho_A = \exp\left(-\frac{1}{2}\left(2q\sigma_\xi\right)^2\right), \tag{1}$$

where $q = k\sin(\alpha)$; k is wave number of the radio wave; α is slip angle; σ_ξ is root mean square height deviation. Somewhat later it was shown in the investigations, carried out by Beard [8], that the reflection coefficient measured experimentally was greater than the predicted one with regard to the correction by Ament in the field of great values of $2q\sigma_\xi$. Starting from these results Miller, Brown and Vegh [9] (*MBV*) assumed that deviation from the mean level ξ of the sea surface was a random variable

$$\xi = H\sin\left(\frac{2\pi}{\Lambda_s}x\right), \tag{2}$$

where H is Gaussian random variable; Λ_s is characteristic wavelength and x is random value uniformly distributed in the interval $(-\Lambda_s/4,\ \Lambda_s/4)$. Thus, it turns out that random rises of the surface ξ have the probability density distribution of the following form:

$$p(\xi) = \frac{1}{2\pi^{3/2}\sigma_\xi}\exp\left(-\frac{\xi^2}{8\sigma_\xi^2}\right)K_0\left(\frac{\xi^2}{8\sigma_\xi^2}\right), \tag{3}$$

where K_0 is modified first genius zero-order Bessel's function or McDonald function. According to the tangent plane approximation the scattered field intensity is defined using the characteristic function corresponding to the probability distribution function. Thus, this model of the sea surface leads to the following kind of the coefficient incorporating the underlying surface roughness ρ_{MBV}:

$$\rho_{MBV} = \exp\left(-\frac{1}{2}\left(2q\sigma_\xi\right)^2\right)I_0\left(\frac{1}{2}\left(2q\sigma_\xi\right)^2\right). \tag{4}$$

Nowadays the *MBV*-model has received wide acceptance when calculating the multiplier of radio wave attenuation over the sea. Specifically, it is used in the program complexes *AREPS*, *TEMPER* etc. But when comparing the experimental data connected with microwave radio waves propagation over the ruffled surface with the theoretical calculations from a number of works [10,11] it was noted that the calculated signals' levels exceed those observed in the experiment. At the same time [12,13] have pointed to an inconsistency between the sea surface statistics built in the *MBV*-model, the experimental data and non-physical nature of the distribution function (3). Also [14] contains numerical estimate of precision of the solutions

obtained with expressions of *MBV* and Ament. For this purpose the method of moments and the multigrid iterative approximation were used [15]. It was mentioned that *MBV*-model provides a good approximation with Rayleigh roughness parameter value more than, and Ament's approximation – with less than 1.5.

Thus, it was proposed in [11] to take into account the shadowing of one sea surface parts with other ones, this is essential with slip angles of propagation. On the other hand, it was proposed in [16] the methods for registration of the non-Gaussian sea disturbance, which more significantly manifests itself with the increase in wind velocity. In the succeeding sections we will give an estimation of these actions on the microwave radio waves propagation in the evaporation duct.

3. ESTIMATE OF THE SHADOW SEA SURFACE

During propagation of radio waves in the duct the wave reflection from the sea surface takes place at narrow slip angles. In such a situation wave incidence angles are comparable with sea surface slope angle and shadowing of one surface parts with other ones takes place. As a result the tangent plane approximation precision decreases (it is expected that the surface is completely lighted and darkening is absent). The problem of estimation of darkening caused by uneven surface was considered by Bass and Fucs [17] using the theory of overshoot of random functions. Statistical function of illumination was expressed in the form of the infinite series, compact expressions are derived from it under the assumption either small or great darkening. Henceforward, the problems of the darkening estimation were considered in the articles by Wagner [18], Smith [19] and Bourlier [20]. To explain the experimental data obtained in the course of the experiment in the tank Smith et al. [21] attempted to modify the coefficient taking account of surface irregularities (4) in an attempt to estimate darkening. It was noted in [22,23], that the frequency shift effect was observed in the interference picture at the propagation route orientation along the wind direction. To estimate this effect in terms for the coherent component of the field the distance, taking into account the difference between the mean value of the sea surface and the mean value of the illuminated part of the sea surface, was introduced, this has brought in an additional phase shift into the reflection coefficient and made it possible to reproduce the frequency shift in the interference pattern. In this case the mean value of the illuminated part of the sea surface was defined using the method of statistical tests and geometrical optics, this is inconvenient for practical use due to sufficiently great computational expenditures. More theoretically grounded for estimation of darkening was presented in the work of Fabro and Bourlier [11], where the probability distribution function of the illuminated height was introduced for estimation of darkening, this function was written as follows:

$$\hat{p}(\alpha,\xi)=\frac{\int_{-\infty}^{\infty} p_{\gamma}(\gamma)S(\alpha;\xi,\gamma)d\gamma}{\int_{-\infty}^{\infty}\int_{-\infty}^{\infty} p_{\xi,\gamma}(\xi,\gamma)S(\alpha;\xi,\gamma)d\xi d\gamma}\,p_{\xi}(\xi), \tag{5}$$

where p_{γ} and p_{ξ} are densities of probability distribution of slopes and height; $p_{\xi,\gamma}$ is joint density of probability distribution of the surface slopes and heights; $S(\alpha;\xi,\gamma)$ is statistical function of illumination of the surface point with the height h and the slope γ, observed at the slip angle α. In the denominator the double integral corresponds to the normalization condition of the form $\int_{-\infty}^{\infty} p(\alpha;\xi)d\xi=1$. The use of Wagner and Smith formula in the straight direct and for any uncorrelated random process results, as has been shown in [20], in

$$\begin{cases}\hat{p}_W=p_{\xi}(\xi)\dfrac{2\Lambda}{1-\exp(-2\Lambda)}e^{-2\Lambda[1-F(\xi)]},\\ \hat{p}_S=p_{\xi}(\xi)(1+2\Lambda)[F(\xi)]^{2\Lambda},\end{cases} \tag{6}$$

where

$$F(\xi')=\int_{-\infty}^{\xi'} p_{\xi}(\xi)d\xi; \tag{7}$$

$$\Lambda(\alpha,\sigma_s)=\frac{1}{\tan\alpha}\int_{\mathrm{tg}\alpha}^{\infty}(\gamma-\tan\alpha)p_{\gamma}(\gamma)d\gamma. \tag{8}$$

Brining forward the Gaussian statistics of the sea surface heights and slopes we obtain

$$\begin{cases}\Lambda(\alpha,\sigma_s)=\Lambda(v)=\dfrac{\exp(-v^2)-v\sqrt{\pi}\,\mathrm{erfc}(v)}{2v\sqrt{\pi}},\\ v=\dfrac{\tan(\alpha)}{\sqrt{2}\sigma_{\gamma}},F(\xi)=1-\dfrac{1}{2}\mathrm{erfc}\left(\dfrac{\xi}{\sqrt{2}\sigma_{\xi}}\right).\end{cases} \tag{9}$$

Then taking into account (6) and (9) the coefficient including the action of the surface imperfection assumes the following form:

$$\rho_{sh}(\alpha)=\int\limits_{-\infty}^{\infty} e^{-j2q\xi}\,p_s(\alpha;\xi)=\frac{1+2\Lambda}{\sqrt{\pi}}\int\limits_{-\infty}^{\infty} e^{-j2q\sqrt{2}\sigma_\xi h-h^2}\,w(h)dh. \qquad (10)$$

In this case the integral in (10) should be calculated numerically. The analysis of the density distribution (6) has shown that it can be approximated with the Gaussian function

$$\hat{p}(h;\alpha)\cong\frac{1}{\hat{\sigma}_h\sqrt{2\pi}}\exp\left[-\frac{(h-\hat{m}_h)^2}{2\hat{\sigma}_h^2}\right] \qquad (11)$$

where the mean height and dispersion of the illuminated height for the Smith expressions assumes the form

$$\begin{cases}\hat{m}_h(v)=\dfrac{1+2\Lambda}{\sqrt{\pi}}\displaystyle\int\limits_{-\infty}^{\infty} he^{-h^2}w(h)dh,\\ \hat{\sigma}_h^2(v)=\dfrac{1+2\Lambda}{\sqrt{\pi}}\displaystyle\int\limits_{-\infty}^{\infty}(h-\hat{m}_h)^2e^{-h^2}w(h)dh,\end{cases} \qquad (12)$$

where $h=\xi\Big/\left(\sqrt{2}\sigma_\xi\right)$ – normalized height; $w(h)=\left[1-\mathrm{erfc}(h)/2\right]^{2\Lambda}$.

Hence we have the following coefficient taking into account the action of the surface imperfection with regard to darkening:

$$\rho_{sh}(\alpha)=\exp\left(-\frac{1}{2}\left(2q\hat{\sigma}_\xi\right)^2\right)e^{-jQ\hat{m}_\xi}, \qquad (13)$$

where $\hat{m}_\xi=\sigma_\xi\sqrt{2}\hat{m}_h$; $\hat{\sigma}_\xi=\sigma_\xi\sqrt{2}\hat{\sigma}_h$.

The obtained coefficient (13) with regard to darkening differs from the coefficient (1) by the availability of the phase multiplier including variation of the optical distance at the cost of variation of the sea surface mean height taking into account darkening and the use of dispersion of the illuminated height.

Method of statistical tests (Monte-Carlo) was used in [13] to check the precision of the solution received according to the above methods of the darkening record (13). As the comparison to the standard solution has shown the above method of the darkening account increases the precision of defining the minima positions of the interferential pattern as compared to the approximation of the tangent plane. But there is a variation from the standard solution obtained using the statistical tests method in the value of the signals levels in minima and maxima, it is the authors' opinion that this is caused by ignoring the diffraction effects when calculating the boundary conditions. Also it should be noted that the algorithm for account of the darkening is unstable at high wind velocities resulting in great irregularities and at high frequencies of radiation.

4. ACCOUNT OF NON-GAUSSIAN STATISTICS OF THE SEA SURFACE

As it was noted above, the *MBV* model (2) assumes that sea surface represents the sine curve with normally distributed amplitude and uniformly distributed phase. Then the density of the height probability distribution appears as (3). But from the experimental data which were obtained in the course of the *Rough Evaporation Duct* (*RED*) experiment [12,24] on the floating platform near the cost of Hawaiian Island, density of the sea surface height probability distribution has the form close to the Gaussian [16]. Also were analyzed densities of probability distributions of the sea waves' amplitudes and phases which differed from those incorporated into *MBV*-model. The Gaussian density of the height probability distribution also results from the central limiting theorem of the probability theory on the assumption that the sea surface is the sum of the Fourier harmonics compounds with a random phase. Hence, inconsistency of the sea surface statistics incorporated into the model can involve reevaluation of the signal value in the reception point and, respectively, the *MBV*-model incorrectness. An explanation for distinction between the Berd experimental data and the Ament reflection coefficient can be the fact that due to nonlinear interaction of the sea waves the statistics differs from the Gaussian form.

Let us consider one of the possible ways of assessment of the non-Gaussian statistics of the sea surface [12]. In accordance with tangent plane approximation the intensity of the coherent scattered field is expressed through the rough surface characteristic function

$$\Phi(q) = \int_{-\infty}^{\infty} e^{jq\xi} p(\xi) d\xi. \tag{14}$$

Expanding the exponent into series we obtain representation of $\Phi(q)$ in the following form

$$\Phi(q) = 1 + \sum_{n=1}^{\infty} \frac{\mu_n}{n!} (jq)^n, \tag{15}$$

where the expansion coefficients μ_n are moments of the random value ξ

$$\mu_n = \left\langle \xi^n \right\rangle = j^{-n} \Phi^{(n)}(0). \tag{16}$$

If ξ is Gaussian random value, then all its central moments are defined through the standard deviation σ_ξ

$$\mu_{2n} = \frac{(2n)!}{2^n n!} \sigma^{2n}, \qquad \mu_{2n+1} = 0. \tag{17}$$

The exponential power (15) expresses the characteristic function through the moments, which can be defined experimentally. But such an approach is of limited utility due to slow convergence of the exponential series. More fast convergence can be obtained for the class of random functions with the density of probability distribution close to the Gaussian one.

Let us consider the generating function of seven invariants $K(q)$ of the random surface ξ

$$K(q) \equiv \ln \Phi(q) = \sum_{n=1}^{\infty} \frac{\kappa_n}{n!} (jq)^n, \tag{18}$$

where κ_n are cumulants.

$$K^{(n)} = \kappa_n = i^{-n} \frac{d^n}{dq^n} \ln \Phi(q) \mid_{q=0}. \tag{19}$$

Provided that $\mu = \langle \xi \rangle = 0,$ we obtain

$$\begin{aligned} &\kappa_0 = 0, \kappa_1 = 0, \\ &\kappa_2 = \mu_2 = \sigma_\xi^2, \kappa_3 = \mu_3, \\ &\kappa_4 = \mu_4 - 3\mu_2^2, \kappa_5 = \mu_5 - 10\mu_2\mu_3 ... \end{aligned} \tag{20}$$

For the Gaussian random value the cumulants $\kappa_n \equiv 0$ with $n > 2$. Then we obtain the reflection coefficient for the tangent plane approximation

$$\begin{aligned} R = Se^{K(2q)} = S \exp\left[-2q^2\sigma_\xi^2\right] \exp\left[(4/3)\left(jq\sigma_\xi\right)^3 \left(\mu_3\sigma_\xi^3\right)\right] \times \\ \times \exp\left[(2/3)\left(q\sigma_\xi\right)^4 \left(\mu_4\sigma_\xi^4\right)\right] ..., \end{aligned} \tag{21}$$

where S is the Fresnel reflection coefficient. The first multiplier $\exp\left[-2q^2\sigma_\xi^2\right]$ describes reflection from the purely Gaussian surface. Nonlinear wave interactions can introduce asymmetry in the density of the high surface probability distribution. Such an asymmetry acts only on the scattered field phase and terms in (21) corresponding to odd cumulants do not act on the field intensity. But the value of the phase essentially acts on the state of minima and maxima of the interferential pattern. The terms corresponding to the even cumulants have an impact on the signal intensity. With small values of $(\sigma_\xi q)$ an impact of deviation from Gaussian on the signal intensity turned out to be small, but if the propagation takes place inside the duct under condition of multiple rereflection then the total effect, in authors' of the methods opinion [16], may be found sufficiently strong.

5. CONCLUSIONS

Results of the numerical computation of the propagation factor in the condition of the radio wave propagation over the sea surface are presented in Figs. 1-3. The propagation factor shows how many decibels change the field when propagating in the duct as compared with propagation in free space. All calculations are carried out using the stepwise partition method, its description was detailed in [1]. Parameters of calculation, such as distance between phase screens and step of the height quantization, were chosen on the basis of the methods, cited in the same source. For the frequency of 7GHz they were equal to 100 and 0.3 m, respectively. Along with the standard *MBV* model (solid line in Figs. 1-3) we present dependences obtained according to the above methods taking into account the darkening (12), (13) (dashed line in Figs. 1-3) and non Gaussian nature of the sea surface statistics (21) (dot-and dash line in Figs. 1-3). Figures 1 and 2 show the height and distance dependence of the attenuation multiplier in the evaporation duct 15 m height at the horizontally polarized transmitting antenna height equal to 7 m and 7 GHz radio frequency radiation. Wind velocity is equal to 7 m/s. The height dependences are given for two receiver ranges: 10 and 100 km. The range dependences are given for the receiver located at the heights of 10 and 30 m. Figure 3 shows the radio waves frequency lowering to 5GHz, the parameters of the duct and transmitting antenna are the same as in the previous preceding Figures, the receiver is located at the height of 10 m and wind velocity corresponds to 7 and 5 m/s.

Vertical profile of the normalized refraction index was of the logarithmic form and was calculated by the formula [1]

$$M(z) = M(0) + 0.125\left(z - z_{ED}\ln\left(z/z_0\right)\right), \tag{22}$$

where $M(z)$ is value of the normalized refraction index at the height of z; $M(0) = 330$ *M*-un.; z_{ED} is the height of the evaporation duct; $z_0 = 1.5 \cdot 10^{-4}$ m is roughness parameter.

The value of the parameters of asymmetry and excess for simulation of the sea surface deviation from the Gaussian corresponds to the maxima in distribution of these parameters from the data of *RED*-experiment and those given in the work of Hristov [16].

Analysis of the height dependence shows variation in the minima position in the interferential pattern for the case of accounting of darkening and for the case of non Gaussian account. But account for darkening makes an even greater impact and results in the extremum position displacement of the interferential pattern by 2-3 m, while the non-Gaussian results in variations no more than for 1 m.

Such variation provides at a sacrifice of shadow and it is observed also in the experimental data, in particular, in [21]. Variation in the interferential pattern minima depth also draws attention. Explanation of these effects is the fact that with the darkening of one part of the surface by other ones the reflection takes place mainly from the planes elevated relative to the sea surface average height at the cost of greater

illumination of higher parts. Variation of the minima depth in the interferential pattern takes place at the cost of decrease in "illumination" of the sea surface part, this corresponds to lesser dispersion of the illuminated height relative to the case of the complete illuminated surface.

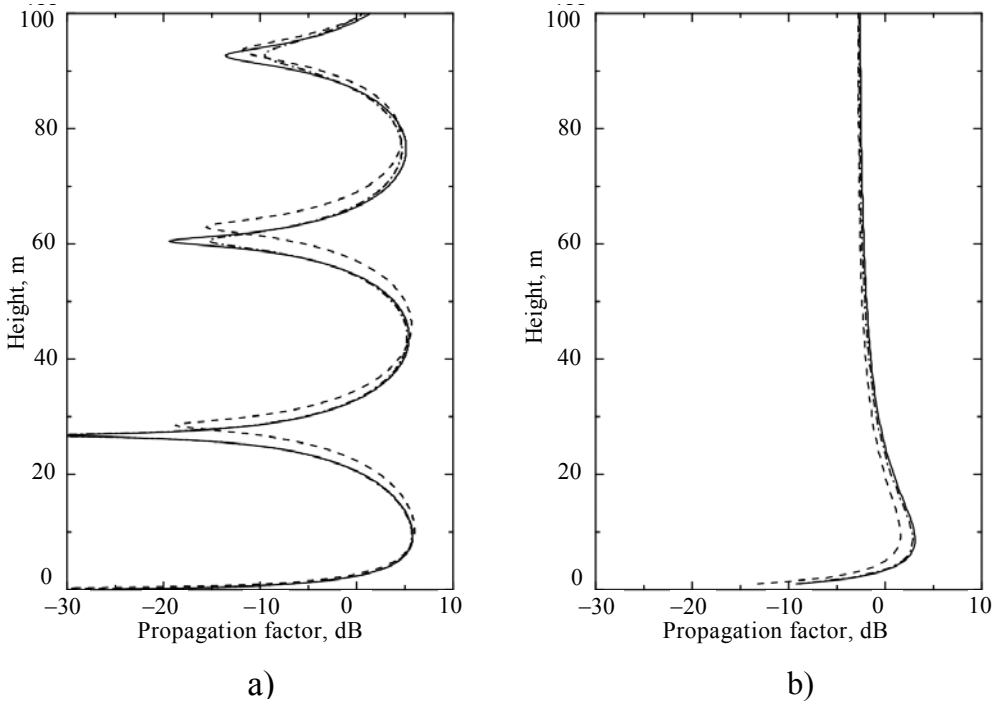

FIG. 1: Height dependence of the propagation factor at a range of: a) – 10 km; b) – 100 km

Figures 1 and 2 show that greater attenuation of the signal inside the duct taking into account darkening and non-Gaussian is observed as moving away from the transmitter. The value of the additional attenuation per unit length constitutes less than 0.1 dB/km taking into account non-Gaussian and of the order of 0.2-0.3 dB taking into account the darkening. Comparison of Figs. 2 and 3 demonstrates that the effects, stipulated by the darkening and non Gaussian, influence greater with the increase in frequency. The influence of these effects increases with the increase in the wind velocity (Fig. 3), this also results from the general physical considerations.

On the basis of the obtained dependence of the attenuation multiplier on the distance and height it may be concluded that with the waveguide propagation the darkening effects should be primarily taken into account as at least in the considered situations they have more essential effect on the propagation of centimeter radio waves than non-Gaussian. Taking into account of these effects results in lowering the signal level in the evaporation duct, this reduces the tendency to overestimation of the

theoretically calculated signal levels in the evaporation duct as compared to the experimental data [10].

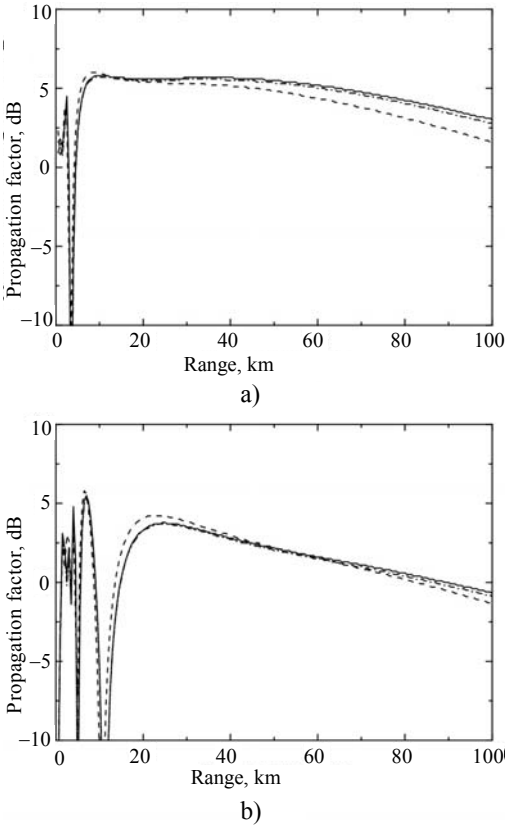

FIG. 2: Distance dependence of propagation factor at the height of: a) – 10 m; b) – 30 m

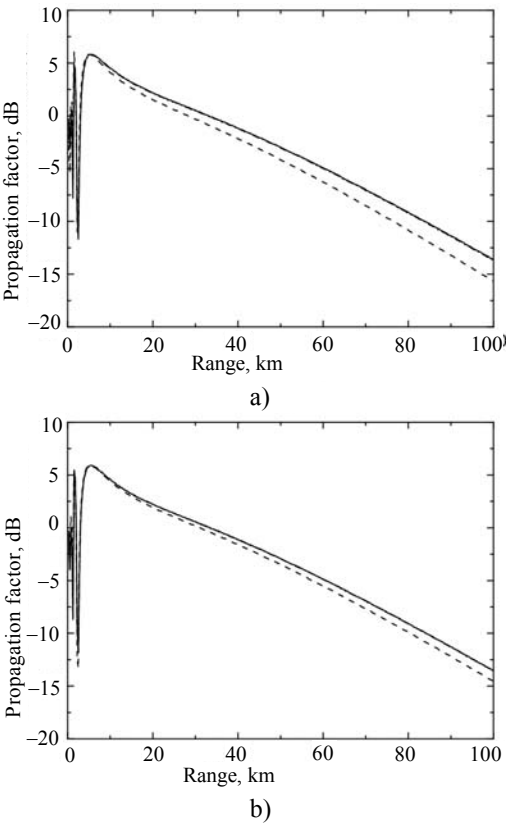

FIG. 3: Distance dependence of the propagation factor for the wind velocity: a) – 7 m/s; b) – 5 m/sc

It should be noted that more rigorous methods of defining the asymmetry and excess parameters against the wind velocity are needed for sufficiently effective taking accounting of non-Gaussian. The shortage of the darkening accounting algorithm is instability which appears with relatively great sea disturbance or with the frequency increase, i.e., with the phase shift in the reflection coefficient. The mentioned shortage should be removed with development more perfect methods of darkening accounting.

REFERENCES

1. Levy, M., (2000), *Parabolic Equation Methods for Electromagnetic Wave Propagation*. London, U.K.: The Institution of Electrical Engineers, – 338 p.

2. Kukushkin, A.V., Freylikher, V.D., and Fuks, I.M., (1987), *Izv. VUZov. Radiofizika*. **30**(7):811-823 (in Russian).
3. Ivanov, V.K., Shalyapin, V.N., and Levadnyi, Yu.V., (2009), Scattering short waves by tropospheric fluctuations in the evaporation duct, *Izv. VUZov. Radiofizika.* (in Russian).
4. Barrick, D.E., (1971), Theory of HF and VHF propagation across the rough sea. Part 1. The effective surface impedance for a slighty rough highly conducting medium at grazing incidence, *Radio Sci*. **6**(5):517-526.
5. Barrick, D.E., (1971), Theory of HF and VHF propagation across the rough sea. Part 2. Application to HF and VHF propagation above sea, *Radio Sci*. **6**(5):527-533.
6. Isakovich, M.A., (1952), *ZhETF*. **23**(3):305-314 (in Russian).
7. Ament, W.S., (1953), Toward a theory of reflection by rough surface, *Proc. IRE*. **41**(1):142-146.
8. Beard, C.I., (1961), Coherent and incoherent scattering of microwaves from the ocean, *IRE Trans. Antennas and Propag*. **9**(5):470-475.
9. Miller, A.R., Brown, R.M., and Vegh, E., (1983), A new derivation for the rough surface reflection coefficient and for the distribution of sea wave elevations, *NRL Report 8744*, Washington, D.C, 4 p.
10. Hitney, H., (1999), Evaporation duct propagation and near-grazing angle scattering from a rough sea, *IGARSS Proc*. 5:2631-2633.
11. Fabro, V., Borlier, C., and Comdes, P.C., (2005), Forward propagation modeling above Gaussian rough surfaces by the parabolic wave equation: introduction of shadowing effect, *Progress in Electromagnetic Research*. 58:243-269.
12. Hristov, T.S. and Friehe, C.A., (2003), EM propagation over the ocean: Analysis of RED experiment data, *12th Conf. Interactions of the Sea and Atmosphere*. P. 1-4.
13. Barrick, D.E., (1998), Grazing behavior of scatter and propagation above any rough surface, *IEEE Trans. on Antennas and Propag*. **46**(1):73-83.
14. Freund, D.E., Woods, N.E., Ku, H.-C., and Awadallah, R.S., (2006), Forward radar propagation over rough sea surface: A numerical assessment of the Miller-Brown approximation using a horizontally polarized 3-GHz line source, *IEEE Trans. on Antennas and Propag*. **54**(4):1292-1304.
15. Donohue, D.J., Ku, H.-C., and Thompson, D.R., (1998), Application of iterative moment-method solutions to ocean surface radar scattering, *IEEE Trans. on Antennas and Propag*. **46**(1):121-132.
16. Hristov, T.S., Anderson, K.D., and Friehe, C.A., (2008), Scattering properties of the ocean surface: The Miller-Brown-Vegh model revisited, *IEEE Trans. on Antennas and Propag*. **52**(4):1103-1109.
17. Bass, F.G. and Fuks, I.M., (1972), *Wave scattering by statistically rough surface*, Nauka, Moscow: 424 p. (in Russian).
18. Wagner, R.J., (1966), Shadowing of randomly rough surfaces, *J. Acoust. Soc Am*. **41**(1):138-147.
19. Smith, B.G., (1967), Geometrical shadowing of a random rough surface, *IEEE Trans. Ant. and Prop*. **13**(5):384-388.
20. Bourlier, C., Bergnic, G., and Saillard, J., (2002), Monostatic and bistatic statistical shadowing functions from one-dimensional stationary random rough surface according to the observation length. Part I. Single scattering, *Waves in Random Media*. **12**(2):145-174.
21. Smith, J.R., Russell, S.J., Brown, B.E. et al., (2004), Electromagnetic forward scattering measurements over a known, controlled sea surface at grazing, *IEEE Trans. Geosci. Remote Sensing*. **42**(6):1197-1207.
22. Smith, J.R. and Mirotznik, M.S., (2004), Rough Surface Scattering Models, *IGARSS Proc. IEEE International*. 5:3107-3110.
23. Smith, J.R. and Mirotznik, M.S., (2005), High Frequency Forward Scattering Models with Shadowing Correction, *Antennas and Propagation Society International Symposium Proc*. **4A**:64-67.
24. Anderson, K.D. and Paulus, R.A., (2000), Rough Evaporation Duct (RED) Experiment, *Proc. of the Battlespace Atmospherics and Cloud Impact on Military Operations*, Fort Collins, Colorado. P. 1-11.

Telecommunications and Radio Engineering, 69(9):785-797 (2010)

MODELING OF ELEVATION ANGLES MEASUREMENT OF LOW-FLYING TARGETS BY MULTIFREQUENCY MONOPULSE RADAR*

Yu. A. Pedenko

A. Usikov Institute of Radio Physics and Electronics,
National Academy of Sciences of Ukraine
12, Academician Proskura St., Kharkiv 61085, Ukraine

*Address all correspondence to Yu. A. Pedenko E-mail: pedenko@ire.kharkov.ua

The statistical computer simulation of measuring elevation angles of low-level targets has been carried out by means of three-frequency monopulse radar above the rough sea under multipath conditions. It is shown that the use of three-frequency monopulse radar substantially decreases errors of elevation angles measurement in comparison with single-frequency version. The use of three-frequency monopulse radar also reduces the possibility of tracking loss. The dependence of these characteristics on frequency spacing has been investigated.

KEY WORDS: *monopulse radar, multifrequency radar, the low-flying target, multipath propagation, angle of elevation, computer simulation technique*

1. INTRODUCTION

It is common knowledge that the radar tracking of low-flying targets takes place under conditions of mulipath propagation associated with radio waves reflection from the dry land or sea surface. Mulipath signals arriving to the radar receiving device input simultaneously with the useful direct signal from the target introduce errors into the measurements of the target coordinates, in particular, angle of elevation, and serve to the autotracking loss [1,2].

In the case of the mirror nature of radar signals reflection from a smooth surface the value and sign of the radar receiver angle discriminator error depend on the interference phase of the direct and mirror reflected signals.

It is also known that under conditions of the diffusion reflection the loss of correlation between the received signals is observed as the difference of the used frequencies increases.

* Originally published in *Radiophysics and Electronics*, Vol. 14, No 1, 2009, pp. 35–42.

It can be assumed that these factors may reduce the elevation angle measurement errors at simultaneous operation of the radar on several frequencies. Taking into account the results obtained in [3] where, in particular, the target tracking loss conditions over the disturbed sea surface in the monopulse radar operation were studied, one may expect that the use of the multifrequency operation will make it possible to reduce the target tracking loss probability.

Currently due to perfection of powerful microwave amplifiers intended for operation in the radar transmitters' output stages, the possibility of the radar simultaneous operation on several frequencies in band up to 20 % and more from the central operating frequency emerged (see, for example [4]). This makes it possible to realize multifrequency measurements of the angle of elevation of target in actual practice. The objective of the present work is to estimate the expected results of the multifrequency operation use through the computer simulation with the technique of simulation of the field over the rough sea surface developed and approved by us [5].

2. INVESTIGATIONS PROCEDURE

Investigations were carried out using the computer numerical simulation performed in three steps. Complex structures of the field in the vertical uniform linear antenna array aperture were calculated in the first step. The fields were created using the target simulator presenting a point isotropic multifrequency radiation source. The procedure described in [5] was used for calculations. As a result a sufficiently great number of the signals field realizations, needed to ensure reliability of inferences about the elevation angle measurement errors, was obtained for each set of geometrical parameters of the track and interface surface roughness.

According to the procedure from [5], the composite signal on each element of the receiving antenna array is formed by summation of the signal from the target, its direct and diffuse reflections. These latter are represented by the discrete signals arriving from the adjacent elemental areas. These areas are located within a "sparkling" surface representing a narrow path extended along the track. The phase center of each of the elemental areas is located randomly within its lengthwise dimension, amplitude of the signal reflected from it is distributed according to the Rayleigh law and phase – uniformly on the interval $0 \ldots 2\pi$. When calculating the distance dependence of the diffusion component the value of the surface scattering bistatic profile was taken constant by distance according to conclusions from [5].

A number of assumptions was used when calculating the field of signals. Hence the phase of reflection, amplitude and location of the phase centers of the areas along the distance, relating to the current realization of the field, were assumed to be the same on all operating frequencies. This was due to the fact that in the frameworks of the used model of the field [5] these values have no direct functional dependence on the signal frequency. Actually, the above-listed values dependence on the operating frequency exists in reality in consequence of the fact that the reflection from each of the areas is a superposition of reflections from the elemental reflectors placed within

the area limits. A consequence of the mentioned assumptions is the fact that the degree of the signals decorrelation on the antenna array at simulation will be less than in actual practice. In this connection the improvements in mulifrequency radar efficiency as compared to the monofrequency radar efficiency by the simulation should be considered as the first limits of such improvement.

As the result of the first stage execution the database was created containing realizations of complex signals on the vertical antenna array $\dot{A}_{kn}$ ($k = 1, 2, \ldots K$ – the serial number of the radar operating frequency; K – amount of the operating frequencies; $n = 1, 2, \ldots N$ – the number of the array element beginning with the lowermost one; N – amount of the array elements). Sufficiently large number of realizations of $\dot{A}_{kn}$, distinct from each other only by a set of random diffusion reflections was calculated for every specified situation defined with the radar height, distance, target elevation angle and the sea disturbance degree.

Amount of realizations for each combination of the track parameters constituted 10000 for each operating frequencies. Amount of the operating frequencies K was chosen small, equal to three, and separation between their extremes was – 0, 4, 8, 12 and 16 % from the center frequency so that they can be easily realized in practice.

At the second stage the elevation angle measurement was simulated using the monopulse method in the autotracking mode. The sum or difference signal were calculated as

$$\dot{U}_{\Sigma(\Delta)k} = \sum_{n=1}^{N} \dot{A}_{kn} \dot{G}_{\Sigma(\Delta)n} \exp\left[j\chi_{kn} \sin\Theta_{\text{PCH}} \right], \tag{1}$$

where $\chi_{kn} = \dfrac{\pi d}{\lambda_k}\left(2n - N - 1\right)$ is phase shift of the n-th element of the array relative to its center; d is antenna array pitch; Θ_{PCH} is elevation angle of the equal signal direction (ESD) of the receiving antenna array, and $\dot{G}_{\Sigma(\Delta)n}$ is aperture function value relating to the n-th element of the array.

The form of the aperture function specifies the parameters of the sum and difference diagrams. In our case they are defined as follows:

$$\begin{aligned} \dot{G}_{\Sigma n} &= \dot{G}_{pn} \cos\left(\chi_n \sin\Delta\Theta\right), \\ \dot{G}_{\Delta n} &= j\dot{G}_{pn} \sin\left(\chi_n \sin\Delta\Theta\right), \end{aligned} \tag{2}$$

where $\dot{G}_{pn}$ is the value of the aperture function of the partial radiation pattern relating to the n-th element of the array, and $\Delta\Theta$ is deviation of the partial radiation pattern in the vertical direction from ESD.

It should be noted that expressions (2) describe the sum and difference diagrams obtained through adding and subtraction of the symmetric partial diagrams with angle diversity being formed, for example, with the mirror antenna equipped with a two-horn radiator. The aperture function of the partial diagram in our case was specified in the form of the cosine pedestal amplitude distribution

$$\dot{G}_{pn} = G_0 + (1 - G_0)\cos\frac{\pi(2n - N - 1)}{2n}, \quad (3)$$

where G_0 is the level of the array-formed aperture edge radiation relative to the maximum. To eliminate additional main lobes of the synthesized radiation patterns the direction between the antenna array elements was chosen to be equal to $\lambda_0 / 2$, where λ_0 is wave length on the central frequency. With the separation between the partial diagrams axes equal to $2\Delta\Theta = \lambda_0 / Nd$ and quantity of the antenna array elements $N = 156$ the vertical antenna array dimension formed 2.5 m. In this case the total radiation pattern width by the level of the half power $\Theta_{0.5}$ with $G_0 = 0.2$ was equal to 17.5 mrad ($\approx 1°$), and the level of the first side lobe of the total radiation pattern amounted to –31.2 dB.

The error signal of measuring the elevation angle was formed as the mean value of the real part of relation of the difference signal to the sum signal received at all wave lengths

$$\delta = \frac{1}{K}\sum_{k=1}^{K} \mathrm{Re}\left(\dot{U}_{\Delta k} / \dot{U}_{\Sigma k}\right). \quad (4)$$

For every realization of the field the elevation angle measurement was performed independently of the previous measurements and was carried out in the following way: equisignal antenna axis of the radar was set at the elevation angle of $0.5\Theta_{0.5}$ relative to the horizon, then according to the angle error sign the axis motion was simulated till this sign alternation. The equisignal axis elevation angle, with which the error signal turned into zero, was taken as the measured target elevation angle.

As it is impossible to cover the whole diversity of the initial conditions in one paper the typical initial conditions taking place in the real situation were chosen. They are listed in Tables 1 and 2, where D is the distance between the radiation source and the radar antenna; h_r is the height of the radar antenna center over the sea surface; $\beta_{\max}$ is the maximum inclination of the sea surface roughness with the uniform distribution of the inclinations, and $\varepsilon_{\text{real}}$ is the radiation source angular height over the interface.

TABLE 1: Track parameters

D, km	h_r, m	β_{max}, rad	$\varepsilon_{real}/\Theta_{0.5}$
2	12	0.05	0.2–0.5

TABLE 2: Roughness parameters (q) and diffuse (ρ_d) and direct (ρ_s) reflection factors corresponding to them

q	ρ_d/ρ_s
0.031	0.10/0.93
0.052	0.20/0.81
0.074	0.30/0.65
0.093	0.36/0.50

Roughness parameters listed in Table 2 were calculated as

$$q = \sigma_h \sin(\psi_s / \lambda_0), \quad (5)$$

where σ_h is the mean square height of roughness (sea waves), and ψ_s is the radio wave slip angle at the direct reflection point. The wave length λ_0 was chose to be equal to 3.2 cm.

The study of errors was carried out in the phase difference range between the direct and reflected signals in the center of the antenna array $\Delta\varphi_0 = 0, 20, 40 \ldots 180°$, relating to the central operating frequency. When simulating, with the rest invariable parameters the specified values of phase differences were set through artificial variation of the mirror signal reflection phase from the interface (in reality the reflection phase with the slip angles of radio waves propagation is close to 180°). The require result could be reached using other means, for example, at the cost of variation of the radar antenna height or the operation frequencies. But the chosen way enhanced the simplification of the simulation process and interpretation of the obtained results. Furthermore, it should be thought that the statistics of errors related to some phase difference $\Delta\varphi_0$, will take place even with the phase difference $\pm\Delta\varphi_0 + 2\pi n$, where n – an integer with on retention of the rest parameters values.

The statistical processing of the obtained data was carried out at the third stage. Here the mean values of the elevation angle measurement errors and mean square deviation of the elevation angle measurement errors were measured depending on the phase difference between the direct and mirror reflected signal for each of the radar operating frequencies separations. There were obtained the mean square measurement errors (averaged by the phase difference range $0 \ldots 2\pi$) as a function of frequency separation value as well as the laws of the target elevation angle measurement error distribution.

3. THE MEAN VALUES OF ELEVATION ANGLE MEASUREMENT ERROR

Let us consider dependences of the elevation angle measurement mean errors $\langle \Delta\varepsilon \rangle$ on the phase difference $\pm\Delta\varphi_0$ between the direct and mirror-reflected signal on the central frequency. Let us lead the discussion using some of the obtained plots presented in Figs. 1(a)-4(a) as illustrations.

The first singularity of the considered dependences consists in that with the increase in the frequencies separation the significant decrease, up to several times as large, of the mean errors absolute values, particularly in the field extremes. In the field minimum this decrease is clearly defined through the whole range of the studied angles, and in the field maximum – with the angular height more than $0.3\Theta_{0.5}$.

The second singularity consists in that with the frequency separation increase the monotone dependence is disrupted of the mean errors variation peculiar to the single

frequency version of the radar operation, for which variation of the mean errors from the negative values in the field maximum to the positive ones in the field minimum is typical. Moreover, with some sufficiently great frequency separations the mean error in the field extremes can change the sigh to the opposite one as compared to the single frequency version. This takes place due to the side frequency signals, where the interference phase changes to the opposite one relative to the central frequency.

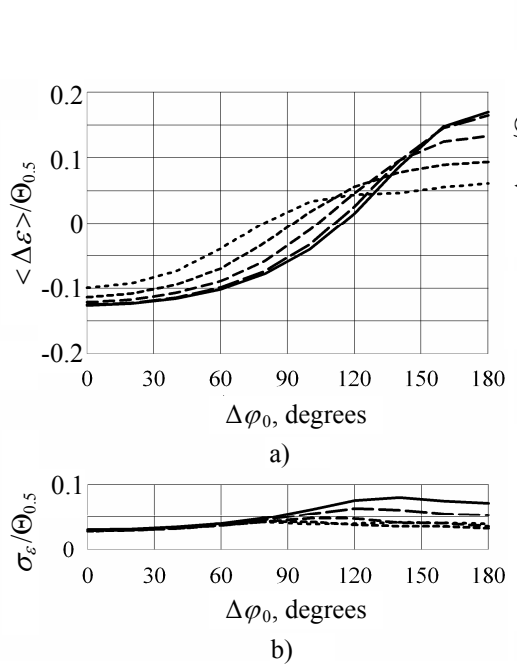

FIG. 1: Mean errors (a) and mean square deviations of errors (b) with $\varepsilon_{\text{real}} = 0.2\Theta_{0.5}$; $\rho_d = 0.36$; $\rho_s = 0.50$: $2\Delta f / f_0 =$ 0 % – ——; 4 % – — —; 8 % – – – –; 12 % – - - - -; 16 % – · · · · · ·

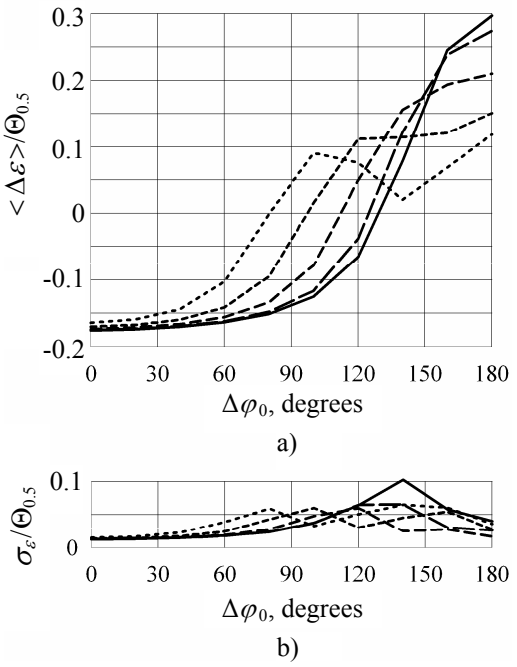

FIG. 2: Mean errors (a) and mean square errors deviations (b) with $\varepsilon_{\text{real}} = 0.2\Theta_{0.5}$; $\rho_d = 0.20$; $\rho_s = 0.81$; the curves notations as on Fig. 1

For each combination of the track geometrical parameters one can choose such frequency separation for which the mean errors curve will be arranged near zero values throughout the range of phase differences $\pm\Delta\varphi_0$. As the analysis of the obtained data has shown the least mean errors at operation on three frequencies are realized if the distinction of phase differences between the direct and reflected signals on the neighbor frequencies is equal about $2\pi/3$. Separation of neighbor frequencies should meet the condition

$$\Delta f \approx \frac{Dc}{6h_r h_t}, \tag{6}$$

valid with $h_r, h_t << D << a_e$, where h_r, h_t are, respectively, radar antenna and target heights; D is distance between the radar and target; c is light speed; a_e is equivalent radius of the Earth. Specifically, the data presented on Figs. 3 and 4 obtained with the elevation angle $0.4\Theta_{0.5}$ and separation $2\Delta f / f_0 = 12$ %, practically correspond to condition (6) which gives the value 12.6 % for the given geometry of the track.

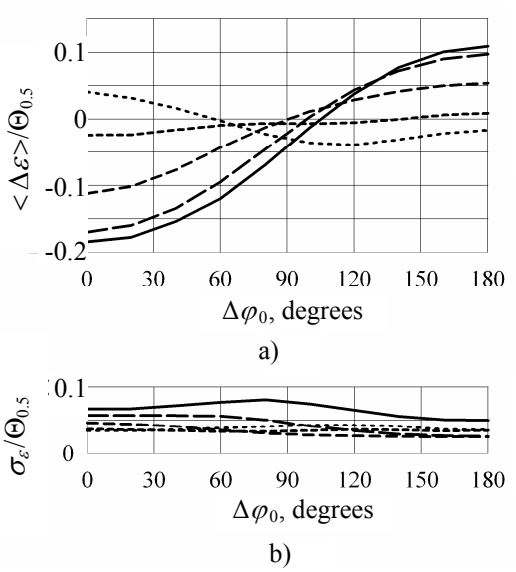

FIG. 3: Mean errors (a) and mean square errors deviations (b) with $\varepsilon_{real} = 0.4\Theta_{0.5}$; $\rho_d = 0.36$; $\rho_s = 0.50$; the curves notations as on Fig. 1

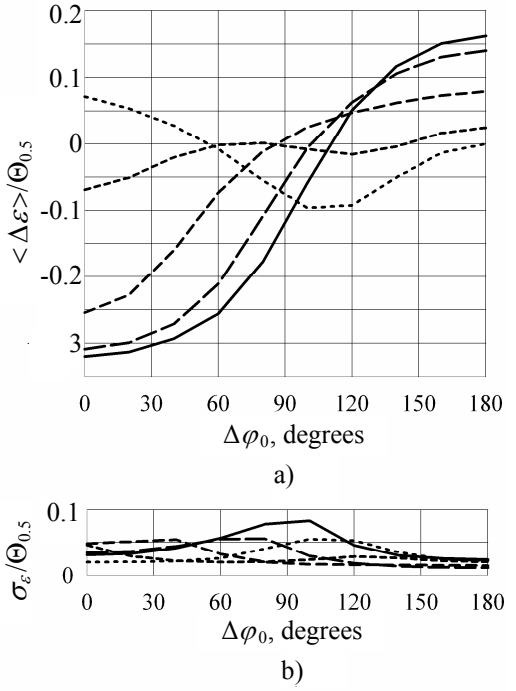

FIG. 4: Mean errors (a) and mean square errors deviations (b) with $\varepsilon_{real} = 0.4\Theta_{0.5}$; $\rho_d = 0.20$; $\rho_s = 0.81$; the curves notations as on Fig. 1

With the angle of elevation of the target $0.5\Theta_{0.5}$ the least mean errors emerged with the value of the frequency separation of 8 and 12 %, this agrees well with the value of 10.0 %, calculated with (6).

4. MEAN SQUARE DEVIATIONS OF ELEVATION ANGLE MEASUREMENT ERRORS

As to the error fluctuations of target elevation angle measurement here their decrease is also observed at transition to the multifrequency measurements condition. The

degree of this decrease depends both on the target elevation angle and on the mirror reflection level, phase difference between the direct and mirror reflections and, naturally, on the frequency separation. Features of errors fluctuations of the elevation angle measurements can be see on Figs. 1(b)-4(b).

Errors fluctuations decrease the most at multifrequency measurements with breaking of the mirror reflection as the target elevation angle increases. Hence with the elevation angle $0.5\Theta_{0.5}$ and mirror reflection coefficient 0.5 the decrease in fluctuations reduces by half and even more throughout the phases difference range already at the frequency separation of 4 %. Further increase in separation does not result in the fluctuations decrease. On the other hand, a twofold decrease in the errors fluctuations with the elevation angle $0.2\Theta_{0.5}$ and the same mirror reflection coefficient takes place only in the area of the phase differences of 90…180°. In this case the frequency separation no less than 8 % is required (see Fig. 1(b)).

As to the great levels of the mirror reflection, here the following should be noted. As it was noted in [3], the considered dependences at single frequency operation are significantly uneven over the phases differences range between the direct and mirror signals, particularly with narrow elevation angles. This manifests itself in the availability of the clearly defined maximum located outside the field extremes domain. In the field maximum the errors fluctuations exceed several times the values in the remainder of the phase difference field. For example, it is seen in Figs. 2(b) and 4(b), where the data at single frequency operation are presented with a solid curve.

Transition to the multifrequency operation with great coefficients of the mirror reflection practically does not decrease the nonuniformity mentioned above. Some decrease of maximums and their displacement along the phases differences axis as well as appearance of new maximums is observed.

5. MEAN SQUARE ERRORS

The most general idea of efficiency of the multifrequency operation conditions can be obtained using for analysis the dependences of the mean square errors on the frequencies separation obtained through averaging in the interval of differences between the direct and reflected signals $0\ldots2\pi$
Errors on

$$\varepsilon_{\text{mse}} = \sqrt{\frac{2\sum_{m=0}^{M}\varepsilon_m^2 - \varepsilon_0^2 - \varepsilon_M^2}{2M}}, \tag{7}$$

where $\varepsilon_m^2 = \langle \Delta\varepsilon_m \rangle^2 + \sigma_{\varepsilon m}^2$; $m = 0, 1, 2 \ldots M$ – phase shift number, with which the m-th values of the mean error and mean square deviation of the error are obtained according to the expression $\Delta\varphi_{0m} = m\pi/M$.

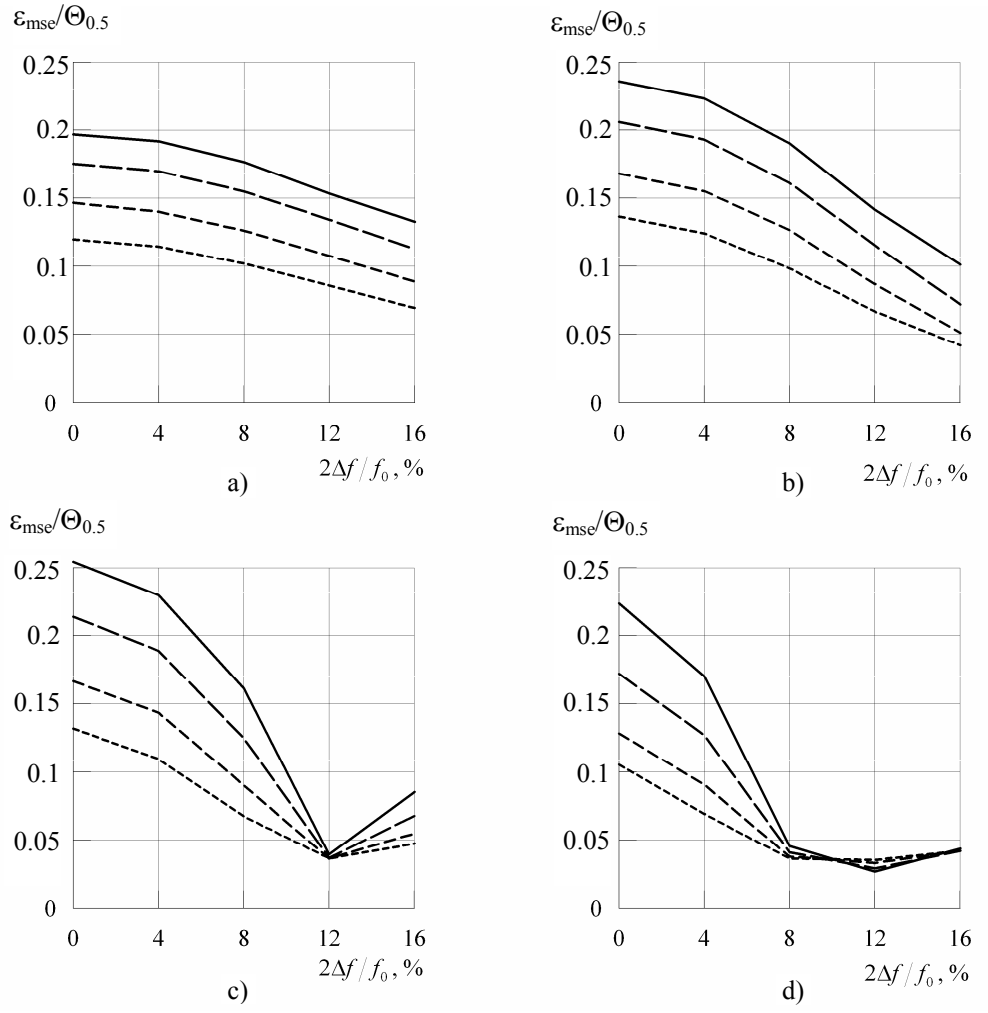

FIG. 5: Mean square errors of the elevation angle measurement: a) – $\varepsilon_{real} = 0.2\Theta_{0.5}$; b) – $\varepsilon_{real} = 0.3\Theta_{0.5}$; c) – $\varepsilon_{real} = 0.4\Theta_{0.5}$; d) – $\varepsilon_{real} = 0.5\Theta_{0.5}$; ρ_d/ρ_s = 0.10/0.93 – ——; 0.20/0.81 – — —; 0.30/0.65 – – – –; 0.36/0.5 – -----

The considered dependences are presented on Fig. 5. Each of four cited plots were obtained at the corresponding radiation source elevation angle from 0.2 to $0.5\Theta_{0.5}$ and contains four curves each, corresponding to different degrees of the underlying surface unevenness.

As seen in plots, measurement of the elevation angle using three frequencies makes it possible to decrease measurement errors. The decrease degree depends both on the underlying surface unevenness and the target elevation angle. The most

essential decrease in errors at the target elevation angles is more than $0.3\Theta_{0.5}$, where it reaches 2…3 and more times.

The analysis of the simulation has shown that the minimal mean square errors of the elevation angle measurement result from such frequencies separation for which the minimal mean error takes place as well, i.e., when the condition (6) is obeyed.

6. THE LAW OF ERRORS DISTRIBUTION OF THE ELEVATION ANGLE MEASUREMENT

The analysis of the error distribution histograms shows that the errors distribution laws both at single frequency and multifrequency operation are described with one of two types. The first type is a symmetric distribution close to the energy region to the normal, but different from the latter by the absence of the side "tails". The second type is an asymmetric distribution characterized by the presence of the gentle left slope and left-side "tail" extending along errors axes in the interval close by meaning to the doubled elevation angle. Figure 6 exemplifies distributions of the second type.

The type of distribution is connected with the phase of interference of the direct and mirror signals reflected from the target. In the case of the single frequency operation the first type distributions correspond to the minimum and maximum of the field. In this case the distributions of the second type correspond to some intermediate phase of interference of the field at the center of the antenna system: with narrow elevation angles this takes place closer to the field minimum, with the increase in the elevation angle this region displaces to the field maximum.

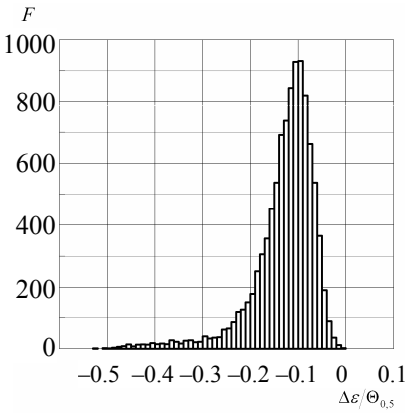

FIG. 6: Histogram of the error distribution of elevation angle measurement of the second type: $\varepsilon_{\text{real}} = 0.3\Theta_{0.5}$; $\rho_d = 0.10$; $\rho_s = 0.93$; $\Delta\varphi_0 = 120°$

To analyze the error distribution law let us consider the elevation angle dependences of the angle discriminator signal errors dependences obtained at simulation, specifically, for the case: $\varepsilon_{\text{real}} = 0.3\Theta_{0.5}$; $\rho_d = 0.10$; $\rho_s = 0.93$; $\Delta\varphi_0 = 120^\circ$.

These dependences were obtained both at the central frequency (Fig. 7(b)), and side frequencies (Figs. 7(a) and 7(c)). Figure 7(d) demonstrates dependences averaged over three frequencies used when measuring the elevation angle.

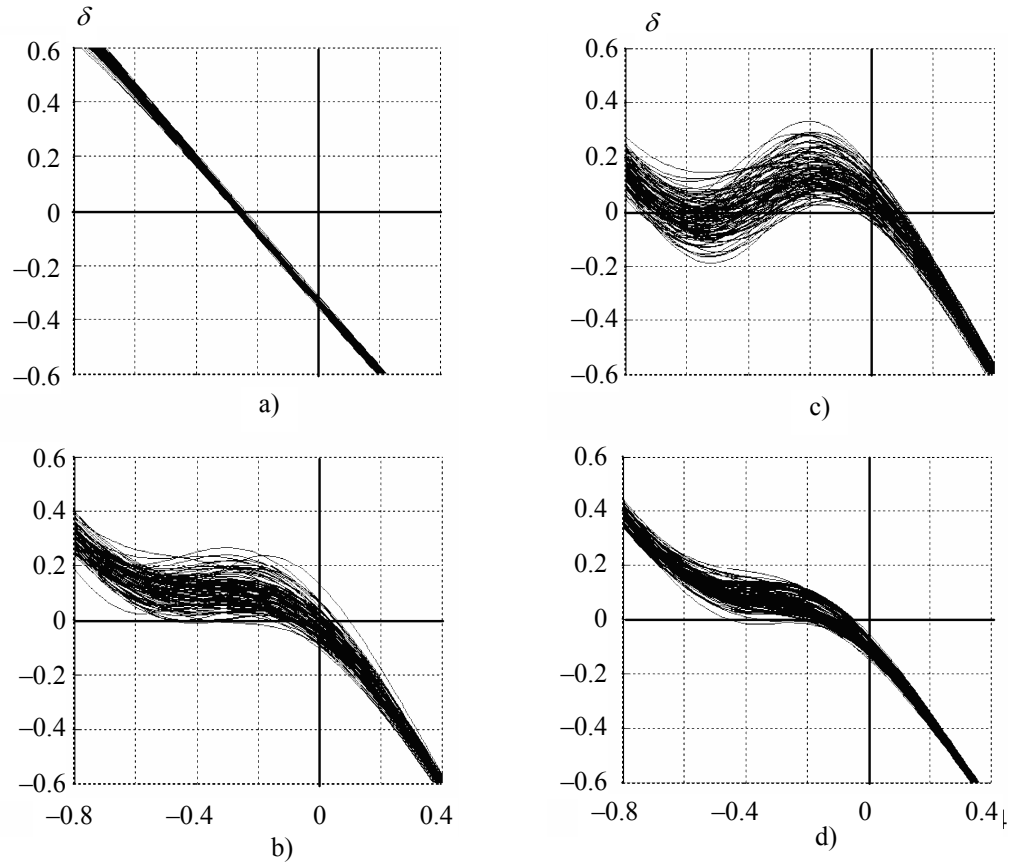

FIG. 7: Elevation angle dependences of the angle discriminator signal: a) – $f = 0.93\, f_0$; b) – $f = f_0$; c) – $f = 1.08\, f_0$; d) – dependence averaged over three frequencies

Thus, the errors distribution of elevation angle measurement depends on the steepness of elevation angle dependence of the angle discriminator signal near its zero value With the great steepness (Figs. 7(a) and 7(c)) we obtain distribution of the first type, and with the small steepness (Figs. 7(b) and 7(d)) – the second one.

With the distributions of the second type the fluctuation component of the elevation angle measurement error exceeds the same fluctuation relating to the distributions of the first type.

The target loss probability as an important characteristic when the radar operates under the automatic tracking conditions. Let us assume that the target loss corresponds to the situation where the measured value of the elevation angle indicates to the point

below the boundary surface below the real target. Using the errors distributions for the whole range of phases differences between the direct and mirror signals it is possible to calculate the target loss averaged probability

$$P = \frac{2\sum_{m=0}^{M} p_m - p_0 - p_M}{2M}, \tag{8}$$

where p_m is probability of that with the given phases difference between the direct and mirror signals the elevation angle measurement error meets the condition $\Delta\varepsilon \le -\varepsilon_{\text{real}}$. The obtained results are shown in Fig. 8.

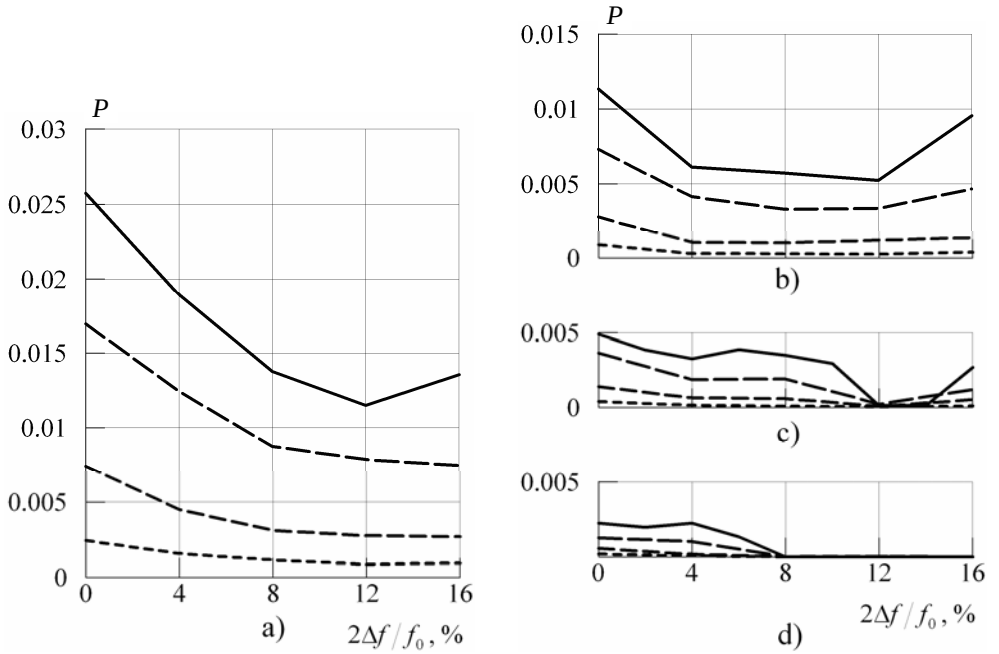

FIG. 8: The target loss probability: a) – $\varepsilon_{\text{real}} = 0.2\Theta_{0.5}$; b) – $\varepsilon_{\text{real}} = 0.3\Theta_{0.5}$; c) – $\varepsilon_{\text{real}} = 0.4\Theta_{0.5}$; d) – $\varepsilon_{\text{real}} = 0.5\Theta_{0.5}$; the curves notations as on Fig. 5

As shown in the indicated pictures the target loss problem becomes the most pressing manifests itself with narrow elevation angles and great levels of mirror reflection from the boundary surface. At the same time the use of the multifrequency operation conditions just in the region of narrow angles gives the stable decrease in the target loss probability with the increase in the frequencies separation. Improvement of this characteristic runs into 2…3 times with relative separations between extreme frequencies of 12 %.

7. CONCLUSIONS

Statistical computer simulation of the monopulse method of the low altitude targets elevation angle measurement using the summarized-difference amplitude radar was carried out with the previously developed model of the field of the multipath signal over the disturbed sea surface. The feature of the measurements consisted in that the measurement was carried out with simultaneous use of three equidistantly separated operating frequencies and formation of the signal of an error – through averaging of the errors signals at these frequencies.

It was found that the transition from the single frequency operating conditions of monopulse amplitude summarized-difference radar to the operation at three frequencies makes it possible to decrease essentially, up to 2…5 times, the mean square errors of the low-altitude targets elevation angle measurements with the elevation angle of the latter of $0.3…0.5\Theta_{0.5}$.

The multifrequency conditions make it possible to reduce the target loss probability. This improvement is 2…3 times in the most unfavorable cases associated with limiting small target elevation angles.

It should be noted that the indicated positive results can be realized in practice as the frequencies separations required for this, do not exceed the limiting ones, mastered in modern microwave engineering.

REFERENCES

1. Barton, D., (1974), Radar tracking at small elevation angles, *TIIER*. **62**(6):37-61 (in Russian).
2. Dax, P.R., (1976), Keep track of than low-flying attack, *Microwaves*. 15:36-53.
3. Razskazovskiy, V.B. and Pedenko, Yu.A., (2006), Radar tracking of low-flying target at the sea surface, *Radiofizika and Elektronika*. **11**(3):377-384 (in Russian).
4. De Hek, A.P. and Hunneman, P.A.H., (2000), Small sized high-gain PHEMT high-power amplifiers for X-BAND applications, *Proc. Gallium Arsenide applications symposium. GAAS 2000*. Paris, pp. 221-223.
5. Razskazovskiy, V.B. and Pedenko, Yu.A., (2003), Millimeter and Centimeter wave field model for the research of the measurement method of elevation angles of low-flying targets, *Radiofizika and Elektronika*. **8**(1):22-23 (in Russian).

Telecommunications and Radio Engineering, 69(9):799-814 (2010)

MOBILE RADIO COMMUNICATION SYSTEMS

OPTIMIZATION OF THE PROFESSIONAL MOBILE RADIO COMMUNICATION NETWORK ARCHITECTURE FOR AN INDUSTRIAL FACILITY*

I. E. Vilinov & A. V. Volodin

Novorossiysk Marine Commercial Harbor,
Novorossiysk, Russian Federation

A summarized description of models for optimization of the network architecture as the basis of the proposed optimization method is given. The main principles of a comprehensive approach to solution of the optimization problem, including the design of system parameters, evaluation of modern information and telecommunication technological advances, introduction of advanced design methods and prospects for the enterprise development and the specific features of the domestic market, are discussed.

KEY WORDS: *network architecture, multicretion optimization, network layout, queuing theory, trunk network, digital network, analog network, broadband network, mobile radio communication networks*

A great number of publications (Gutkin, 1975; Nikolaev and Bruk, 1985; Okunev and Plotnikov, 1976; Shevchuk and Yagolnikov, 1996; Volodin, 2001; Pavlov, 2002; Vilinov and Volodin, 2001; Vilinov et al., 2003) are devoted to issues of optimization of radio communication facilities that play all the more important role in production-technological and management activities of industrial enterprises. However, the interest in new methods for improving quality, optimization, and synthesis of professional mobile radio communication (PMRC) networks as a factor of boosting the production efficiency remains as high as before. The appearance of new modern telecommunication and information technologies on the market defines the urgency of new research for further increasing the efficiency

*Originally published in *Telecommunications*, no. 1, pp. 20–27, 2008.

of technological achievements used by the production sector. Given the increased scopes, variety and diversity of problems solved, the quality of newly designed PMRC networks should be assessed on the basis of multicretion optimization, using the entire range of the recent developments in the field of systemic approaches, modern principles of scalarization, decomposition, and aggregation techniques, and methods of hierarchical structured synthesis and sequential decision-making (Okunev and Plotnikov, 1976; Shevchuk and Yagolnikov, 1996; Volodin, 2001; Pavlov, 2002; Vilinov and Volodin, 2001; Vilinov et al., 2003; Samoilenko, 2005).

At the same time, the requirements to the depth of scientific developments go hand in hand with the requirements to the practical use of a comprehensive approach that ensures an adequate assessment not only of the level of new standards and technologies appearing on the market, but also the real opportunities of their introduction into the production processes. Therefore, to increase the level of detailing of the issues discussed, it is necessary to decompose not only the structure of the newly built network, but also the process of optimization and its constituent operations.

Given the above, this work discusses the problem of the network optimization not for all stages of the multistage synthesis (Gutkin, 1975; Shevchuk and Yagolnikov, 1996; Pavlov, 2002), but only for its initial external system level, i.e., for optimization of the designed network architecture. It is also based on the assumption that the stages of hardware synthesis of the network (Gutkin, 1975; Vilinov and Volodin, 2001), including substantiation and description of its individual components (Methods, 2005), represent a separate problem.

As in (Methods, 2005), the network architecture means the organizational and technological aggregation of individual subsystems, containing information about characteristic principles of the system construction and its connections: internal connections between subsystems and external connections with supersystems, their current status, and future development trends.

As seen from the definition, the architecture ensures the dynamic development of the system, its capacity for increasing the range of telecommunication services provided, and the possibility for a broad introduction of modern specialized and universal applications. Nevertheless, the absence of the required scientific and methodological facilities at production enterprises prevents them from making a justified choice of concrete technologies, optimized for the given enterprise, among the multiple range of competitive technologies offered on the market. This brings about an unacceptable delay in the application of new technologies, accompanied by reduced production efficiency during this period, while errors that may be made in selecting the technologies do not give the required effect in terms of

labor productivity and lead to inadequate costs for the enterprise vis-a-vis the projected effect of application of new technologies and additional financial costs related to final development of the commissioned network.

The objective of this work is to develop a method for multicretion optimization of the future PMRC network architecture for a modern industrial enterprise.

In line with the synthesis problem stated in (Shevchuk and Yagolnikov, 1996), the optimization problem in general means the search for an architecture **A** with an optimal quality vector **T**, possessing the set N_x of the indicators x_n, according to the stated set of requirements x and the selected preference criterion. In analytical terms, a comprehensive aggregated optimization procedure can be presented as follows:

$$\mathbf{A} \rightarrow \text{opt}\,\mathbf{T}(x) = \{x_n\}_{n=1}^{N_x} \in \mathbf{T}(x) \subset \mathbf{E}_x \subset \mathbf{E}_{var}, \tag{3}$$

where $\mathbf{T}(x)$ is the set of possible architecture options, belonging to the set $\mathbf{E}_x$ of implemented systems. In turn, $\mathbf{E}_x$ belongs to a conventionally chosen set $\mathbf{E}_{var}$ of the network options (variants), differing from each other, *inter alia*, by the composition of the basic data, taking into account the complex dynamics of improved quality of performance and resultant from analysis of the above networks in correlation with the development trends and enterprise's capacities for practical introduction, as well as the specific features of the domestic market.

Conventional presentation of the stated options as a separate set is justified by the need to emphasize the impact of the implemented networks' features on the value of their quality vector and the character of solution of the subsequent optimization problems, as well as to underline, additionally, the importance of the comprehensive approach to the search of justified solutions as regards future development and the lines for improvement of the existing radio communication network.

Figure 1 shows the structural layout of the proposed model for optimization of the network architecture. In order to give a clear and compact imaging of the basic operations, the methods used and the stages of optimization, the model layout is based on the above-mentioned expression (1) for an aggregated optimization problem and operator's presentation of the discussed network structures and individual resources. As seen from Fig. 1, the operator's unit includes 11 operators shaping systemic parameters and an operator shaping the requirements to the PMRC network architecture. Figure 1 shows operators related to solution of other model optimization problems, including analysis of the existing network, analysis of the opportunities of modern technologies, shaping of the requirements to hard-

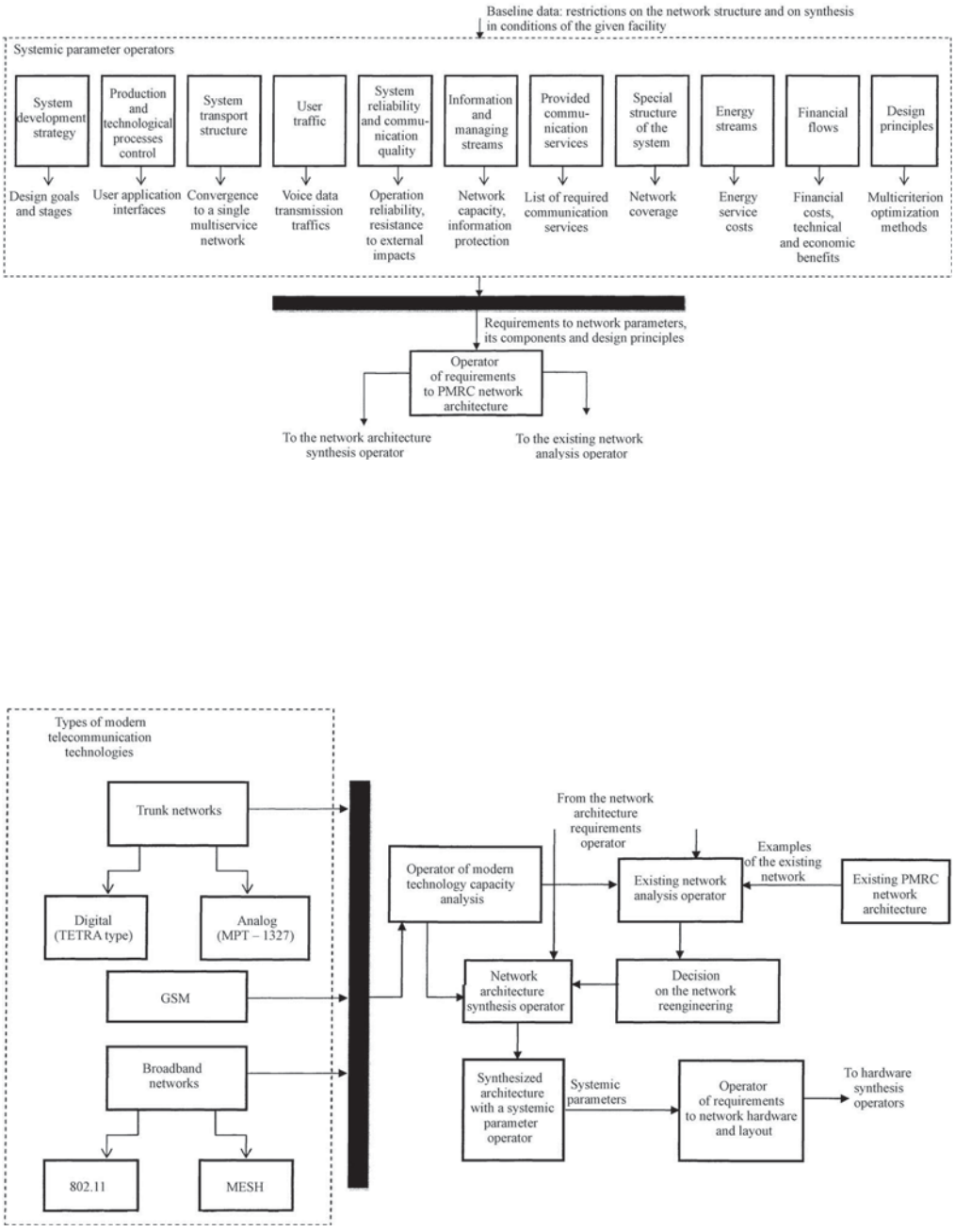

FIG. 1: The structural layout of the network architecture optimization model

ware and network layout, synthesis of the network architecture, as well as the list of the information and telecommunication technologies discussed.

The completeness and the quality of presentation of the entire aggregate of systemic parameters are especially important in conditions of the required multicriterion approach and the known difficulties related to its application for optimization of complex systems (Gutkin, 1975; Shevchuk and Yagolnikov, 1996; Pavlov, 2002). In solving a complex optimization problem, they should ensure the development of a uniform information base, required both for synthesis of the network and analysis of subsystem options and for qualitative expertise of the operations made. They are used as the base for developing particular and integral system quality indicators, making it possible to shape an image of the corporate network and its subsystems. They are the main information base used to substantiate the required material resources and assess the efficiency of their use. In view of the above, the requirements to the quality of systemic parameters developed for new radio communication networks and the use of a comprehensive approach for their development become all the more important. Disclosing the significance of the comprehensive approach and its content for the development of systemic parameters, it is also necessary to point to the need of its preservation when requirements to specific subsystems are developed. This is needed to achieve the required degree of interrelation between the designed network and its supersystem, or, in other words, to ensure maximum correspondence between the requirements to the subsystem and the parameters of the would-be integrated system.

The composition of the developed aggregate of operators, typical systemic parameters and the relevant requirements to individual subsystems (in this case, to the PMRC network) are presented in Fig. 1, and in more detail in Table 1. Each of the presented operators determines the relevant parametrical direction, related to the assessment of the system performance quality or the character and scale of the facility operation for development of the system. The system parameters for a comprehensive telecommunication and information-control network as a supersystem option, most widely used by industrial enterprises, have been developed.

The operator presentation of systemic parameters allows, in addition to the above visual clarity, the development of the entire aggregate of basic data, required for individual optimization model operations even in conditions of possible absence of a completed implemented supersystem. In case of optimization of the network architecture, it is especially important for the development of requirements to the performance efficiency (operational reliability, capacity, coverage area, user's traffic, etc.), the quantity and quality of services provided and the ensuring of the required connections, i.e., external and internal, vertical and horizon-

TABLE 1

Nos.	System operator	Systemic parameters	General and operational and technical requirements to the subsystem
1	System development strategy	1.1. Purpose 1.2. Objectives 1.3. Priority of subsystem tasks and equipment, construction stages	1.1. Purpose 1.2. Objectives 1.3. Total number of general production radio communication network users 1.3. Total number of general production radio communication network users
2	Production and technological processes management	2.1. List of automated business processes (currently and for the futur 2.2. List of SCADA subsystems and other specialized applications as automated management facilities	2.1. Main structural units and groups: users of technological mobile radio communication network 2.2. Number of technological radio communication network users (currently and for the future) 2.3. Territorial distribution of structural units, groups and individual users unified by a technological sign 2.4. Structural unit communication plans 2.5. Requirements: – to interfaces of the universal and user applications used; – levels of provided communication services by user categories
3	System "transport structure"	3.1. Types of the communication lines used and theirparameters (FOLs, cables, radio channels, numberof couplers, informationtransmission rates, etc.)	3.1 Requirements to convergence communication lines and services into a single multiservice network

Continued Table 1

Nos.	System operator	Systemic parameters	General and operational and technical requirements to the subsystem
4	User traffic	4.1. Spatial and time distribution of user traffic (number and duration of communications, time dialup parameters) (according to calculations and statistical studies f the daily average traffic structure)	4.1. Requirements: – to data transmission and voice information; – voice traffic parameters; – data transmission traffic parameters
5	System reliability and communication quality	5.1. Trouble-free operation probability 5.2. System service life 5.3. Troubleshooting time 5.4. Parameters of external destabilizing factors (environment temperature, humidity, salt fog, noise, mechanical impacts, etc.)	5.1. Requirements: – to subsystem operation reliability; – control over reliability of the network – spare parts, tools and accessories; – resistance to external destabilizing impacts; – communication quality, among other, in conditions of destabilizing impacts
6	Information and managing streams	6.1. Number and parameters of information streams (incoming and outgoing information) at different system sections 6.2. Tolerated denialof user services 6.3. Informationtransmission rate 6.4. Maximum allowedinformation delay time 6.5. Number of usersand their categories 6.6. Future growthof information scopesand user numbers	6.1. Requirements: – to capacity of individual channels and the subsystem (PMRC network) as a whole; – probable denial of user services; – maximum information delay; – scope and operative access to processed information, given the user categories and network development prospects; – information protection
7	Provided communication services	7.1. List of required communication services	7.1. Requirements: – to types of communication services provided to users; – level of services by user categories

Continued Table 1

Nos.	System operator	Systemic parameters	General and operational and technical requirements to the subsystem
8	Spatial structure of the system	8.1. Spatial distribution of users, groups and structural units in the service area 8.2. Territorial location of telecommunication facilities in the service area 8.3. Specific terrain features in the coverage area	8.1. Territorial distribution of structural units, groups and individual users of the subsystem (PMRC network) by categories and types of required radio communication (general production or technological radio communication) 8.2. Requirements: – to the coverage area (currently and for the future); – the territorial location of telecommunication facilities in the subsystem; – the needs of relay stations organization and parameters; – the density of user load for various area of the network
9	Energy streams	9.1. Electrical parameters of the system network equipment and maintenanc and repair measuring devices	9.1. Requirements to energy resources for the network equipment and measuring devices
10	Financial flows	10.1. Financial costs of design, construction, operation, maintenance and repair of the network and equipment	10.1. Requirements: – to justification of required financial costs, – financial analysis and investment assessment
11	Design principles	11.1. Systemic approach as the basis of design of complex optimized systems 1.2. Basic principles of modern design of competitive systems: – network openness; – versatility; – scalability and modularity; – progressing design	11.1. Requirements: – to implementation of modern methods of multicriterion optimization of the designed network; – introduction of advanced design methods

tal, a close interconnection of each of the networking stages, from design to introduction and use.

In addition, the parameters and requirements in the discussed case can be developed without a reference to a strict organizational structure of the facility, but, rather, based on the needs of specific production and technological processes, taking into account the degree of their automation and development prospects. As a result, the so-called process method of network design, more progressive and maximally adapted to production needs, is implemented. Figure 2 gives the list of the requirements to the design process as an essential stage of multicriterion optimization of the organized network, in the form of a hierarchical structure of particular design problems and methods of their solution.

The final version of the requirements to the subsystem and architecture synthesis is developed after the completion of all work, indicated by the model operators for the solution of respective optimization problems (see Fig. 1). The required work also includes a cycle of experimental studies, as shown in the scheme in Fig. 2 and related, in this case, to testing radio facility capacities and assessing the communication quality, constructing and analyzing diagrams of spatial and time distribution of user traffic, calculating the capacity, and justifying the time parameters of user traffic and options of the network load, frequency radio channels and user terminals.

The values of basic network quality indicators can be estimated in quantitative terms by means of known mathematical relationships of the queuing theory and radio communication. For example, quantitative analysis of information streams and user service quality estimation can be made using materials form the works (Ventsel, 1988; Goryainov et al., 1980). In this case, the radio channel capacity and the load can be calculated using Erlang's formulas.

1. For a system with denials (losses), when information exchange between users is made without managers and the operation mode efficiency is determined by the denial probability P_{den}, Erlang's B formula is used used:

$$P_{\text{den}} = \frac{\alpha^n}{n!}\left[\sum_{k=0}^{n} \frac{\alpha^k}{k!}\right]^{-1},$$

where n is the number of allocated channels, $\alpha = \lambda / \mu$ is the network load (erlang), $\lambda = \lambda_1 N_{\text{us}}$ is the network input flow (dialup) intensity, μ is the service flow intensity, an inverse mean service time value t_{ser}, $\alpha = \alpha_1 N_{\text{us}}$, N_{us} is the network

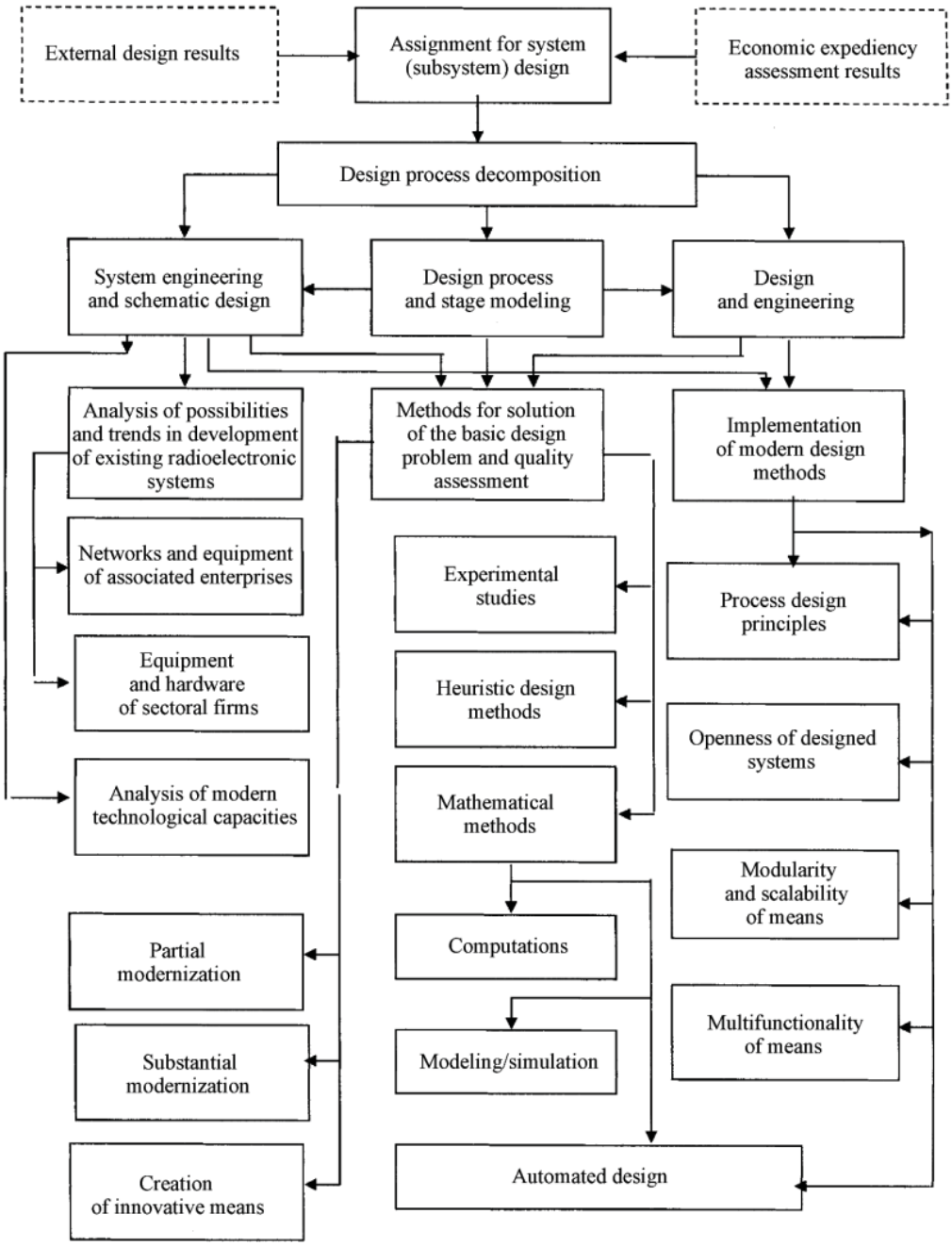

FIG. 2: System of a hierarchical structure of particular design problems and methods

user number, $\alpha_1 = \lambda_1 / \mu$ is one user load, and λ_1 is the incoming flow intensity per user.

2. For a system with waiting and queue organization, when the information exchange between users is made by means of a manager, Erlang's *C* formula is used which can assume one of the following two forms, depending on the calculated parameter:

$$P_{\text{wait}} = \frac{\alpha^n}{n!}\left[\sum_{k=0}^{n} \frac{\alpha^k}{k!} + \frac{\alpha^{n+1}}{n!\,(n-\alpha)}\right]^{-1},$$

where P_{wait} is the probability of the call queuing, or

$$P_{\text{den (wait)}} = \frac{\alpha^n}{n!}\left(\frac{\alpha}{n}\right)^s \left[\sum_{k=0}^{n} \frac{\alpha^k}{k!} + \frac{\alpha}{n!}\sum_{s=1}^{m}\left(\frac{\alpha}{n}\right)^s\right]^{-1},$$

where $P_{\text{den(wait)}}$ is the denial probability of the network with queuing and a limited number of calls waiting in line, m is the number of calls limiting the queuing line, and s is the number of call of queuing.

For estimation and justification of the energy capacities of the organized network architecture, the following equation (Krivistkii, 1979) is used, based on the given coverage area:

$$P_{\text{rec}} = \frac{P_{\text{tr}}\, G_{\text{tr}}\, G_{\text{rec}}\, \eta_{\text{tr}}\, \eta_{\text{rec}}\, \lambda^2}{16\pi^2 r^2}\, \nu^2,$$

where P_{rec} is the signal power at the receiver input, P_{tr} and G_{tr} are the transmitter power, W, and the transmitter antenna gain, respectively, G_{rec} is the receiver antenna gain, η_{tr} and η_{rec} are the efficiency of the transmitter and receiver antenna and feeder transmission lines, λ is the wavelength, m, r is the distance between the transmitter and receiver antennas, m, established from the result of terrain analysis and selected from direct visibility condition:

$$r \le (3.6 \ldots 4.1)\left(\sqrt{h_1 + \sqrt{h_2}}\right),$$

TABLE 2

Nos.	Operations performed	Main results
1	Analysis of the existing PMRC network	1.1. Development of the list of the existing network drawbacks 1.2. Decision of the expediency of the network reconstruction 1.3. Decision of the need of radio equipment update
2	Analysis of the condition of similar work operations in associated enterprises	2.1. Detailing general requirements to the network infrastructure 2.2. Adjustment (towards decrease) of costs related to the network integration 2.3. Detailing the developed preference criteria
3	Analysis of modern technological capacities	3.1. Determination of the range of compared technologies (see Fig. 1) 3.2. Development of a comparison table of different technology parameters (see Table 3)

here h_1 and h_2 are the elevations of the transmitter and receiver antennas, m, $\nu^2 = \dfrac{P_{\text{rec}}}{P_{0\text{rec}}}$ is the free space field propagation factor, and $P_{0\text{rec}}$ is the power at the receiver input during signal propagation in a free space.

As shown conventionally in formula (1) and in the form of specific individual operations in Fig. 1, the solution of the architecture synthesis problem is related to the required preliminary solution of a series of analysis problems, inter alia, problems of analysis of the features and trends in development of the existing networks at associated enterprises, the results of inventory of business processes at the given facility, economic evaluation of the expediency of organization of a new network, and the results of comparative assessment of modern technological capacities. The presence of such integrated information allows a substantial reduction of the set dimensions in formula (1) and, accordingly, decreasing the level of synthesis problem solution complexity in general (Shevchuk and Yagolnikov, 1996).

TABLE 3

Nos.	Modes and functional capacities	Trunk network		Broadb and network		GSM
		TETRA	MPT 1327	802.11	MESH	
1	Voice communication	+	+	–	–	+
2	Assignment of service priorities and classes	+	+	–	–	–
3	Priority and emergency call	+	+	–	–	1*
4	Address group and individual calls	+	+	–	–	1*
5	Call queuning	+	+	–	–	–
6	Confidentiality of talks	+	–	–	–	–
7	Duplex communication	+	–	–	–	–
8	Output to PABX and PSTN	+	+	–	–	–
9	Possibility for limiting talks duration	+	+	–	–	–
10	Possibility for talks recording	+	+	–	–	–
11	Possibility for organizing computer manager workplaces	+	+	+	+	–
12	Call set-up time, sec	0.3	0.5	–	–	6–20
13	Data transmission	+	+	+	+	+
14	Short message services, SDS	+	+	–	–	–
15	Selecting the cover area	+	+	+	+	–
16	Channel switching	+	–	+	+	+
17	Package switching	+	–	+	+	+
18	Facility location	+	–	–	+	–
19	Presence of explosion-protected radio sets	+	–	–	+	–
20	Capability of operating in conditions of destabilizing impacts	+	+	+	+	2*
21	Mean terminal service life	Up to 10 years	No data	No data	No data	2 years
22	System reliability monitoring	+	+	+	+	3*
23	System recovery time monitoring	+	+	+	+	4*

Continued Table 3

Nos.	Modes and functional capacities	Trunk network		Broadb and network		GSM
		TETRA	MPT 1327	802.11	MESH	
24	System development monitoring	+	+	+	+	5*
25	Monitoring of projects implemented around the world	~600	~1000	No data	8	No data
26	Monitoring of projects implemented in the Russian Federation	22	~100	No data	0	No data

1* These modes are not the main modes for GSM, and their implementation requires additional equipment.

2* Implemented in part. Side-mounted headsets are not designed for operation in unfavorable climatic and noise conditions.

3* System reliability is defined by the operator and is out of control by the customer.

4* Operator cannot guarantee the system recovery time after a failure.

5* The system development is defined by the operator and is out of control by the customer.

Note. Data in Table 3 were developed using materials from (Technical Assignment, 2005).

An additional simplification of the problem can be made by a limitation of the preference criteria range, which takes into account the specific features of development of the given facility. In such conditions, the synthesis problem as the final stage of the architecture optimization can be solved using engineering synthesis methods based on the principles of convolution of the vector network-efficacy criterion, given the above limitations of the preference criteria system. Such an approach, oriented towards maximum use of the preliminary analysis results as well as statistical data, obtained during experimental and computational studies, allows a substantial simplification of the practical problem on optimization of the newly organized network.

The method proposed in this work has been tested, as individual practical methods, by the OJSC Novorossiysk Marine Commercial Harbor (NMCH) for justification of future development of the existing PMRC network and for identification of the main lines of its development.

The main stages of the optimization process and the content of its individual operations have been selected according the recommendations given in this work. The list of operations performed and the main results obtained are presented in Table 2.

CONCLUSIONS

The proposed method of the network architecture optimization is developed for a general case of the PMRC network being produced, aims at overcoming difficulties related to practical introduction of modern information and telecommunication technologies at production facilities, takes into account the specific features of development of the domestic market, and can be used for developing versatile scientific and practical tools for solving optimization problems in radio communication networks of different downsizing levels.

REFERENCES

Dremov, A. N., A decisive step towards integration, *Tekhnologii i Sredstva Svyazi*, no. 2, 2001.

Goryainov, V. T., Zhuravlev, A. G., and Tikhonov, V. I., *Statisticheskaya radiotekhnika. Primery i zadachi* (Statistical Radio Engineering. Examples and Tasks), Moscow: Sovetskoe Radio Press, 1980.

Gutkin, L. S., *Optimizatsiya radioelektronnykh ustroistv po sovokupnosti pokazatelei kachestva* (Optimization of Radio-Electronic Devices by the Range of Quality Indicators), Moscow: Sovetskoe Radio Press, 1975.

Krivistkii, B. Kh., *Spravochnik po radioelektronnym sistemam* (Reference Book on Radioelectronic Systems), vol. 1, Moscow: Energiya Press, 1979.

Metody opredeleniya trebovanii k arkhitekture i komponentam sistemy professionalnoi mobilnoi radiosvyazi (Methods for Determination of Requirements to the Architecture and Components of a Professional Mobile Radio Communication System), RKK "Mobilnye Radiosistemy", 2005.

Nikolaev, V. I. and Bruk, V. M., S*istemotekhnika: metody i prilozheniya* (System Engineering: Methods and Applications), Leningrad: Mashinostroenie Press, 1985.

Okunev, Yu. B. and Plotnikov, V. G., *Printsipy sistemnogo podkhoda k proektirovaniyu v tekhnike svyazi* (Principles of a Systemic Approach to Communication System Design), Moscow: Svyaz Press, 1976.

Pavlov, Yu. S., Multicriterion assessment of system efficacy by a sequential decision method, *Proc. Int. Scientific and Practical Conf. "Radio Detection and Ranging, Navigation and Communication*," Voronezh, vol. 2, pp. 1042–1047, 2002.

Samoilenko, A. P., Principles of construction of integral criteria for quantitative assessment of efficiency of automated technological processes management systems, *Izv. Vyssh. Uchebn. Zaved., Elektromekhanika*, 2005.

Shevchuk, V. I. and Yagolnikov, S. V., A sequential hierarchical method of synthesis of conflict-resistant radioelectronic systems, *Konfliktno-Ustoichivye Radioelektronnye Sistemy*, no. 1, 1996.

Tekhnicheskoe zadanie i tekhniko-ekonomicheskoe obosnovanie reorganizatsii professionalnoi mobilnoi radiosvyazi OAO "NMTP": Otchet o NIR (Technical Assignment and Feasibity Study on Reorganizatiomn of a Professional Mobile Radio Communication System: Report on R&D), St. Petersburg: CJSC "TsNIIMF", 2005.

Ventsel, E. S., *Issledovanie operatsii. Zadachi, printsipy, metodologiya* (Operation Research. Tasks, Principles, Methods), Moscow: Nauka Press, 1988.

Vilinov, I. E. and Volodin, A. V., Method of quality assessment for the updated regional communication network, Vestnik RGUPS, Rostov-on-Don, pp. 10–14, 2001.

Vilinov, I. E., Volodin, A. V., and Karpov, E. A., Basic principles of the conceptual construction of a corporate integrated communication network, *Proc. IV Interregional Scientific and Practical Conf.* "*Innovative and Double Technologies of Regional Production*," Rostov-on-Don: FGUP VNII Gradient, 2003.

Volodin, A. V., Increasing efficacy of design of conflict-resistant radioelectronic systems, *Proc. of the Interregional Scientific and Practical Conf.* "*Theory and Practice of Development of Radio Equipment in Market Conditions*," Rostov-on-Don: FGUP VNII Gradient, 2001.

Telecommunications and Radio Engineering, 69(9):815-837 (2010)

APPLIED RADIO PHYSICS

RECONSTRUCTION OF PERMITTIVITY PROFILE OF STRATIFIED LOSSY DIELECTRIC USING NEWTON-KANTOROVICH ITERATIVE SCHEME

S.G. Alexin & O.O. Drobakhin

Dnepropetrovsk National University
72, Gagarin Ave., Dnepropetrovsk, 49010, Ukraine

*Address all correspondence to O.O. Drobakhin E-mail: drobakhino@mail.ru

The equations specifying the general Newton-Kantorovich iterative scheme for the case of lossy stratified dielectric structures are presented. Both dispersive and non-dispersive permittivity models are considered. The improvement of the scheme assuming non-dispersive permittivity model is proposed. The advantage of modified scheme is shown by numerical experiments. The problem of reflecting interfaces localization in non-dispersive case is considered. The new approaches to the spectral analysis order choosing and the main spectral components selection are proposed and utilized in numerical experiments.

KEY WORDS: *permittivity, reconstruction, iterativescheme, numerical experiment*

1. INTRODUCTION

The problem of 1-D permittivity profile $q(k,x)$ reconstruction based on the microwave multifrequency measurements of reflected data is related with medical tomography, geoexploration, non-destructive testing of dielectric industrial products and building constructions etc. In many practical applications objects under consideration correspond the stack of homogeneous layers that allows transforming to the parametric problem of layers parameters (viz permittivity $q_n(k)$ and thickness d_n) determination. A lot of methods developed provide variety of approaches to the problem solving. The discrete analog of the Gel'fand-Levitan method [1] performs layer-by-layer reconstruction after transformation the measured data to time-domain. The method of dynamic deconvolution [2] is another one providing successive reconstruction being founded on frequency-domain data treatment and parametrical spectral analysis. The idea of successive correction of layer parameter estimates has

found implementation in the Newton-Kantorovich iterative scheme [3-6]. The improvement the last method is the object of the paper.

The first aim pursued by this paper is specification of basic method to the case of stratified lossy dielectric. The general method described in [3-4] provides integral equations allowing reconstruction both continuous and discrete permittivity profiles. But authors of [3-4] didn't notice that integral equations can be simplified in the case of stratified structure. The second aim is improvement of the reconstruction stability providing by the method. The aim is achieved by the Riccati equation treatment in more natural coordinate. The third aim is development of the concept of reflecting interfaces localization. The concept is based on parametrical spectral analysis and includes preliminary solving of the problem of spectral analysis order choosing and subsequent spectral components data treatment. The treatment has the aim of main spectral components selection and increasing the accuracy of them utilizing information containing in the echo spectral components.

2. NEWTON-KANTOROVICH ITERATIVE SCHEME

Newton-Kantorovich iterative scheme (NKIS) provides reconstruction of permittivity profile (PP) through numerical solving of the Riccati differential equation connecting permittivity function $q(k,x)$ and reflection coefficient $r(k,x)$:

$$\frac{dr(k,x)}{dx} = 2jk\sqrt{q(k,x)}r(k,x) + \frac{1-r^2(k,x)}{4q(k,x)}\frac{dq(k,x)}{dx}, \tag{1}$$

where k is wavenumber of free space, x is geometrical coordinate, and $q(k,x)$ is complex-valued dispersive permittivity function. In accordance with [3-4] the equation provides more accurate inversion being considered in terms of electrical coordinate z instead of geometrical one x:

$$z(x) = \int_0^x \sqrt{\varepsilon(x')}dx' . \tag{2}$$

The initial data for reconstruction is vector of reflection coefficient values measured in plane just before the structure, $r(k_m, z_0 - 0)$, on the grid of wavenumbers $k_1, k_2, \ldots k_M$. The derivation of the method is based on supposition that initial-estimate PP-function $q(k,z)$ gets small variation $\Delta q(k,z)$ that produce corresponding variance of reflection coefficient $\Delta r(k,z)$. Requirement of $\Delta r(k,z)$ minimization in plane $z = z_{\max}$ beyond the structure leads to iterative scheme giving sequence of variations $\Delta q(k,z)$ providing correction of the initial profile $q(k,z)$. The $z_{\max}$ value must be

greater than the electric thickness of the structure under consideration (SUC). The parameter $z_{\max}$ is free to choose parameter of the method. Despite the fact that method was developed on the basis of differential equation, involvement of generalized function concept (the Heaviside step function and the Dirac delta-function) allows correct implementation of the method for the reconstruction of discrete profiles.

2.1 NKIS in the Lossless Case

If in a given frequency band the SUC has properties of an ideal dielectric then complex PP function becomes real, $q(k,z)=\varepsilon(z)$, that transforms equation (1) to more simple one being the base for NKIS modification development:

$$\frac{dr(k,z)}{dz}=2jkr(k,z)+\frac{1-r^2(k,z)}{4\varepsilon(z)}\frac{d\varepsilon(z)}{dz}. \tag{3}$$

Our previous paper [5] provides equations concretizing general NKIS [3-4] for the case of lossless stratified structure (Fig. 1).

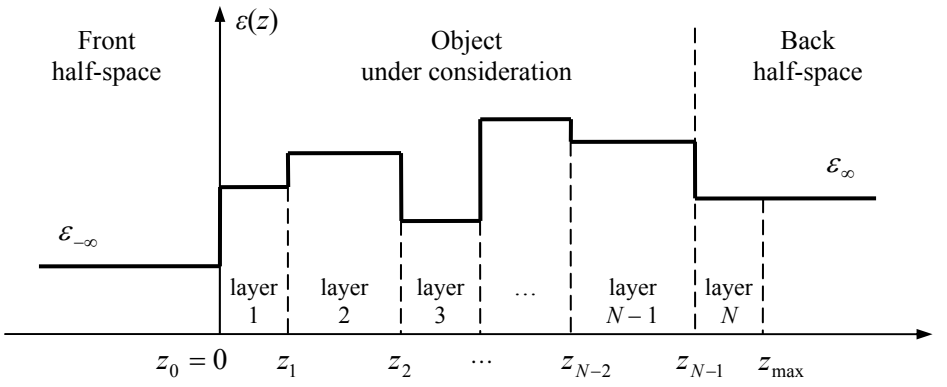

FIG. 1: Geometry of the problem in the case of lossless stratified structure under consideration

Initial permittivity profile in discrete case can be presented by the vector of layers permittivity $\boldsymbol{\varepsilon}=\left(\varepsilon_1 \quad \varepsilon_2 \quad \ldots \quad \varepsilon_N\right)^{\mathrm{T}}$. Iterative scheme launched provides successive correction of $\boldsymbol{\varepsilon}$-vector using sequence of correcting vectors $\boldsymbol{\Delta\varepsilon}=\left(\Delta\varepsilon_1 \quad \Delta\varepsilon_2 \quad \ldots \quad \Delta\varepsilon_N\right)^{\mathrm{T}}$. The vector of summands is obtained at iterations by the solution of overdetermined system of linear algebraic equations (SLAE). The latter can be written in matrix form:

$$\mathbf{A}\boldsymbol{\Delta\varepsilon}=\mathbf{Q}. \tag{4}$$

The coefficients of matrix **A** having size $M \times N$ and the coefficients of vector **Q** having height M are given by:

$$\begin{aligned} A_{mn} &= \frac{j}{2\varepsilon_n}\Big[\exp(jk_m Z_n) + r^2(k_m, z_n - 0)\exp(-jk_m Z_n)\Big]\times \\ &\times \prod_{i=n}^{N-1}\left(\frac{1-r^2(k_m, z_i + 0)}{1-r^2(k_m, z_i - 0)}\right)\exp\big[2jk_m(z_{\max} - z_n)\big]\sin(k_m Z_n), \\ Q_m &= -r(k_m, z_{\max}) - \frac{1-r^2(k_m, z_{\max})}{4}\frac{\varepsilon_\infty - \varepsilon_N}{\varepsilon_N}, \end{aligned} \tag{5}$$

where z_n is the electrical coordinate of n^{th} interface, $z_{\max} = z_N$ is electrical depth of reconstruction, $Z_n = z_n - z_{n-1}$ is electrical thickness of layer n, and $r(k_m,\ldots)$ is reflection coefficient values obtained by transformation of initial reflectometry data $r(k_m, z_0 - 0)$ through structure reconstructed by the moment. The equation for matrix **A** coefficients presented above corresponds to the case of Π-shape basis which is used for the purpose of construction of correcting summand expression [5].

The least-squares method with conventional Tikhonov regularization is proposed in [3-4] to be used for solving of (4). The method gives solution in following form:

$$\mathbf{\Delta\varepsilon} = \left(\mathbf{A}^{\mathrm{H}}\mathbf{A} + \gamma\mathbf{I}\right)^{-1}\mathbf{A}^{\mathrm{H}}\mathbf{Q},$$

where $\mathbf{A}^{\mathrm{H}}$ is Hermitian conjugation of matrix **A**, γ is regularization coefficient, and **I** is unity matrix of size $N \times N$.

After system solving corrected vector of permittivity is obtained as:

$$\mathbf{\varepsilon}^{(p+1)} = \mathbf{\varepsilon}^{(p)} + \mathrm{Re}\big(\mathbf{\Delta\varepsilon}\big),$$

with upper index denoting the number of iteration.

Before the reconstructive scheme launching, the interface electrical coordinates z_n have to be obtained. The problem will be considered in the next chapter.

Our next investigations have been concentrated on the problem of lossy dielectric PP reconstruction.

2.2 Basic Variant of NKIS in the Lossy Case

Authors of basic works [3-4] treated with dispersive permittivity model of type

$$q(k, x) = \varepsilon(x) - j\eta_0\sigma(x)/k, \tag{6}$$

with $\eta_0 = 120\pi$ Ohm being characteristic impedance of free space and $\sigma(x)$ being conductivity profile. Following by the authors, let's introduce in the Riccati differential equation (1) new coordinate z using definition (2). The new form of the Riccati equation will be as following:

$$\frac{dr(k,z)}{dz} = 2jk\sqrt{\frac{q(k,z)}{\varepsilon(z)}}r(k,z) + \frac{1-r^2(k,z)}{4q(k,z)}\frac{dq(k,z)}{dz}. \tag{7}$$

Comparing the expression (7) with the equation (3) corresponding to lossless case, one can note that permittivity function occurs in (7) not only in full form $q(k,z)$ but also in form $\varepsilon(z) = \mathrm{Re}\big(q(k,z)\big)$, as opposed to (3) where permittivity function meets only in full form $\varepsilon(z)$. This is the reason why inversion of equation (7) relatively $q(k,z)$ cannot be achieved in so simple way as inversion of the equation (3) relatively $\varepsilon(z)$. For the purpose of the problem solving the authors split $q(k,z)$ - function into 2 parts and provide simultaneous inversion of (7) relatively profiles $\varepsilon(z)$ and $\sigma(z)$.

In the case of stratified dielectric and Π-shape basis introducing vectors of correcting terms $\mathbf{\Delta\varepsilon} = \begin{pmatrix}\Delta\varepsilon_1 & \Delta\varepsilon_2 & \dots & \Delta\varepsilon_N\end{pmatrix}^{\mathrm{T}}$ and $\mathbf{\Delta\sigma} = \begin{pmatrix}\Delta\sigma_1 & \Delta\sigma_2 & \dots & \Delta\sigma_N\end{pmatrix}^{\mathrm{T}}$ are obtained form overdetermined system of linear equations that can be written in matrix form:

$$\begin{pmatrix}\mathbf{A} & \mathbf{B}\end{pmatrix}\begin{pmatrix}\mathbf{\Delta\varepsilon} \\ \mathbf{\Delta\sigma}\end{pmatrix} = \mathbf{Q}$$

with

$$A_{mn} = jk_m\left(I_1 + j\frac{\eta_0\sigma_n}{k_m\varepsilon_n}I_2\right)g, \quad B_{mn} = \eta_0\big(I_1 + I_2\big)g,$$

$$Q_m = -r(k_m, z_{\max}) - \frac{1-r^2(k_m, z_{\max})}{4}\frac{q_{m\infty} - q_{mN}}{q_{mN}}.$$

Miscellaneous parameters are given by:

$$I_1 = \frac{1}{2jk_m}\sqrt{\frac{\varepsilon_n}{q_{mn}}}\Big(\alpha^* + r^2(k_m, z_{n-1} + 0)\alpha\Big),$$

$$I_2 = 2r(k_m, z_{n-1} + 0)Z_n \exp\left(-2jk_m\sqrt{\frac{q_{mn}}{\varepsilon_n}}z_{n-1}\right),$$

$$\alpha = \exp\left(2jk_m\sqrt{\frac{q_{mn}}{\varepsilon_n}}z_{n-1}\right) - \exp\left(2jk_m\sqrt{\frac{q_{mn}}{\varepsilon_n}}z_n\right), \quad q_{mn} = \varepsilon_n - j\eta_0\sigma_n/k_m,$$

$$g = \frac{1}{2\sqrt{\varepsilon_n q_{mn}}} \exp\left[2jk_m \left(z_{n-1}\sqrt{\frac{q_{mn}}{\varepsilon_n}} + \sum_{i=n}^{N} Z_i \sqrt{\frac{q_{mi}}{\varepsilon_i}} \right) \right] \prod_{i=n}^{N-1} \left(\frac{1 - r^2(k_m, z_i + 0)}{1 - r^2(k_m, z_i - 0)} \right),$$

α^* denotes complex conjugation of α.

Following system solving, the corrected vectors of permittivity and conductivity values are obtained as:

$$\boldsymbol{\varepsilon}^{(p+1)} = \boldsymbol{\varepsilon}^{(p)} + \mathrm{Re}(\Delta\boldsymbol{\varepsilon}), \qquad \boldsymbol{\sigma}^{(p+1)} = \boldsymbol{\sigma}^{(p)} + \mathrm{Re}(\Delta\boldsymbol{\sigma}).$$

We will also consider iterative scheme that corresponds to non-dispersive permittivity model of type

$$q(x) = \varepsilon(x) - j\varepsilon''(x). \tag{8}$$

Introducing the vector of correcting terms $\Delta\boldsymbol{\varepsilon}'' = \left(\Delta\varepsilon_1'' \quad \Delta\varepsilon_2'' \quad \ldots \quad \Delta\varepsilon_N''\right)^{\mathrm{T}}$ brings linear system of type

$$\left(\mathbf{A} \quad \mathbf{B}\right)\begin{pmatrix}\Delta\boldsymbol{\varepsilon} \\ \Delta\boldsymbol{\varepsilon}''\end{pmatrix} = \mathbf{Q} \tag{9}$$

giving variations of real and lossy parts of permittivity by

$$\boldsymbol{\varepsilon}^{(p+1)} = \boldsymbol{\varepsilon}^{(p)} + \mathrm{Re}(\Delta\boldsymbol{\varepsilon}), \qquad \boldsymbol{\varepsilon}''^{(p+1)} = \boldsymbol{\varepsilon}''^{(p)} + \mathrm{Re}(\Delta\boldsymbol{\varepsilon}'').$$

The new equations for coefficients of matrix **A** and vector **Q** can be obtained from corresponding dispersive-case equations after the substitution $\sigma_m \to \frac{k_n \varepsilon_m''}{\eta_0}$. The new equation for coefficients of matrix **B** will be following:

$$B_{nm} = k_n (I_1 + I_2) g,$$

with I_1, I_2 and g given by the dispersive-case formulas after corresponding substitution.

2.3 The Problem of Interfaces Localization in the Lossy Case

As in the lossless case, the interface coordinates $z_n \left(n = 0,1,...,N-1\right)$ must be obtained before iterative scheme launching. If dispersive model of permittivity assumed,

parametric spectral analysis (PSA) methods cannot longer be utilized for this purpose. The reason is that dispersion of permittivity makes model of frequency domain reflection coefficient (FDRC) as sum of exponentials no longer correct in general case. If one knows electrical thickness of layers $Z_n = d_n\sqrt{\varepsilon_n}$ from somewhere the NKIS can be used for ε_n, σ_n and d_n values obtaining but in general case the data absence is critical.

Our further consideration will imply validity of non-dispersive model of permittivity (8) in the frequency band of measurements. The permittivity model allows PSA methods using for obtaining of z_n. But one feature of PSA implementation must be noted. In the lossless case delay of second spectral component gives electrical coordinate of second interface $z_1 = d_1\sqrt{\varepsilon_1}$, while in the lossy case the spectral component delay equals to $\xi_1 = d_1\sqrt{q_1} = d_1\sqrt{\varepsilon_1 - j\varepsilon_1''}$ that isn't electrical coordinate of second interface. That is the reason why the spectral component delay must be recalculated as following: $z_1 = \sqrt{\mathrm{Re}\left(\xi_1^2\right)}$. For the structure having more than 1 layer other main spectral component delays must also be recalculated by:

$$z_n = z_{n-1} + \sqrt{\mathrm{Re}\left[\left(\xi_n - \xi_{n-1}\right)^2\right]}, \qquad n > 1. \tag{10}$$

The problem of PP reconstruction in the lossy case has peculiarity that consists in the fact that main spectral component delays $\xi_n\left(n = 0,1,...,N-1\right)$ bring information about loss-angle tangent by themselves. The tangent can be calculated without NKIS launching by simple formula [7]:

$$\tan\delta_n = \frac{\varepsilon_n''}{\varepsilon_n} = \frac{-\mathrm{Im}\left(\Xi_n^2\right)}{\mathrm{Re}\left(\Xi_n^2\right)},$$

with $\Xi_n = \xi_n - \xi_{n-1}$ being the lossy-case analog of electrical depth Z_n of layer *n*. The information about loss-angle tangent allows express imaginary part of permittivity through real part or vice versa and substitute this equation in SLAE instead of ε_n'' or ε_n respectively. This operation halves amount of unknown parameters of SLAE what now has to be solved relatively only ε_n or ε_n'' respectively.

If the halving has been done, the accuracy of $\tan\delta_n$ estimates is specified by PSA method only; if the halving hasn't done, the accuracy of $\tan\delta_n$ is specified by both PSA method and NKIS. The first case can look more preferable at the first sight. But it is the fact that information regarding $\tan\delta_n$ consists not only in spectral component delays ξ_n and ξ_{n-1} but also in all sequential main spectral components delays and amplitudes such as in delays and amplitudes of sequential echo spectral components. If

the noise present in FDRC-data, using only two delays ξ_n and ξ_{n-1} is deficient relatively gathering information about PP and as a result noise level in $\tan\delta_n$-value will be higher that can be achieved in principle. The full data of FDRC including relations between spectral components must be utilized in estimation process what means that $\tan\delta_n$ must be leaved as free parameter before NKIS launching. The problem of interfaces localization will be considered detailed in the next chapter.

2.4 Riccati Equation Treatment in More Natural Coordinate

Comparing equations (3) and (7) one can see that conversion of the original Riccati equation (1) from *x*-coordinate to *z*-coordinate by transformation (2) simplified basic equation in lossless case but didn't in lossy case. Equation (7) corresponding lossy case in comparison with (1) include not only full permittivity function $q(k,z)$ but also its real part what makes impossible inversion of the equation relative $q(k,z)$. As a result the complex permittivity profile has to be split into two profiles corresponding to real and imaginary parts and then inversion has to be taken relatively these two parts apart. This brings SLAE with the vector of unknowns having doubled height.

The numerical simulation has shown that stability of reconstruction relatively initial estimate of PP in the lossy case much worse than in the lossless case. Moreover if exact profile is lossless, loss-assuming iterative scheme provides worse stability than corresponding scheme assuming loss absence. The problem can be related with the form of differential equation underlying in the foundation of NKIS.

The transformation of type

$$\xi(x)=\int_0^x\sqrt{q(x')}dx'=\int_0^x\sqrt{\varepsilon(x')-j\varepsilon''(x')}dx'$$

converts basic equation (1) to equation

$$\frac{dr(k,\xi)}{d\xi}=2jkr(k,\xi)+\frac{1-r^2(k,\xi)}{4q(\xi)}\frac{dq(\xi)}{d\xi} \tag{11}$$

that coincides by form with equation (3) corresponding *z*-coordinate and lossless case. This means that inversion of (11) relative $q(\xi)$ brings same iterative scheme that inverts (3) relatively $\varepsilon(z)$. The scheme (4) was found to be more stable that scheme (9) that is the reason why the new scheme is expected to be more stable that (9) too.

The new scheme supposes that vector of complex correcting terms $\mathbf{\Delta q}=\begin{pmatrix}\Delta q_1 & \Delta q_2 & \dots & \Delta q_N\end{pmatrix}^{\mathrm{T}}$ can be found from linear system of type

$$\mathbf{A\Delta q}=\mathbf{Q}\,.$$

The equations for coefficients of matrix **A** and vector **Q** can be obtained from equations (5) (lossless scheme derived after *z*-coordinate introducing) by replacements $\varepsilon \to q$, $z \to \xi$ and $Z \to \Xi$. After system solving corrected vector of complex permittivity is given by:

$$\mathbf{q}^{(p+1)} = \mathbf{q}^{(p)} + \Delta\mathbf{q} .$$

Note that the correcting vector has just complex elements, and operation of real part taking is no longer necessary.

Some features of the new scheme must be noted. Firstly, ξ coordinate is complex in opposite to *z*-coordinate. As a result main spectral components delays shouldn't be recalculated after PSA as it was done in the case of *z*-coordinate (see equation (10)). Secondly, choose of parameter $\xi_{\max}$ (the analog of $z_{\max}$) now have an influence on loss-angle tangent of last layer being the part of back half-space. In the case of non-lossy environment the imaginary part of $\xi_{\max}$ should be taken equal to imaginary part of ξ_{N-1}; real part of $\xi_{\max}$ is free to choose parameter.

Unfortunately, if one assumes dispersive model of permittivity, the ξ-coordinate introducing by

$$\xi(x,k) = \int_0^x \sqrt{q(x',k)}\,dx'$$

don't remove the problem of PSA methods non-applicability. The coordinates of interface ξ_n becomes wavenumber-dependent.

3. THE PROBLEM OF INTERFACES LOCALIZATION

Before the NKIS launching, layer interface coordinates (z_n or ξ_n) have to be obtained. The localization of interfaces is important stage of reconstruction that essentially determines final result. There are some approaches to the localization proposed, but the problem is still urgent because of disadvantages inherent to the approaches. The widest class of approaches is based on PSA implemented in one or another form. All PSA methods suppose preceding solving of problem of order choosing and subsequent problem of main spectral components selection. Both the problems are still poorly referenced.

3.1 Interfaces Localization Methods Overview

The problem of reflecting interfaces localization is usually solved with use of PSA methods applied to reflection coefficient data [5]. This approach has two weak points

being inherent to PSA principally. At first, PSA gives spectral components corresponding to multiple reverberations of probing wave in SUC. As a result, those ones corresponding to first reflection from the each interface (i.e., giving electrical coordinate of interface) cannot be simply identified. Using all the components obtained gives additional degrees of freedom for profile variation in the process of reconstruction what is not desired. At second, some structures demonstrate compensation of main spectral component(s) by those ones corresponding to echo. This leads to absence of energy in the spectral distribution in the place of the actual interface. As a result, the interface cannot be found and adequate basis cannot be designed for PP representing.

An original method of interfaces localization was proposed in [3-4]. The method implies preliminary approximate PP reconstruction using NKIS with exponential basis and following interfaces identification as points where spatial distribution of $|d\varepsilon(z)/dz|$ reaches local maxima. After this discrete basis can be designed and discrete reconstruction can be carried out. This approach to z_n obtaining also has some disadvantages. Firstly, time-consuming numerical integration has to be made. Secondly, this method demands low-frequency reflection coefficient data available, or otherwise exponential basis will not be able to reproduce PP with adequacy.

Two approaches can be used in composition producing hybrid approach [6]. The approach imply matching of PSA data with spatial distribution of $|d\varepsilon(z)/dz|$. Hybrid approach provides high accuracy of z_n and at the same time has suppressed sensitivity to false interfaces and vanishing interfaces problems. Unfortunately there is low velocity of performance and low-frequency data criticality problems remained in hybrid approach being inherited from the maxima-searching method.

3.2 The Problem of Spectral Analysis Order Choosing

It is known that layered dielectric structure being irradiated by the impulse, produces infinite number of reflected impulses. That means that fully-adequate spectral model can be provided only if order of PSA is chosen to be equal to infinity. But condition of finiteness of frequency grid sample amount constricts the maximal order of PSA to half of the amount. Moreover, noise presence in FDRC-data often makes surplus maximal order choosing because some of spectral components obtained might be fictive ones produced by noise. It is evident that spectral analysis order choosing must be grounded on the level of noise. There are two opinions relatively the problem of order choosing. The first one is expressed in proposition of preliminary choosing of wittingly large order and subsequent decreasing of it until stopping condition becomes true. The second one comes to the opposite proposition of preliminary choosing of wittingly low order and subsequent increasing of it.

Let's consider the second approach implementation in couple with PSA method based on rational approximation in the Fourier-conjugate domain [8]. The PSA method supposes conversion of FDRC-data to time domain by inverse discrete Fourier transform (IDFT):

$$x_m = \frac{1}{N}\sum_{n=0}^{N-1} X_n e^{j2\pi\frac{mn}{N}} \tag{12}$$

and consideration of x_m as function of argument $\zeta_m = e^{j2\pi\frac{m}{N}}$. It can be shown that table function $x_m(\zeta_m)$ provides particular values of sum of pole functions; every pole function describes one spectral component. Pole positions and magnitudes giving delays and magnitudes of spectral components can be obtained by $x_m(\zeta_m)$ -table approximation with rational function. The approximation is useful to be preceded by rational interpolation using points corresponding to maxima of the discrete function. The interpolation gives initial estimate for approximation procedure.

If one provides growing order of spectral analysis sequentially picking up spectral components with less and less energy, on some iteration all the spectral components remained would be considerably sunk in the noise. Next maxima of residual signal chosen for interpolation may be only the spike of the noise but not actual spectral component. It leads to the idea that order growing must be stopped when maxima of residual signal becomes less than some threshold. In other words, the order must be grown until spectral analysis becomes picking up fictive spectral components produced by the noise. The choice of the threshold must be based on the properties of noise presented in FDRC-data.

Let's suppose FDRC-data has noise with independent real and imaginary parts of all the samples that have zero mean values and variances σ^2. It can be shown that Fourier transform (12) gives time-domain signal having noise with independent normally distributed real and imaginary parts with zero mean values and variances σ^2 / N. Let's introduce stochastic variable ψ being maximum of square modulus of noise samples η_m in time domain,

$$\psi = \max_{m=0}^{N-1} |\eta_m|^2 .$$

It can be proved that ψ has distribution with cumulative distribution function (CDF) of form:

$$F_\psi(y) = \left(1 - e^{-\lambda y}\right)^N$$

with $\lambda = \frac{N}{2\sigma^2}$. Let's introduce probability p that stochastic variable ψ overcomes some threshold ψ_{th}. In other words p is probability that noise spike would be confused with actual spectral component. Inversion of CDF $F_\psi(y)$ provides equation expressing ψ_{th} through p by:

$$\psi_{th} = F_{\psi}^{-1}(p) = \frac{-1}{\lambda}\ln\left(1 - \sqrt[N]{1-p}\right). \quad (13)$$

The growing of spectral analysis order must be stopped when maximum of modulus square of residual signal becomes less than threshold. The parameter *p* can be used for control of sensitivity of spectral analysis. If *p* tends to zero, threshold is growing, and spectral analysis order growing would be stopped soon. Then PSA becomes rough passing only components having large amplitude. If *p* tends to unity, threshold is decreasing and order growing would be stopped a long way off. Then PSA becomes sensitive passing not only actual spectral components with small amplitude but also fictive noise-produced ones.

It is important that all main spectral components must be greater then threshold, otherwise they wouldn't be picked up by spectral analysis and NKIS couldn't reconstruct PP with adequacy.

If PSA is used for the purpose of interfaces localization, the information consisting in echo impulses isn't usually utilized. But this information can be involved in reconstruction process for increasing of accuracy. Let's consider this concept in details.

3.3 The Concept of Estimation of Interfaces Electrical Depth

After spectral analysis performing simple concept can be used for selection of the spectral components corresponding to the first reflection from interfaces. The concept is based on the statement that all the echo spectral components have delays being linear combination of delays of the main spectral components with natural-number coefficients.

Let's introduce notation $z_{(n_1,n_2,n_3,\ldots)}$ for delay of impulse formed after n_1 reverberations in first layer, n_2 reverberations in second layer etc. The delay is expressed through electrical depths of layers as following:

$$z_{(n_1,n_2,n_3,\ldots)} = \sum_k n_k Z_k \ .$$

The notation z_n (with no parentheses and only one index) corresponds to spectral component obtained by PSA having sequence number $n\left(n = 0,1,\ldots\right)$. The notations $\sigma^2_{(n_1,n_2,n_3,\ldots)}$ and σ_n^2 will be used for variances of $z_{(n_1,n_2,n_3,\ldots)}$ and z_n respectively. Let's assume firstly that SUC is known to be lossless in the frequency band of measurements. This allows throw off imaginary parts of as delays and so magnitudes of spectral components after PSA performing.

Let's suppose that PSA has given *M* spectral components with electrical coordinates z_n and corresponding magnitudes $R_n\left(n = 0,1,\ldots,M-1\right)$. The coordinate of the earliest spectral component z_0 is frequently known to be equal to zero, thus it

can be replaced by 0 explicitly. The second component coordinate has to be seen as stochastic variable. If low noise level assumed, z_1 can be used as estimate of true value of first layer electrical thickness Z_1. It can be shown that PSA method based on rational interpolation in the Fourier-conjugate domain provides variance of z_1 (and thus Z_1) as following:

$$D[Z_1] = D[z_1] = \sigma_1^2 = \frac{1}{N}\left(\frac{C}{2\Delta\omega}\right)^2 \left|\frac{(\zeta_i - p_1)(\zeta_k - p_1)}{a_1 p_1 (\zeta_k - \zeta_i)}\right|^2 \left(|\zeta_i - p_1|^2 + |\zeta_k - p_1|^2\right)\sigma^2, \quad (14)$$

$$a_1 = R_1 g_1,\ g_1 = \frac{1}{N}(1/p_1)^{N-1+\alpha}\left(1 - p_1^N\right),\ \alpha = \omega_{\min}/\Delta\omega,$$

$$p_1 = \exp\left(j2\pi\frac{z_1}{N\Delta z}\right),\ \Delta z = \frac{C}{2N\Delta\omega},$$

$$\zeta_i = \exp(j2\pi i/N),\ i = \mathrm{floor}(z_1/\Delta z),\ \zeta_k = \zeta_i \exp(j2\pi/N),$$

where C is the light speed, $\omega_{\min}$ is the first frequency of frequency grid of FDRC-measurements, $\Delta\omega$ is step of frequency grid, N is number of frequencies in grid, and σ^2 is remain for notating of variance of real and imaginary parts of noise presented in FDRC-data. The variance of Z_1 is seen to be dependent from delay z_1 and magnitude R_1 of the spectral component.

The data of Z_1-value and $D[Z_1]$-value provides information about expected coordinate of the first echo impulse of the first layer $z_{(2)}$ and can be used for weighting window construction for searching of this impulse. Probability distribution function (PDF) of $z_{(2)}$ expectation has a form of Gaussian curve with mean value $\mu_{(2)} = 2Z_1$ and variance $\sigma_{(2)}^2 = 2^2 D[Z_1]$. The third spectral component z_2 given by PSA may be first echo of first layer (thus having type $z_{(2)}$) or may correspond to new interface (thus having type $z_{(1,1)}$). True type of z_2 can be described by matching PDF of z_2 disposition with PDF of $z_{(2)}$ expectation.

Let's illustrate the principle of decision taking on the following example. Figure 2 shows four earliest spectral components obtained by PSA having delays z_0, z_1, z_2 and z_3. The decision must be taken whether z_2 or z_3 correspond to echo. The first spectral component z_0 is assumed having zero delay, as opposed to other three components having uncertainty of delay value. The uncertainties can be taken into account by PDF-functions of spectral components disposition $w_1(z)$, $w_2(z)$ and $w_3(z)$ respectively. The PDF-function of $z_{(2)}$-component expectation notated as $w_{(2)}(z)$ can

be produced from function $w_1(z)$ by doubling of mean value and quadruplicating of variance. The function $w_{(2)}(z)$ has to be matched with functions $w_2(z)$ and $w_3(z)$ for the purpose of decision taking. The matching can be formalized by the way of comparison of correlation coefficients being given by integration of PDF-function product:

$$\theta = \int_{-\infty}^{\infty} w_c(z) w_m(z) dz = \frac{1}{\sqrt{2\pi(\sigma_c^2 + \sigma_m^2)}} \exp\left(\frac{-(z_c - z_m)^2}{2(\sigma_c^2 + \sigma_m^2)} \right), \tag{15}$$

where index "m" notes parameters of spectral component-model and index "c" notes parameters of spectral component-candidate to model. It can be seen that the closest z_c to z_m and the least variances σ_c^2 and σ_m^2, the larger coefficient of correlation would be. The candidate having the largest value of the coefficient is assumed to correspond to the model.

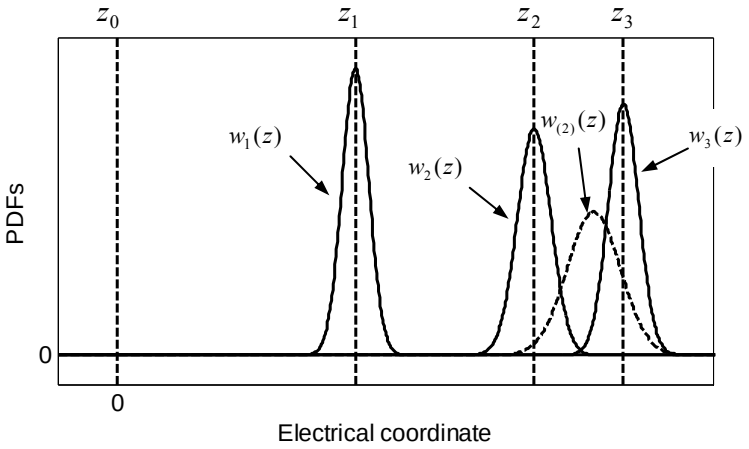

FIG. 2: The explanation of concept of spectral component types determination by the way of matching of probability distribution functions of spectral component expectation and spectral component disposition

In general case impulse-candidate has to be matched with series of models every of which corresponds to some path of probing impulse in the structure. The PDF of expectation of spectral component $z_{(n_1, n_2, \ldots, n_m)}$ is Gaussian curve with mean value

$$\mu_{(n_1, n_2, \ldots, n_m)} = \sum_{k=1}^{m} n_k Z_k$$

and variance

$$\sigma^2_{(n_1,n_2,\ldots,n_m)} = \sum_{k=1}^{m} n_k^2 D[Z_k]$$

with Z_k and $D[Z_k]$ (k = 1, 2, …, m) having been calculated previously. If satisfactory model is found, the impulse could be used for correction of values of electrical thickness of layers and recalculation of corresponding variances. If there no satisfactory model for the impulse-candidate, the impulse must be assumed to be the new main spectral component (thus corresponding to the first reflection from the new interface).

The method of estimation of interfaces electrical depth can be formalized to the algorithm presented below.

1. Calculation of variances of spectral component delays σ_1^2, σ_2^2, …, σ_{M-1}^2 by equation of type (14).

2. Initialization of vector-columns of electrical thickness of layers **Z**, variances of electrical thickness **D**, matrix **F** containing the serial numbers of layers passed through before corresponding spectral component formed (matrix of indices of spectral components) and weighting matrix **W** by following:

$$\mathbf{Z} = z_1,\ \mathbf{D} = \sigma_1^2,\ \mathbf{F} = 1,\ \mathbf{W} = 1/\sigma_1^2.$$

Initially the vectors and matrix are scalars but they will be expanded later.

3. Opening the cycle enumerating spectral components having delays z_2, …, z_{M-1}. Let's consider that k is the index of the following spectral component.

3.1 Searching for model of spectral component $\{z_k, \sigma_k^2\}$ utilizing comparison of coefficients of correlation calculated by (15). Simple enumeration of models can be used for the purpose. The vectors **Z** and **D** are used for spectral models construction. Let's consider that z_k is obtained to correspond to impulse of type $z_{(n_1,n_2,\ldots,n_m)}$. Auxiliary vector-row **n** is handy to be composed as following:

$$\mathbf{n} = \begin{pmatrix} n_1 & n_2 & \cdots & n_m \end{pmatrix}.$$

Two situations can have place: the component z_k may correspond to echo impulse or may correspond to new main impulse. If z_k corresponds to echo impulse, the matrix of indices **F** is extended by following

$$\mathbf{F} \to \begin{pmatrix} \mathbf{F} \\ \mathbf{n} \end{pmatrix}.$$

If z_k corresponds to new main impulse (in this case all the elements of vector **n** equals to 1), matrix **F** is extended by following

$$\mathbf{F} \to \begin{pmatrix} \mathbf{F} & \mathbf{0} \\ \mathbf{n} & \end{pmatrix}$$

with **0** being zero vector-column of height of matrix **F**.

3.2 Extending of the weighting matrix **W** by following

$$\mathbf{W} \to \begin{pmatrix} \mathbf{W} & \mathbf{0} \\ \mathbf{0}^{\mathrm{T}} & 1/\sigma_k^2 \end{pmatrix}.$$

3.3 Recalculation of vector-column of electrical thickness of layers **Z** using least-squares method with weighting:

$$\mathbf{Z} = \mathbf{U}\mathbf{z},$$

where $\mathbf{z} = \begin{pmatrix} z_1 & z_2 & \cdots & z_k \end{pmatrix}^{\mathrm{T}}$ and rectangular matrix **U** given by:

$$\mathbf{U} = \left(\mathbf{F}^{\mathrm{T}}\mathbf{W}\mathbf{F}\right)^{-1}\mathbf{F}^{\mathrm{T}}\mathbf{W}.$$

3.4 Recalculation of vector-column of layers electrical thickness variance **D** utilized in the process of spectral models matching:

$$\mathbf{D} = \mathbf{U}^2\mathbf{\Sigma}$$

with $\mathbf{U}^2$ being matrix obtained from matrix **U** through element wise squaring, $\mathbf{\Sigma} = \begin{pmatrix} \sigma_1^2 & \sigma_2^2 & \cdots & \sigma_k^2 \end{pmatrix}^{\mathrm{T}}$.

3.5 Closing the cycle of variable *k*.

4. At the end electrical depths of interfaces and corresponding variances can be recalculated from the data of electrical thickness of layers as following:

$$\mathfrak{Z}_k = \sum_{m=1}^{k} Z_m, \quad D[\mathfrak{Z}_k] = \sum_{m=1}^{k} D[Z_m]. \qquad (k = 1,2,...,N)$$

Owing to the echo spectral component data utilizing, the accuracy of result is higher than could be achieved using only main spectral components.

3.4 The Method of Electrical Depths Estimation in the Lossy Case

If the SUC is known to be lossy, the algorithm of electrical thickness estimation has to be modified.

Firstly, the replacement of notations have to be done: $z \to \xi$ and $Z \to \Xi$ for scalar values and $\mathbf{z} \to \boldsymbol{\xi}$, $\mathbf{Z} \to \boldsymbol{\Xi}$ for vectors. The new variables are assumed to be complex-valued.

Secondly, electrical coordinates $\xi_n = \xi'_n - j\xi''_n$ and magnitudes $R_n = R'_n + jR''_n$ given by PSA have to be remained complex-valued.

Thirdly, variances of both real and imaginary parts of ξ_n (as long as $\xi_{(n_1,n_2,\ldots,n_m)}$) have to be introduced. But it can be proved that variance of ξ'_n is equal to variance of ξ''_n then notation σ_n^2 can be remained for both variances. The statement is also true for spectral component-models $\xi_{(n_1,n_2,\ldots,n_m)}$. The variance of σ_n^2 can be calculated by equation of type (14), but new equation for reference point index must be used: $i = \text{floor}(\xi'_n / \Delta z)$. The Δz notation can be remained.

Fourthly, speaking strictly, the matching of spectral component-candidate with spectral component-model has to be performed by both real and imaginary parts. The coefficient of correlation becomes the product of two coefficients, corresponding to matching of real part of delay and imaginary part of delay:

$$\theta = \theta'\theta'',$$

$$\theta' = \frac{1}{\sqrt{2\pi(\sigma_c^2 + \sigma_m^2)}} \exp\left(\frac{-(\xi'_c - \xi'_m)^2}{2(\sigma_c^2 + \sigma_m^2)} \right), \quad \theta'' = \frac{1}{\sqrt{2\pi(\sigma_c^2 + \sigma_m^2)}} \exp\left(\frac{-(\xi''_c - \xi''_m)^2}{2(\sigma_c^2 + \sigma_m^2)} \right).$$

But in practically feasible situations the matching of imaginary parts of delays is useless because high closeness of ξ''_c and ξ''_m and relatively large sum of variances σ_c^2 and σ_m^2. As a result coefficient θ'' is essentially determined by variance but not closeness of spectral components and then becomes spurious. Therefore the coefficient can be considered equaling to 1.

Then the algorithm presented above can be utilized without subsequent modifications.

The concept of electrical depths estimation has a few weak points have to be noted. Firstly, the algorithm errs in the case when structure has electrical thickness of layers being multiples. This is the case when main spectral components are overlaid on echoes and would be interpreted as echoes. Secondly, it is evident that probability of errs rise with rising number of impulse-candidate. This caused by growing density of impulses-candidates and impulses-models on one hand and growing variance of PDF of impulse expectation on other hand.

4. NUMERICAL EXPERIMENT

The first series of experiments dealt with two modifications of NKIS assuming non-dispersive permittivity model of type (8). The structure under consideration had been

chosen to have 4 layers with parameters presented in Table 1. FDRC-data was synthesized numerically in frequency band 8-12 GHz and had 256 equidistantly spaced frequencies. After FDRC synthesis complex additive noise was introduced in the data. The noise had uniform distribution of real and imaginary parts and fell into square with side 10^{-4} on complex plane.

TABLE 1: Parameters of structure under consideration

	Layer 1	**Layer 2**	**Layer 3**	**Layer 4**
d_n, mm	100	90	85	45
ε_n	2	5	4	3
$\tan\delta_n$, 10–2	1	2	0	4

Firstly the problem of spectral analysis order choosing was solved. The probability that noise spike would be confused with actual spectral component had been chosen as $p = 10^{-3}$. The threshold corresponding to the p value and noise level was calculated by (13) and was $\psi_{th} = 8.1 \cdot 10^{-11}$. The order of spectral analysis had been grown until maximum of modulus square of residual signal became less than threshold. The order of spectral analysis reached was $M = 11$.

After PSA performing electrical depth of interfaces were estimated using the approach proposed. The model-enumeration conception gave that spectral components obtained has types presented in Table 2. The values of depths obtained and corresponding variances are presented in Tables 3 and 4. The tables also include the values obtained utilizing only main spectral components data. Comparing the results one can see that the approach proposed lessen the variances and improved accuracy of interface coordinates.

TABLE 2: The type of spectral components obtained by PSA

The number of spectral component obtained (by delay growing)	**The index of spectral models matched**
1*	0
2*	1
3	2
4*	1 1
5	2 1
6*	1 1 1
7*	1 1 1 1
8	1 1 1 2
9	2 1 1 1
10	1 2 2 1
11	3 1 2 1

* The components marked by asterisk are determined to be the main ones.

TABLE 3: Electrical depth of interfaces ξ_n, 10^2 mm

	ξ_1	ξ_2	ξ_3	ξ_4
Exact values	1.4142 –j0.0071	3.4268 -j0.0272	5.1268 -j0.0272	5.9064 -j0.0428
Obtained using only main spectral components data	1.4142 –j0.0071	3.4260 –j0.0273	5.1316 –j0.0301	5.9051 –j0.0429
Obtained using all the spectral components data	1.4142 –j0.0071	3.4265 –j0.0273	5.1275 –j0.0278	5.9056 -j0.0427

TABLE 4: The variance of real part of electrical depth of interfaces $D[\xi_n']$, mm^2

	$D[\xi_1']$	$D[\xi_2']$	$D[\xi_3']$	$D[\xi_4']$
Achieved using only main spectral components data	0.0082	0.7502	1.0551	2.7505
Achieved using all the spectral components data obtained	0.0082	0.5766	0.7354	1.2503

After electrical depths obtaining PP was reconstructed using two modifications of NKIS. The first one is based on z-coordinate and implies linear system solving relatively vector $(\Delta\varepsilon \quad \Delta\varepsilon'')^{\mathrm{T}}$, the second one is based on ξ-coordinate and implies system solving relatively vector $\Delta\mathbf{q} = \Delta\boldsymbol{\varepsilon} - j\Delta\boldsymbol{\varepsilon}''$. The initial profile for reconstruction was chosen to be an air ($q = 1$). The parameter of regularization γ used in linear system solving was equal to 0.

The first observation made concerned the first modification. There was strict dependence of the fact whether iterative process converges from the parameter of reconstruction depth. The scheme is realized to converge if the norm of correcting vector becomes monotonic vanishing starting from some iteration. The parameter $z_{\max}$ was traced in ranges 650-750 mm with step 10 mm. The first modification of NKIS has shown divergence in 6 cases from 11. Only 5 values of $z_{\max}$ (670, 680, 720, 730 and 740 mm) provide the norm of correcting vector $(\Delta\varepsilon \quad \Delta\varepsilon'')^{\mathrm{T}}$ tending to zero. The regularization couldn't repair the situation. Furthermore it was noticed that in cases of scheme breaking exact profile wasn't attractive point for the iterative scheme. Being chosen as initial profile, exact profile produced diverged iterative scheme.

In opposite to the first modification, the second modification of NKIS provided convergence in all the cases when $\mathrm{Re}(\xi_{\max})$ traced in ranges 650-750 mm with step 10 mm.

The speed of reconstruction was examined with use of dependence of the following parameter form iteration number:

$$\rho = \lg\left(\sum_{m=1}^{M} \left| r(k_m, z_{\max}) \right|^2 / \sum_{m=1}^{M} \left| r(k_m, z_0 - 0) \right|^2 \right).$$

The ρ-parameter is logarithm of relation of L_2-norms of reflection-coefficient vectors corresponding sections $z_{\max}$ and $z_0 - 0$ (or $\xi_{\max}$ and $\xi_0 - 0$ respectively if ξ-coordinate used). The numerator responses to residual reflection coefficient beyond the structure obtained by transformation of the vector of initial data $r(k_m, z_0 - 0)$ through the structure reconstructed by the moment. The denominator brings only normalizing function giving zero-valued ρ-parameter before 1st iteration if the first modification of NKIS is used.

The ρ-parameter dependencies was obtained using the both modifications of NKIS assuming $z_{\max} = \mathrm{Re}(\xi_{\max}) = 720$ mm (see Fig. 3). Comparing Fig. 3(a) and 3(b) one can note that second modification of NKIS provided sharp decreasing of ρ-parameter that obtained final value after 4th iteration. The figure shows existence of non-exceeded threshold specified by noise level in FDRC-data. The first modification of NKIS was a great distance away from the threshold even after 20th iteration.

The profiles of permittivity and loss-angle tangent reconstructed by first modification of NKIS are shown in Fig. 4. Corresponding profiles reconstructed by second modification are shown in Fig. 5. The figures show advantage in accuracy of the second modification. The first modification made rough error assuming negative loss-angle tangent of back half-space. The second one brought the profile $\varepsilon(x)$ that even visually coincides with exact one.

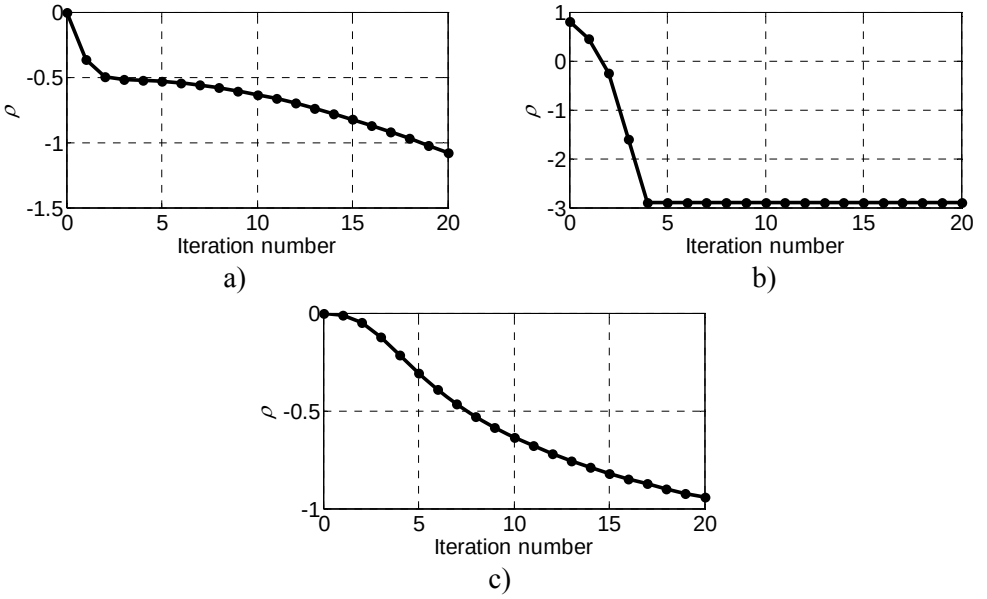

FIG. 3: Convergence process of various modifications of NKIS:
a – the modification supposing non-dispersive permittivity model and assuming *z*-coordinate,
b – the modification supposing non-dispersive permittivity model and assuming ξ-coordinate,
c – the modification supposing dispersive permittivity model

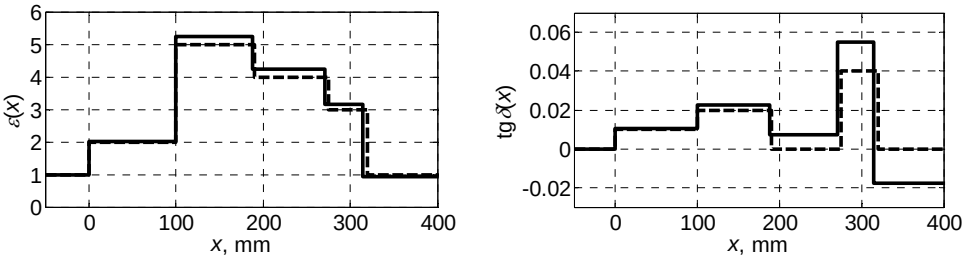

a) b)

FIG. 4: Results of reconstruction by the modification of NKIS supposing non-dispersive permittivity model and assuming z-coordinate: a – reconstructed permittivity profile (solid line) overlaid on exact one (dash line), b – reconstructed profile of loss-angle tangent (solid line) overlaid on exact one (dash line)

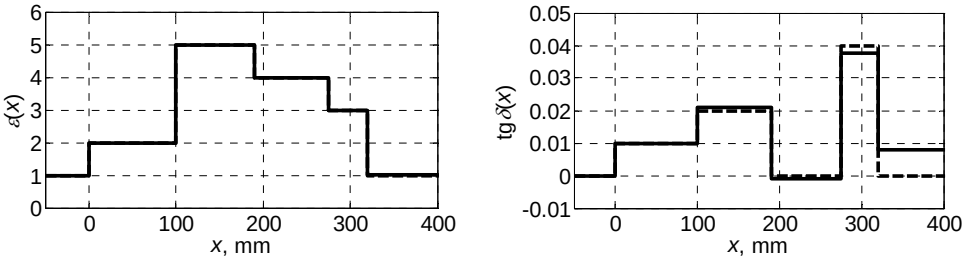

a) b)

FIG. 5: Results of reconstruction by the modification of NKIS supposing non-dispersive permittivity model and assuming ξ-coordinate: a – reconstructed permittivity profile that visually coincides with exact one, b – reconstructed profile of loss-angle tangent (solid line) overlaid on exact one (dash line)

Analogous testing was carried out for NKIS modification assuming dispersive model of permittivity of type (6) that is the case when z-coordinate is used and linear system is solved relatively vector $(\Delta\varepsilon \quad \Delta\sigma)^{\mathrm{T}}$. The structure under testing had same values of d_n and ε_n as previous one. The values of conductivity σ_n had been chosen so that new structure got at the central frequency of the band the same values of complex permittivity q_n as previous one. This attained by choosing $\sigma_n = k_{\mathrm{mean}}\varepsilon_n \tan\delta_n / \eta_0$. So long as the depth of interfaces z_n couldn't longer be obtained with use of PSA, they were chosen to be equal to exact ones. The series of NKIS launching with various $z_{\max}$ has been shown that the modification has ties between the fact of scheme convergence and $z_{\max}$-value, as it had place for non-

dispersive model of q_n. The convergence occurs in 4 cases from 11 ($z_{\max}$ = 670, 680, 690, 720 mm).

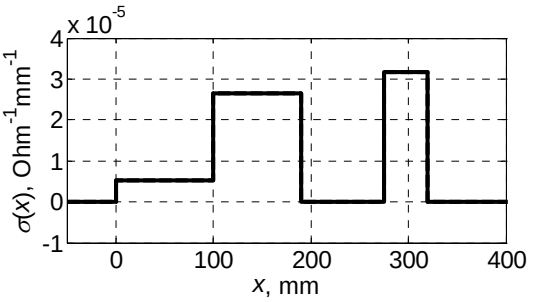

FIG. 6: The profile of conductivity reconstructed by the modification of NKIS supposing dispersive permittivity model (the profile visually coincides with exact one)

Figure 3(c) shows ρ-parameter vs iteration number obtained for $z_{\max} = 720$ mm. Comparing the Figure with Fig. 3(a) one can note more slow convergence in the dispersive case. The reconstructed profiles of conductivity (Fig. 6) and permittivity (not shown) visually coincide with exact ones. So high accuracy of reconstruction can be accounted for using of exact values of interface electrical coordinates.

5. CONCLUSIONS

1. The equations specifying NKIS for the case of lossy stratified material have been derived and presented. The equations are obtained after integrals taking in explicit form in the equations provided by the basic works [3-4]. As a result the reconstruction is performed much faster because the scheme having been specified excludes numerical integration.
2. The new coordinate is proposed to be introduced in the Riccati equation being the foundation for NKIS development. The treatment of the equation in more natural coordinate provides solving of the problem relative to complex permittivity, which is opposite to basic variant of method providing solving the individual values of real and imaginary parts of permittivity. The stability and accuracy advantage of the new modification of method is shown numerically.
3. The new approach to spectral analysis order choosing is proposed. The approach is based on tolerated probability assignment that fictive noise-produced spectral component would be picked up by spectral analysis. The approach supposes growing of the order until specified probability is reached.
4. The new approach to interface electrical depths estimation is proposed. The approach performs spectral analysis results treatment discerning main spectral components and echo ones by the way of matching of probability distribution

functions of spectral component expectation and spectral component disposition. The data of echo components is involved as long as the data of main ones for the purpose of interface depths estimation. The estimation is based on the least-squares method with weighting. The approach proposed has advantage in comparison with simple selection of main spectral components that has been shown numerically.

REFERENCES

1. Aki, K. and Richards, P.G., (1980), *Quantitative Seismology. Theory and methods*, W.H. Freeman & Co, San Francisco.
2. Robinson, E.L., (1982), Spectral Approach to Geophysical Inversion by Lorenz, Fourier, and Radon Transforms, *Proc. IEEE*, 70:1039-1054.
3. Mikhnev, V.A. and Vainikainen, P., (2000), Two-Step Inverse Scattering Method for One-Dimensional Permittivity Profiles, *IEEE Trans. Antennas and Propagation*, 48:293-298.
4. Mikhnev, V. and Vainikainen, P., (2000), Iterative Step-Like Reconstruction of Stratified Dielectric Media from Multifrequency Reflected-Field Data, *Subsurface Sensing Technologies and Applications*, 1:65-78.
5. Alexin, S.G., Drobakhin, O.O., and Tkachenko, V.O., (2009), Modification of the Newton-Kantorovich Iteration Procedure for Piecewise-Constant Real Permittivity Profile Reconstruction, *Telecommunications and Radio Engineering*, **68**(16):1411-1421.
6. Alexin, S.G. and Drobakhin, O.O., (2009), Inverse Problem Solving for Layered Dielectric Structure using Newton-Kantorovich Iterative Scheme with Increased Accuracy, *Proc. DIPED-2009*: 227-231.
7. Miller, E.K. and Lager, D.L., (1982), Inversion of One-Dimensional Scattering Data using Prony's Method, *Radio Science*, **17**(1):211-217.
8. Andreev, M.V., Borulko, V.F., Drobakhin, O.O., and Saltykov, D.Yu., (2004), Rational Representation in Spectrum Conjugate Domain for Parameters Determination of Reflecting Structures, *Proc. MMET*04*, pp. 16-1-1:449-451.

Telecommunications and Radio Engineering, 69(9):839-845 (2010)

INVESTIGATION INTO OPTOELECTRONIC AVIATION ANGLE METER BY THE DESIGN-OF-EXPERIMENTS METHOD

A.S. Oganesyan, M.V. Thehovsky, N.D. Koshevoy, & V.A. Gordienko

National Aerospace University "Kharkkiv Aviation Institute", Kharkiv 61085, Ukraine

*Address all correspondence to A.S. Oganesyan E-mail: artyom.oganesyan@gmail.com

This paper considers both an aviation angle meter to measure the aircraft control surface angles and the operation of angle meter electronic bloc. A description is given of the process of synthesizing mathematical models of this particular device using the design-of-experiments method.

KEY WORDS: *angle meter, infrared light-emitting diode (LED), design of experiments, full factorial experiment, orthogonal central composition full factorial experiment*

1. FORMULATION OF THE PROBLEM

In testing aviation equipment, as the scheduled operations are underway, it is necessary to obtain the most accurate measurements, to afford digital output to interface devices and provide for on-line testing process.

One of the constituent elements of the scheduled operations is to measure aircraft control surface angles.

The aim of the present paper is to give an appropriate description of electronics-based facility that determines the control surface deviation in terms of the disturbance assigned from the control column. In addition, we think it fit to suggest the techniques for constructing the mathematical model of an object under study, namely, an aviation angle meter.

2. DESCRIPTION OF THE BASIC PART OF THE FACILITY TO BE USED

The aviation angle meter we propose is built around electronic components whose purpose is to determine the angular deviations of aircraft control surfaces [1]. The schematic of the angle meter installation on an aircraft is presented in Fig. 1.

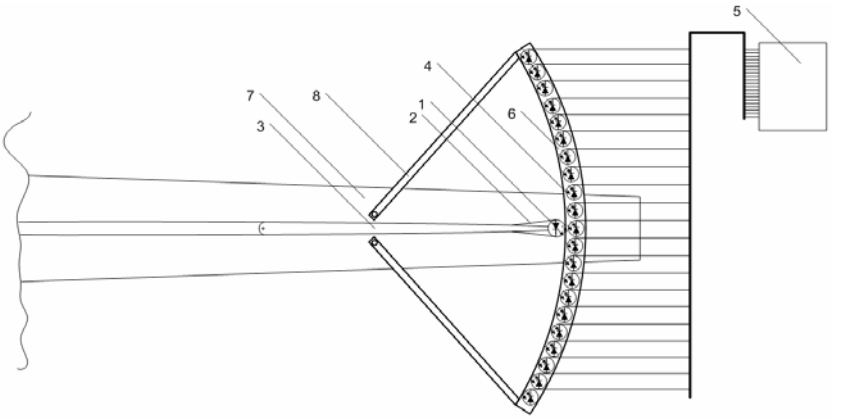

FIG. 1: The functional diagram of angle meter installation

Referring to Fig. 1, 1 is the infrared LED that acts as a signal-producing source; 2 is the clamp for attaching the LED to the control surface 3 (in this particular case the control surface is the yaw rudder); 4 is the metallic arc on which the signal receivers are mounted, i.e., the photodiodes 6 operating in the infrared; 5 is the electronic signal-processing unit. Physically, the entire system is connected to fuselage 7 by means of stiff rods. The electronic unit (shown in Fig. 2) of the above device is intended to address a common issue relevant to intensifying two adjacent optical receivers [2]. Receiving a signal and deriving a correct value at the electronic unit output with a signal coming simultaneously from two adjacent photodiodes are effected as follows. All the IR receivers are divided into 2 groups: even and odd ones. The signals from the first 8 odd photodiodes are fed into the comparator circuit CC1, the signals from the first 8 even photodiodes enters into the CC2 circuit, the signals from the second 8 odd photodiodes are fed into the CC3 circuit and so forth. The signals are subsequently processed in two separate channels. Either an 8-bit word is generated as it comes out of the channels (in case the second channel is “empty” or a word corresponding to the average arithmetic meaning of words is likewise generated (if a signal differing from zero is existent in both of the channels). 8-bit words are assigned by the memory cells (Flesh 1, Flesh 2, …, Flesh N).

The aim of the present study into the aviation angle meter described above is to construct a mathematical model describing the response of the receivers to the change in the infrared LED position. The output signal of the photodiode (or a signal of the phototransistor which is better suited to be utilized) is voltage. The factors affecting the photodiode (or phototransistor) output voltage are 1) the distance to the LED (ΔX); 2) an interval between the central axes of the receiver and the radiator (ΔY); 3) an angle of LED inclination with respect to the receiving device (β). At the same time one should take account of the response of not only a single receiving element, but also those elements that are close to it (see Fig. 3). Thus, it is necessary that 3 expressions be derived:

$$U_1 = f(\Delta X, \Delta Y, \beta);$$
$$U_2 = f(\Delta X, \Delta Y, \beta);$$
$$U_3 = f(\Delta X, \Delta Y, \beta).$$

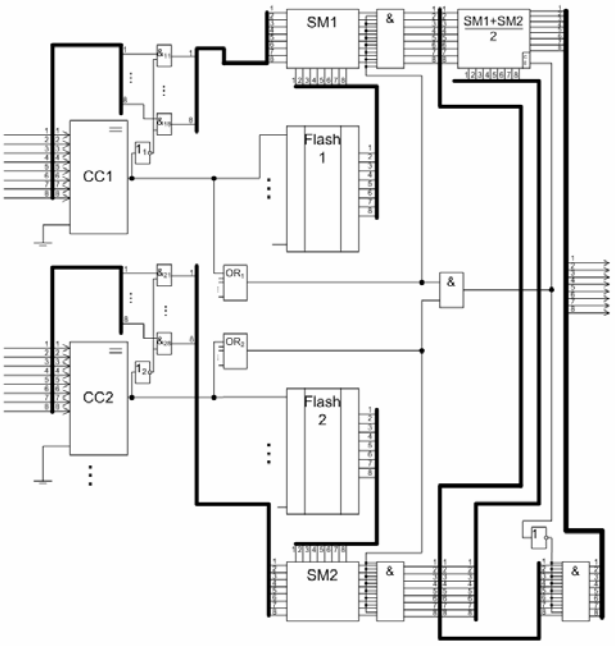

FIG. 2: The functional electronic block diagram

The optimal method for deriving mathematical models of this kind is the design of experiments. Using this method makes easy to conduct a relatively small series of experiments through far less cumbersome calculations, to obtain the sought-for mathematical model, to judge its adequacy and to highlight significant and insignificant coefficients of regression equations.

The primary objective is to determine the boundaries of the factor space domain. Decisions on the limiting values are made in view of the fact that IR LED (of BIR-BM 1331 type produced by Bright LED Electronics) serves as a radiator whereas the IR photoresistors of BPT-BP 2931 (also produced by Bright LED Electronics) are of use as signal receivers. In view of the overall dimensions of the receivers (the plastic lens is 3.00 mm in diameter) and the strength properties of the metal the duralumin arc is mode from, the gap between the adjacent diodes in drilling the holes should be 2.00 mm. Thus, the interval $\Delta Y = R + \frac{1}{2}l$, where R is the radius of the photoresistor plastic lens; l is the spacing between the adjacent receivers, i.e., $\Delta Y = 2.5$ mm. The distance to the LED may not be more than an accuracy of the arc and clamp setting.

The extreme value of the ΔX distance is assumed to be equal to 4.0 mm. The angle of the radiator axis is similarly chosen with respect to the receiver axis. The extreme value of β are experimentally taken to be $\pm 3.5^0$. The experiment involving two levels of each of three factors is referred to as the full factorial experiment (FFE) 2^3.

According to theory of design of experiments, it is common practice to designate the factors by x_1, x_2, x_3 and their interactions by $x_1x_2, x_1x_3, x_2x_3, x_1x_2x_3$. The levels and the intervals of factor variation are listed in Table 1. Using these symbols one can write the aim-oriented mathematical model as:

$$U = b_0 + b_1x_1 + b_2x_2 + b_3x_3 + b_{12}x_1x_2 + b_{13}\ x_1x_3 + B_{23}x_2x_3 + b_{123}x_1x_2x_3\,.$$

TABLE 1: The levels and factor variation intervals

Factors	**Levels of factors**			**Variation intervals**	**Dimensionality**
	-1	0	+1		
$x_1(\beta)$	-3.5	0	3.5	3.5	degree
$x_2(\Delta Y)$	-2.5	0	2.5	2.5	mm
$x_3(\Delta X)$	0	2	2	2	mm

The design-of-experiments matrix for a given problem will take on the form in view of the interaction effect (see Table 2).

TABLE 2: Matrix of FFE 2^3 design including the interaction effect

No	x_1	x_2	x_3	x_1x_2	x_1x_3	x_2x_3	$x_1x_2x_3$	U_1	U_2	U_3
1	-1	-1	-1	+1	+1	+1	-1	U_{11}	U_{21}	U_{31}
2	+1	-1	-1	-1	-1	+1	+1	U_{12}	U_{22}	U_{32}
3	-1	+1	-1	-1	+1	-1	+1	U_{13}	U_{23}	U_{33}
4	+1	+1	-1	+1	-1	-1	-1	U_{14}	U_{24}	U_{34}
5	-1	-1	+1	+1	-1	-1	+1	U_{15}	U_{25}	U_{35}
6	+1	-1	+1	-1	+1	-1	-1	U_{16}	U_{26}	U_{36}
7	-1	+1	+1	-1	-1	+1	-1	U_{17}	U_{27}	U_{37}
8	+1	+1	+1	+1	+1	+1	+1	U_{18}	U_{28}	U_{38}

The coefficients for each of three mathematical models are calculated from the following formulas:

$$b_0 = \frac{\sum U_i}{N};\ b_j = \frac{\sum_{i=1}^{N} x_{ji}U_i}{N}\,.$$

Once the mathematical models verify the hypothesis on their adequacy. To do so one can make use of the F-criterion (Fisher criterion) [3]:

$$F = \frac{S_{ad}^2}{S_{\{U\}}^2},$$

where S_{ad}^2 is the adequacy variance; $S_{\{U\}}^2$ is the optimization parameter variance.

When using the Fisher criterion, the hypothesis verification can be reduced to the comparison with a tabular value. As far as this particular problem is concerned, the model will be recognized as an adequate one of the F-criterion value does not exceed 6.9. Otherwise, one has to go on to a non-linear mathematical model. To this end it is best to make use of the orthogonal center compositional full factorial experiment (OCCFFE).

With using (OCCFFE) it is required that the boundaries of the factor-space domain should be extended to a value of α. For the experiment 2^3, $\alpha = 1.2154$. If the factor space is unlimited, then α is counted off from the experiment center in positive and negative directions. This can be done involving the factors x_1 and x_2. However, for x_3 the space is limited space at point of 0 mm. Therefore for this particular factor the point of the experiment center has to be shifted in such a way that the coded value of $-\alpha$ corresponded to the real value of 0 mm. Upon hawing extended the factor-space domain by this procedure we obtain the following levels and intervals of factor variations (see Table 3)

TABLE 3: Levels and intervals of factor variations for OCCFFE 2^3

Factors	**Factor levels**					**Variation intervals**	**Dimensio-nality**
	$-\alpha$	-1	0	+1	$+\alpha$		
$x_1(\beta)$	-4.25	-3.50	0.00	3.50	4.25	3.50	degree
$x_2(\Delta Y)$	-3.00	-2.50	0.00	2.50	3.00	2.50	mm
$x_3(\Delta X)$	0.00	0.40	2.40	4.40	4.80	2.00	mm

As the orthogonal compositional plan is being used, the mathematical model in the general case will take on this form

$$U = b_0 + b_1 x_1 + b_2 x_2 + b_3 x_3 + b_{12} x_1 x_2 + b_{13}\, x_1 x_3 + B_{23} x_2 x_3 +$$
$$+ b_{11}\left(x_1^2 - a\right) + b_{22}\left(x_2^2 - a\right) + b_{33}\left(x_3^2 - a\right),$$

where a is the displacement parameter for the experiment 2^3 $a = 0.7303$.

In this instance the design-of experiments matrix will be of the form as shown in Table 4:

TABLE 4: OCCFFE 2^3 design matrix

No	z_1	z_2	z_3	z_4	z_5	z_6	z_7	z_8	z_9	U_1	U_2	U_3
	x_1	x_2	x_3	x_1x_2	x_1x_3	x_2x_3	x_1^2-a	x_2^2-a	x_3^2-a			
1	-1	-1	-1	1	1	1	1-a	1-a	1-a	U_1	U_1	U_1
2	1	-1	-1	-1	-1	1	1-a	1-a	1-a	U_2	U_2	U_2
3	-1	1	-1	-1	1	-1	1-a	1-a	1-a	U_3	U_3	U_3
4	1	1	-1	1	-1	-1	1-a	1-a	1-a	U_4	U_4	U_4
5	-1	-1	1	1	-1	-1	1-a	1-a	1-a	U_5	U_5	U_5
6	1	-1	1	-1	1	-1	1-a	1-a	1-a	U_6	U_6	U_6
7	-1	1	1	-1	-1	1	1-a	1-a	1-a	U_7	U_7	U_7
8	1	1	1	1	1	1	1-a	1-a	1-a	U_8	U_8	U_8
9	$+\alpha$	0	0	0	0	0	α^2-a	-a	-a	U_9	U_9	U_9
10	$-\alpha$	0	0	0	0	0	α^2-a	-a	-a	U_{10}	U_{10}	U_{10}
11	0	$+\alpha$	0	0	0	0	-a	α^2-a	-a	U_{11}	U_{11}	U_{11}
12	0	$-\alpha$	0	0	0	0	-a	α^2-a	-a	U_{12}	U_{12}	U_{12}
13	0	0	$+\alpha$	0	0	0	-a	-a	α^2-a	U_{13}	U_{13}	U_{13}
14	0	0	$-\alpha$	0	0	0	-a	-a	α^2-a	U_{14}	U_{14}	U_{14}
15	0	0	0	0	0	0	-a	-a	-a	U_{15}	U_{15}	U_{15}

The coefficients for a given mathematical model will be calculated from the following formulas [4]:

$$b_0 = \frac{\sum_{i=1}^{N} U_i}{N};\ b_p = \frac{\sum_{i=1}^{N} z_i U_i}{2^3 + 2a^2};\ b_s = \frac{\sum_{i=1}^{N} z_i U_i}{2^3};\ b_u = \frac{\sum_{i=1}^{N} z_i U_i}{2a^4},$$

where b_p are the coefficients of linear terms; b_s are the coefficients of interactions; b_u are the coefficients of quadratic terms. The truth of the adequacy hypothesis is verified by the method similar to the FFE.

3. CONCLUSIONS

To summarize the foregoing, we can conclude that in the present paper a special emphasis has been placed upon the patterns of mathematical models describing the responses of the aviation angle meter photoreceivers. Certain type of models are given and the regression coefficients are calculated both for linear and quadratic functions. The quadratic model is used to interpolate the sought for expression $U = f(\Delta X, \Delta Y, \beta)$ in case a linear model is inadequate.

REFERENCES

1. Koshevoy, N.D. and Oganesyan, A.S., (2007), A universal photoelectric sensor of aircraft control surface angular displacement, *Sbornik nauchnykh trudov KNU*, Kiev: 34-37 (in Russian).
2. Oganesyan, A.S., Koshevoy, N.D., and Tsehovsky, M.V., (2009), Circuitry designing of an optical device for measuring a turning angle of the aircraft control surface, *Svetotekhnika and Elektroenergetika*. **10**(3):75-78 (in Russian).
3. Adler, Yu.P., Markova, E.V., and Granovsky, Yu.V., (1976), *The design of experiments in searching optimal conditions*, Nauka, Moscow: 279 p. (in Russian).
4. Akhnazarova, S.L. and Kafarov, V.V., (1985), *Methods of optimizing an experiment in chemical technology*, Vyshsaya Shkola, Moscow: 327 p. (in Russian).